UCLA
UCLA Electronic Theses and Dissertations

Title
Viral Reprogramming of Metabolism as an Approach to Identify Metabolic Vulnerabilities in Cancer

Permalink
https://escholarship.org/uc/item/3160m91h

Author
Thaker, Shivani K

Publication Date
2019

Peer reviewed|Thesis/dissertation

eScholarship.org Powered by the California Digital Library
University of California

UNIVERSITY OF CALIFORNIA

Los Angeles

Viral Reprogramming of Metabolism as an Approach to Identify Metabolic Vulnerabilities in Cancer

A dissertation submitted in partial satisfaction of the requirements for the degree

Doctor of Philosophy in Molecular and Medical Pharmacology

by

Shivani Thaker

2019

© Copyright by

Shivani Thaker

2019

ABSTRACT OF THE DISSERTATION

Viral Reprogramming of Metabolism as an Approach to Identify Metabolic Vulnerabilities in Cancer

by

Shivani Thaker

Doctor of Philosophy in Molecular and Medical Pharmacology

University of California, Los Angeles, 2019

Professor Heather R. Christofk, Chair

Cancer cells and viruses reprogram cell metabolism towards increased nutrient uptake and anabolism. Unlike cancer cells, viruses undergo intense selection for efficiency, only upregulating metabolic nodes critical for their rapid replication. Viruses are therefore powerful tools to identify essential metabolic pathways in cancer cells. A previous study from our lab reported that adenovirus infection increases host cell anabolic glucose metabolism. Specific glycolytic genes are activated by binding of viral protein E4ORF1 with cellular transcription factor MYC, which is upregulated in many cancers. Here, we show that adenovirus infection also upregulates glutamine metabolism through E4ORF1-induced MYC activation, leading to increased levels of glutaminase and glutamine transporters. Inhibition of glutaminase reduces optimal replication of adenovirus and other diverse viruses, including HSV-1 and influenza. Glutaminase inhibitors are also currently in clinical trials to treat certain types of cancers. This study serves as a proof-of-principle that metabolic enzymes and pathways important for adenovirus infection converge on critical metabolic enzymes in cancer.

The specific compilation of metabolic genes altered by adenovirus infection, that may also be critical for cancer cell proliferation, is currently undefined. We find that adenovirus infection leads to upregulation of an enzyme involved in fructose metabolism, ketohexokinase, which supports optimal virus replication and lung tumor growth. We further show that lung cancer cells can convert glucose via the polyol pathway into fructose, which can then be metabolized by ketohexokinase. Our model for how ketohexokinase promotes anabolism is by allowing cells to bypass negative feedback on a heavily regulated enzyme in glycolysis, phosphofructokinase, and allowing increased glucose utilization into nucleotides. Since KHK deficiency is a clinically benign, targeting KHK in lung cancer have limited systemic toxicities in patients.

Finally, numerous viruses in addition to adenovirus have been found to reprogram host cell metabolism, but whether the flavivirus Zika virus alters metabolism and whether viruses have unique effects on different host cells remains unclear. We find that Zika virus differentially alters glucose metabolism in both human cells and mosquito cells by increasing glucose use in the TCA cycle in human cells, while increasing glucose utilization into the pentose phosphate pathway in mosquito cells. Zika virus infection of human cells leads to selective depletion of nucleotide triphosphates, leading to AMP-activated protein kinase activation and cell death. Our findings suggest that the differential metabolic reprogramming during Zika virus infection of human versus mosquito cells determines whether or not cell death occurs and demonstrates that viruses can have contrasting effects depending on the host cell. Taken together, this dissertation (i) describes virally induced metabolic changes in both adenovirus and Zika virus and (ii) utilizes the evolutionary efficiency of adenovirus infection as an approach to identify important metabolic enzymes in anabolism and cancer.

The dissertation of Shivani Thaker is approved.

Utpal Banerjee

Jing Huang

Siavash K. Kurdistani

Heather R. Christofk, Committee Chair

University of California, Los Angeles

2019

For my four loving grandparents.

TABLE OF CONTENTS

FIGURES AND TABLES

Chapter 1

Chapter 2

Chapter 3

Chapter 4

Chapter 5

ACKNOWLEDGMENTS

These past four and a half years pursuing a Ph.D. have been incredibly formative and would not have been the same without the support of numerous individuals both inside and outside of the lab. First and foremost, I'd like to thank my labmates, past and present, who have become more like family over these past four and a half years. I'd like to express my gratitude towards Minh Thai, a former postdoctoral fellow in the lab, for his patience and willingness to train me when I first joined the lab with very limited experience in mammalian cell culture and biochemistry. He taught me most of the technical skills that allowed me to pursue this work. I'd like to thank former graduate students in the lab and friends Abby Krall and BJ Sullivan for their wisdom and entertainment and for sharing in all of the laughs, tears, and mostly failed experiments in lab these past years. Our relationship has really grown over the years and I'm lucky to have gone through graduate school with them. I'd like to thank my former undergraduate student, Lisa Situ, for her seemingly unlimited energy, positive attitude, and hard work in lab. I'd like to thank Ernst for running and analyzing my many metabolomics, for his effort in helping me wrap up the KHK project. I'd like to thank the rest of my labmates, Wen Gu, James Ch'ng, Pete Mullen, Andy Cicchetto, Suzi Shapira, and the rest of "Club Christofk" for the good times in lab. Finally, I'm grateful for all of our lab managers, Carolina Espindola, Katie Machado, Lisa Situ, and Sarah Jobbins for all of their effort to keep the lab running smoothly.

I'd like to thank all of our collaborators at UCLA that helped make the science possible. I'd especially like to thank Milica Momcilovic and David Shackelford for all of their collaboration on the *in vivo* aspects of the ketohexokinase project. Milica has always been an extremely responsible, enthusiastic, and respectful collaborator and it's been great to have had the opportunity to work with her. I'd like to thank Ren Sun, Vaithi Arumugaswami, and their respective labs for their collaboration on the viral aspects of the Zika project.

Transitioning between medical school and graduate school has been tough, and I'd like to thank my MSTP classmates for sharing the medical and graduate school journey with me.

I have great respect for my thesis committee members Dr. Utpal Banerjee, Dr. Siavash Kurdistani, and Dr. Jing Huang and thank them for their guidance and valuable feedback on my work and for inspiring me to be a better scientist. I've been fortunate to also have my undergraduate mentor, Dr. Banerjee, on my committee and would like to thank him for making me passionate about science early on and for teaching me how to think. Without his mentorship and support at a critical period in my training, I wouldn't be on the path I am now.

Importantly, I'd like to thank my Ph.D. mentor, Dr. Heather Christofk, for her continuous support, mentorship, optimism, and generosity throughout my graduate training. Heather has been approachable and caring and I greatly appreciate her commitment to my training. I've learned so much under her guidance on how to be a better scientist, writer, presenter, and thinker. I've admired her ability to effectively handle so many tasks- whether professional or personal- and work so well with people. It's been a fantastic opportunity to work in her lab and I'm grateful for the experience.

I'd like to thank my parents, Kartik and Jigna, and my brother, Kunal, for their unconditional support in all of my endeavors. I am so fortunate to have them in my life.

Finally, I'd like to thank my husband Pradeep for his patience, optimism, support, and companionship in every possible way throughout graduate school. He continuously inspires me with his hard work and genuine care for others.

There are many others that I haven't specifically gotten to thank that have contributed to my graduate training and experience whom I am thankful for.

The research presented in this thesis was performed under the direction of Dr. Heather R. Christofk and was supported by an NIH NIGMS training grant, UCLA Virology and Gene Therapy Training Grant, UCLA Tumor Immunology Training Grant, UCLA Medical Scientist Training Program Grant, and the UCLA Dissertation Year Fellowship.

PREFACE

Chapter 1. Parts of this manuscript are under peer review: **Thaker SK**, Ch'ng J, Christofk, HR. Viral Hijacking of Cellular Metabolism. BMC Biology. 2019 (under review)

Chapter 2. A version of this manuscript is published: Thai M*, **Thaker SK***, Feng J, Du Y, Hu H, Wu TT, Graeber TG, Braas D, Christofk HR. MYC-induced reprogramming of glutamine catabolism supports optimal virus replication. *Nature Communications*. 2015;6. doi:10.1038/ncomms9873. *equal contribution

Chapter 3. A version of this manuscript is published: **Thaker SK**, Chapa T, Garcia G Jr, Gong D, Schmid EW, Arumugaswami V, Sun R, Christofk HR. Differential Metabolic Reprogramming by Zika Virus Promotes Cell Death in Human versus Mosquito Cells. *Cell Metabolism*. 2019; pii: S1550-4131(19)30064-6. doi: 10.1016/j.cmet.2019.01.024.

Chapter 4. Ketohexokinase is an important metabolic enzyme in lung cancer.

Chapter 5. Conclusions and Future Directions.

VITA

EDUCATION

University of California Los Angeles (UCLA) 2008-2012

Bachelor of Science, Molecular, Cell & Developmental Biology and Minor in Biomedical Research

summa cum laude, Phi Beta Kappa, Highest Departmental Honors, College Honors

UCLA David Geffen School of Medicine

Doctor of Medicine, Medical Scientist Training Program 2012-

Doctor of Philosophy, Molecular and Medical Pharmacology 2014-

ACADEMIC POSITIONS

Undergraduate Student Researcher, UCLA 2010-2012

Advisor: Dr. Utpal Banerjee

Examined signaling pathways altered upon oncogenic activation that lead to changes in cell metabolism using Drosophila melanogaster as a genetic model.

Graduate Student Researcher, UCLA, Los Angeles, CA 2014-

Advisor: Dr. Heather Christofk

Investigating how viruses rewire host cell metabolism and use of viruses to identify important metabolic enzymes in cancer cells.

PUBLICATIONS

1. Thai M*, **Thaker SK***, Feng J, Du Y, Hu H, Wu TT, Graeber TG, Braas D, Christofk HR. MYC-induced reprogramming of glutamine catabolism supports optimal virus replication. Nat Commun. 2015. *Equal contributions

2. Wang CW, Purkayastha A, Jones KT, **Thaker SK**, Banerjee U. In vivo dissection of tumor growth and the Warburg effect. eLife. 2016;5.
3. **Thaker SK**, Chapa TJ, Garcia GJ, Gong D, Schmid EW, Arumugaswami V, Sun R, Christofk HR. Differential metabolic reprogramming by Zika virus promotes cell death in human versus mosquito cells. Cell Met; 2019 (In press).
4. **Thaker SK,** Ch'ng J, Christofk HR. Viral Hijacking of Cellular Metabolism. (under review, BMC Biology)
5. **Thaker SK**, Momcilovic M, Schmid E, Zemke NR, Su T, Liu X, Mao Z, Jung M, Kurdistani SK, Berk AJ, Braas D, Shackelford D, Christofk HR. Ketohexokinase is important for lung tumor growth. (in preparation)

SELECTED PRESENTATIONS

1. Ketohexokinase is important for lung tumor growth. Keystone Symposia Conference Tumor Metabolism; 25 Feb 2019; Keystone, CO. (short talk)

HONORS, AWARDS, AND DISTINCTIONS

2008-2012	Regents Scholar, UCLA
2010	Whitcome Summer Research Fellowship, UCLA
2011	Dean's Prize, Undergraduate Science Poster Day, UCLA
2011	Emil Reisler Award, UCLA
2011-2012	Senior Undergraduate Research Scholar, UCLA
2015-2017	Tumor Immunology Institutional Training Grant, UCLA
2017-2018	Interdisciplinary Training in Virology and Gene Therapy Grant, UCLA
2018-2019	Dissertation Year Fellowship, UCLA

CHAPTER 1

Introduction: Metabolic reprogramming by cancer cells and virus infection

Although it has been known for over half a century that viral infection alters host cell metabolism, the mechanisms and consequences of virus-induced metabolic reprogramming have only begun to be studied over the last decade (Figure 1). Viruses clearly rely on host cell machinery to propagate. Therefore, it is not surprising that viral infection triggers metabolic reprogramming in host cells to facilitate optimal virus production. Metabolic phenotypes conferred by virus infection often mirror metabolic changes seen in cancer cells, such as upregulation of nutrient consumption and anabolism. Given their rapid evolution and intense selection for efficiency, viruses are powerful tools to study cellular metabolic reprogramming mechanisms towards increased nutrient consumption and anabolism. We hypothesize that understanding viral strategies used to make host cells amenable to virion production may provide insight into important metabolic nodes in cancers.

Here, we discuss a few examples of metabolic reprogramming by different viruses and the use of viruses as a guide to identify critical metabolic nodes for cancer anabolism to lay the foundation for the dissertation. The work presented in the later chapters will discuss (i) adenovirus infection-induced changes in host cell glutamine metabolism through viral protein E4ORF1 binding to and activation of cellular transcription factor MYC, (ii) the use of adenovirus infection to identify metabolic enzymes important for anabolism and tumor growth, specifically the enzyme ketohexokinase, which is involved in fructose metabolism, and (iii) how another virus, Zika virus, differentially alters metabolism of human versus mosquito cells, leading to cell death specifically in human cells.

Virus infection induces metabolic reprogramming in host cells

Adenovirus is a double-stranded DNA virus that relies entirely on host cell machinery for replication (O'Shea, 2005a). Several early studies in the 1950s through 1970s described increases in glycolysis during adenovirus infection (Bardell, 1977; Fisher and Ginsberg, 1957). However, recent technological advances have enabled more detailed analysis of the metabolic

changes induced during adenovirus infection and potential mechanisms by which metabolic reprogramming may occur. A previous study in our lab demonstrated that wild-type adenovirus 5 (ADWT) infection of human breast epithelial and bronchial epithelial cells leads to increased glucose consumption and lactate production as well as decreased oxygen consumption rates (Thai et al., 2014). Glucose is used to generate pentose phosphate pathway intermediates and nucleotides during infection, likely to support viral genome replication (Thai et al., 2014). The ADWT-induced increases in glycolysis are mediated by early adenovirus gene product E4ORF1 binding to cellular MYC to direct transcription of specific glycolytic enzymes, including HK2 and PFKM, and an adenovirus containing the D68A point mutation in E4ORF1 that prevents binding to MYC does not replicate as well as ADWT (Thai et al., 2014).

Several other viruses have also been shown to modulate aspects of metabolism in infected cells (Figure 2). Recent studies have utilized improved technologies including liquid chromatography coupled to mass spectrometry (LC-MS) and isotope tracers to analyze the metabolic changes induced by viral infection of host cells. HSV-1 infection leads to increased levels of glycolytic intermediates upstream of phosphoenolpyruvate (PEP) (Vastag et al., 2011). HSV-1 upregulates pyrimidine nucleotide biosynthesis by increasing aspartate generation both through elevated glucose flux into the TCA cycle through pyruvate carboxylase (PC) and from glutamine anaplerosis, followed by subsequent metabolism by glutamic-oxaloacetic acid transaminase 2 (GOT2) to form aspartate, which contributes to the pyrimidine backbone (Vastag et al., 2011) (Grady et al., 2013). Consistently, knockdown of PC and GOT2 decrease optimal HSV-1 replication (Vastag et al., 2011). Since aspartate is an important source of carbons for nucleotide synthesis, knockdown of enzymes that deplete aspartate, including argininosuccinate synthetase (AS1), increases viral titers by increasing aspartate availability for virus replication (Grady et al., 2013). Additionally, HSV-1 infected cells use glutamine to generate aspartate, which is important for supporting pyrimidine synthesis. Since HSV-1 is a large double-stranded DNA virus with a genome of approximately 152 base pairs, viral

replication necessitates a large pool of nucleotides (Smith et al., 2014). Interestingly, HSV-1 encodes some of its own nucleotide metabolism enzymes including thymidine kinase, dUTPase, uracil-DNA glycosylase, and ribonucleotide reductase (Boehmer and Lehman, 1997). It's been hypothesized that HSV-1 has evolved to promote nucleotide biosynthesis in host cells since the virus infects and replicates in non-proliferative cell types including neurons.

Human cytomegalovirus (HCMV) is a member of the herpesvirus family that promotes increased glycolytic flux (Munger et al., 2008), likely through inducing increased expression of several glycolytic enzymes and activity of PFK (Munger et al., 2006). HCMV also promotes increased U-$^{13}C_6$-glucose labeling of TCA cycle intermediates, particularly citrate, which is kinetically labeled by glucose more rapidly in HCMV-infected cells compared to mock controls (Munger et al., 2008). HCMV infection promotes glutaminolysis as infected cells consume more glutamine and generate more glutamate than uninfected cells (Chambers et al., 2010). Consistently, the enzyme activities of glutaminase (GLS) and glutamate dehydrogenase (GDH) are also elevated upon HCMV infection (Chambers et al., 2010). Since glucose is routed towards lipid synthesis during HCMV infection, glutamine is used to replenish the TCA cycle in host cells and contributes to increased ATP production. Glutamine withdrawal decreases virus titer.

Flaviviruses are a genus of positive, single-stranded RNA viruses that are typically transmitted to humans through arthropod vectors, including mosquitoes, and undergo lytic replication (Jordan and Randall, 2016). The *Flaviviridae* family includes viruses known to cause serious diseases including Dengue virus (DENV), West Nile virus (WNV), Japanese encephalitis virus (JENV), and Zika virus (ZIKV). As with many other viruses, DENV infection of primary HFF cells increases glycolysis and alters levels of glycolytic intermediates compared to uninfected cells (Fontaine et al., 2015). DENV infection of HFFs also induces upregulation of GLUT1 protein levels and increases in hexokinase 2 (HK2) mRNA and protein levels post-infection (Fontaine et al., 2015). Consistently, glucose withdrawal in host HFF cells leads to a nearly 2-

log decrease in DENV replication, and 2-DG treatment of HFF and immortalized endothelial (TIME) cells during infection reduces virus replication (Fontaine et al., 2015).

While all the previously mentioned viruses alter the metabolism of host mammalian cells, interestingly, viruses that infect invertebrate hosts have also been shown to alter metabolism. The invertebrate virus white spot syndrome virus (WSSV) that infects shrimp hemocytes induces glycolysis in infected cells versus normal cells PI3K-Akt-mTOR-dependent manner (Chen et al., 2011; Su et al., 2014). The fact that metabolic reprogramming by viruses is conserved throughout species, even in invertebrates, provides further evidence that metabolic reprogramming is critical for replication of diverse viruses.

Gaps of Knowledge in Virus Metabolism Studies

While diverse viruses have been shown to reprogram host cell metabolism, many of the molecular mechanisms by which viruses induce these changes remains unknown. A number of viruses, including HSV-1, encode their own metabolic enzymes – usually involved in nucleotide biosynthesis - to facilitate viral replication in host cells. For instance, VACV encodes its own thymidylate kinase, and HSV-1 encodes RRM2. For those viruses that rely on hijacking host cell machinery for metabolic reprogramming, a major gap remains in the identification of the viral gene products that interact with host cell factors to modulate host cell metabolism. It remains unknown whether different viruses display tropism for specific cell types and different downstream effects depending on the metabolic environment and machinery present in the cells. Additionally, it remains unclear whether the same virus can have contrasting effects on different types of host cells.

Viruses as Cancer Discovery Tools and Therapies

DNA viral proteins and tumor cell mutations converge on many of the same molecular pathways to promote viral or cellular replication, including anabolic pathways. Key oncogenes and tumor

suppressor genes, including Src kinase, p53, PI3-kinase, and others, were originally discovered by identifying host pathways that DNA viral proteins interact with to promote replication (O'Shea, 2005b). While new tools are continually being developed to further cancer research, cancer genome instability and short evolutionary life-span make it difficult to distinguish passenger versus molecular drivers of tumorigenesis (O'Shea, 2005b). On the other hand, viruses, such as adenoviruses, have evolved to be efficient and alter key pathways in host cells that enable them to replicate effectively.

Since adenoviruses have undergone strong selective pressure for efficiency, and they completely rely host cell machinery for replication, the specific metabolic nodes they hijack for their replicative needs may represent especially important metabolic nodes for anabolism (Figure 3). As a proof-of-principle, we have found that adenovirus infection increases GLS protein levels and activity. GLS is already a cancer metabolism drug target – the GLS inhibitor CB-839 is currently being used in clinical trials to treat certain types of solid and hematological malignancies that also rely on GLS activity. We found that treatment of adenovirus infected cells with CB-839 reduces viral titers. We provide another example of a virally-induced metabolic enzyme, ketohexokinase, which we find is important for both virus replication and lung tumor growth. These results are examples that metabolic enzymes and pathways critical for optimal virus replication may also be important for cancer cell proliferation. Understanding how a rapidly replicating virus like adenovirus alters host cell metabolism during infection will likely reveal critical anabolic nodes that are important in different cancers, just as understanding how viruses reprogram host cell signaling and transcriptional machinery helped identify key oncogenes and tumor suppressor genes in the 1970s and 1980s.

SUMMARY

While many studies have demonstrated that viruses reprogram cell metabolism and rely on metabolic changes for optimal virus replication *in vitro*, significant work remains to determine

mechanistically what viral proteins interact with host cell machinery to induce such alterations and characterize whether the same metabolic perturbations occur during infection *in vivo*. We provide a molecular mechanism by which adenovirus infection increases glutamine metabolism in infected cells – through viral E4ORF1 binding and activation of cellular MYC. We also use the approach of determining which metabolic enzymes are upregulated during adenovirus infection to identify enzymes important in cancer growth as well. Through this method, we have identified the enzyme ketohexokinase to play an important role in adenovirus infection and lung tumor growth. Finally, several studies suggest that the metabolic characteristics of a cell type or tissue may determine virus tropism, therefore it will be interesting for future studies to determine whether there is different viral affinity for and replication across tissue types depending on the metabolic environment. Additionally, whether differential metabolic reprogramming by a virus across multiple species impacts how specific species cope with viral replication remains unknown. To address this, we show that Zika infection differentially alters metabolism of human versus mosquito cells, which leads AMPK activation and cell death specifically in human cells.

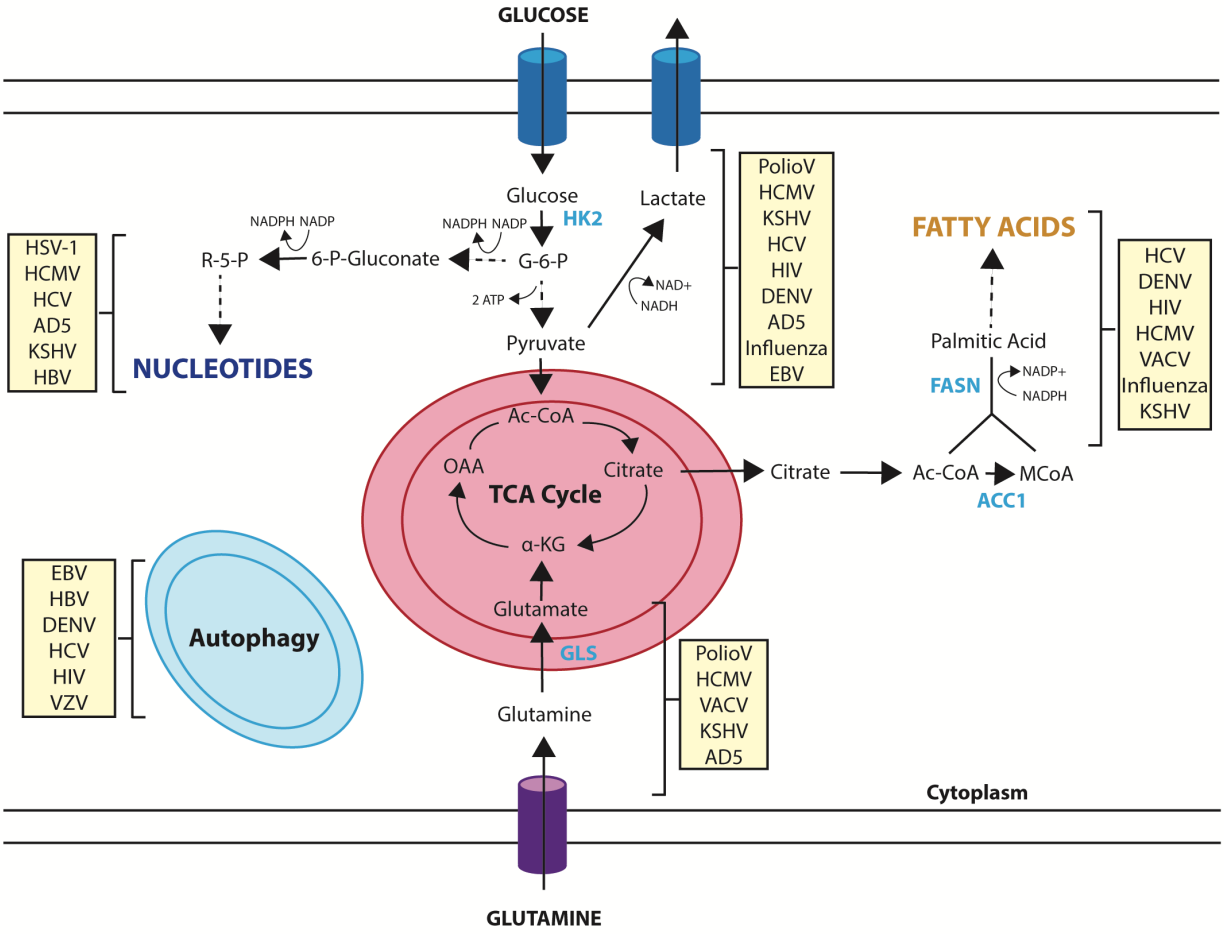

Figure 1. Schematic of metabolic pathways altered by virus infection.

Virus	Metabolic Changes	Mechanism	References
Adenovirus (ADWT)	Increased glycolysis and increased glutaminolysis	E4ORF1-mediated activation of cellular MYC	Fisher et al., Proc Soc Exp Biol Med, 1957; Thai et al, Cell Met, 2014; Thai and Thaker et al., Nature Comm, 2015
Human cytomegalovirus (HCMV)	Increased glycolysis and nucleotide synthesis; greater increases in TCA cycle and lipid biosynthesis; increased anaplerotic use of glutamine	CAMPKK-AMPK signaling necessary; increased GLUT4 translocation to plasma membrane; ?	Munger et al., Nat Biotech, 2008; Chambers et al., J Virol, 2010; Vastag et al., PLoS Pathog, 2011; Terry et al., PNAS, 2012; Yu et al., J Virol, 2011
Herpesvirus-1 (HSV-1)	Increased glycolysis and anaplerotic influx to TCA cycle through pyruvate carboxylase feeding increased pyrimidine nucleotide synthesis	Increased PFK-1 activity; ?	Vastag et al., PLoS Pathog, 2011; Abrantes et al., Biochem Biophys, 2012.
Influenza A	Increased glycolysis	?	Ritter et al., BMC Syst Biol, 2010
Dengue Virus (DENV)	Increased fatty acid biosynthesis	DENV NS3 recruits FAS to sites of viral replication; ?	Heaton et al., PNAS, 2010
Vaccinia virus (VACV)	Increased glutamine production for synthesis of purines and pyrimidines and anaplerosis	VACV protein C16 stabilizes HIF-1α;	Fontaine et al., J Virol, 2014

Figure 2. Non-oncogenic viruses and metabolic alterations on host cells during infection.

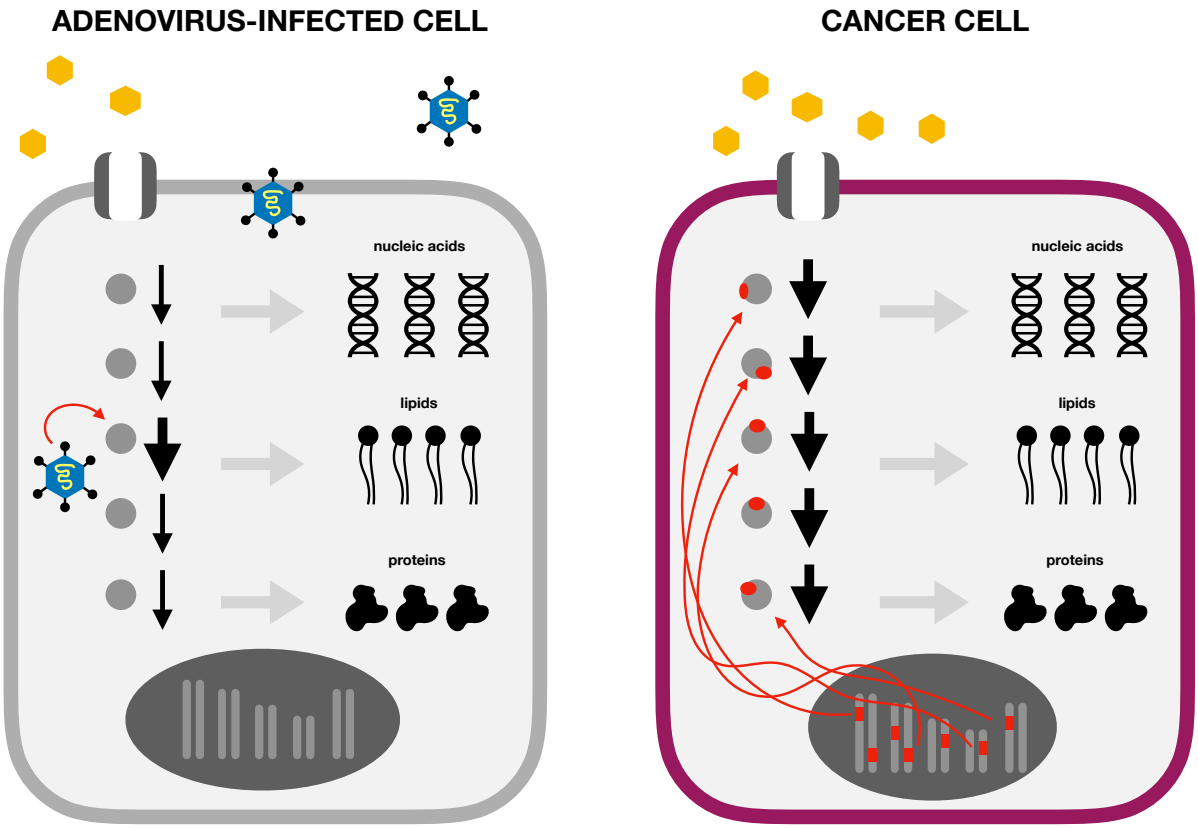

Figure 3. Comparison of wild type adenovirus-infected cell and cancer cells. While cancer cells have numerous mutations and perturbation of whole metabolic pathways (green), adenovirus-infected cells upregulate only key metabolic nodes for virion replication.

REFERENCES

Bardell, D. (1977). Glucose uptake and lactic acid production of adenovirus type 5-infected HEp-2 cells cultured under exponential growth and stationary phase conditions. Microbios *20*, 139-144.

Boehmer, P.E., and Lehman, I.R. (1997). Herpes simplex virus DNA replication. Annu Rev Biochem *66*, 347-384.

Chambers, J.W., Maguire, T.G., and Alwine, J.C. (2010). Glutamine metabolism is essential for human cytomegalovirus infection. Journal of virology *84*, 1867-1873.

Chen, I.T., Aoki, T., Huang, Y.T., Hirono, I., Chen, T.C., Huang, J.Y., Chang, G.D., Lo, C.F., and Wang, H.C. (2011). White spot syndrome virus induces metabolic changes resembling the warburg effect in shrimp hemocytes in the early stage of infection. Journal of virology *85*, 12919-12928.

Fisher, T.N., and Ginsberg, H.S. (1957). Accumulation of organic acids by HeLa cells infected with type 4 adenovirus. Proceedings of the Society for Experimental Biology and Medicine. Society for Experimental Biology and Medicine (New York, N.Y.) *95*, 47-51.

Fontaine, K.A., Sanchez, E.L., Camarda, R., and Lagunoff, M. (2015). Dengue virus induces and requires glycolysis for optimal replication. Journal of virology *89*, 2358-2366.

Grady, S.L., Purdy, J.G., Rabinowitz, J.D., and Shenk, T. (2013). Argininosuccinate synthetase 1 depletion produces a metabolic state conducive to herpes simplex virus 1 infection. Proc Natl Acad Sci U S A *110*, E5006-5015.

Griffiths, P., Baraniak, I., and Reeves, M. (2015). The pathogenesis of human cytomegalovirus. J Pathol *235*, 288-297.

Jordan, T.X., and Randall, G. (2016). Flavivirus modulation of cellular metabolism. Curr Opin Virol *19*, 7-10.

Kohio, H.P., and Adamson, A.L. (2013). Glycolytic control of vacuolar-type ATPase activity: a mechanism to regulate influenza viral infection. Virology *444*, 301-309.

Krall, A.S., Xu, S., Graeber, T.G., Braas, D., and Christofk, H.R. (2016). Asparagine promotes cancer cell proliferation through use as an amino acid exchange factor. Nat Commun *7*, 11457.

Landini, M.P. (1984). Early enhanced glucose uptake in human cytomegalovirus-infected cells. J Gen Virol *65 (Pt 7)*, 1229-1232.

McArdle, J., Moorman, N.J., and Munger, J. (2012). HCMV targets the metabolic stress response through activation of AMPK whose activity is important for viral replication. PLoS Pathog *8*, e1002502.

Munger, J., Bajad, S.U., Coller, H.A., Shenk, T., and Rabinowitz, J.D. (2006). Dynamics of the cellular metabolome during human cytomegalovirus infection. PLoS Pathog *2*, e132.

Munger, J., Bennett, B.D., Parikh, A., Feng, X.J., McArdle, J., Rabitz, H.A., Shenk, T., and Rabinowitz, J.D. (2008). Systems-level metabolic flux profiling identifies fatty acid synthesis as a target for antiviral therapy. Nat Biotechnol *26*, 1179-1186.

O'Shea, C.C. (2005a). Viruses - seeking and destroying the tumor program. Oncogene *24*, 7640-7655.

O'Shea, C.C. (2005b). Viruses: tools for tumor target discovery, and agents for oncolytic therapies - an introduction. Oncogene *24*, 7636-7639.

Ritter, J.B., Wahl, A.S., Freund, S., Genzel, Y., and Reichl, U. (2010). Metabolic effects of influenza virus infection in cultured animal cells: Intra- and extracellular metabolite profiling. BMC Syst Biol *4*, 61.

Smallwood, H.S., Duan, S., Morfouace, M., Rezinciuc, S., Shulkin, B.L., Shelat, A., Zink, E.E., Milasta, S., Bajracharya, R., Oluwaseum, A.J., et al. (2017). Targeting Metabolic Reprogramming by Influenza Infection for Therapeutic Intervention. Cell Rep *19*, 1640-1653.

Smith, S., Reuven, N., Mohni, K.N., Schumacher, A.J., and Weller, S.K. (2014). Structure of the herpes simplex virus 1 genome: manipulation of nicks and gaps can abrogate infectivity and alter the cellular DNA damage response. Journal of virology *88*, 10146-10156.

Su, M.A., Huang, Y.T., Chen, I.T., Lee, D.Y., Hsieh, Y.C., Li, C.Y., Ng, T.H., Liang, S.Y., Lin, S.Y., Huang, S.W., et al. (2014). An invertebrate Warburg effect: a shrimp virus achieves successful replication by altering the host metabolome via the PI3K-Akt-mTOR pathway. PLoS Pathog *10*, e1004196.

Taubenberger, J.K., and Morens, D.M. (2008). The pathology of influenza virus infections. Annu Rev Pathol *3*, 499-522.

Thai, M., Graham, N.A., Braas, D., Nehil, M., Komisopoulou, E., Kurdistani, S.K., McCormick, F., Graeber, T.G., and Christofk, H.R. (2014). Adenovirus E4ORF1-induced MYC activation promotes host cell anabolic glucose metabolism and virus replication. Cell Metab *19*, 694-701.

Vastag, L., Koyuncu, E., Grady, S.L., Shenk, T.E., and Rabinowitz, J.D. (2011). Divergent effects of human cytomegalovirus and herpes simplex virus-1 on cellular metabolism. PLoS Pathog *7*, e1002124.

Vysochan, A., Sengupta, A., Weljie, A.M., Alwine, J.C., and Yu, Y. (2017). ACSS2-mediated acetyl-CoA synthesis from acetate is necessary for human cytomegalovirus infection. Proc Natl Acad Sci U S A *114*, E1528-E1535.

Wang, P., Xu, J., Wang, Y., and Cao, X. (2017). An interferon-independent lncRNA promotes viral replication by modulating cellular metabolism. Science *358*, 1051-1055.

Yu, Y., Maguire, T.G., and Alwine, J.C. (2011). Human cytomegalovirus activates glucose transporter 4 expression to increase glucose uptake during infection. Journal of virology *85*, 1573-1580.

Yu, Y., Maguire, T.G., and Alwine, J.C. (2012). Human cytomegalovirus infection induces adipocyte-like lipogenesis through activation of sterol regulatory element binding protein 1. Journal of virology *86*, 2942-2949.

Yu, Y., Maguire, T.G., and Alwine, J.C. (2014). ChREBP, a glucose-responsive transcriptional factor, enhances glucose metabolism to support biosynthesis in human cytomegalovirus-infected cells. Proc Natl Acad Sci U S A *111*, 1951-1956.

Yu, Y., Pierciey, F.J., Jr., Maguire, T.G., and Alwine, J.C. (2013). PKR-like endoplasmic reticulum kinase is necessary for lipogenic activation during HCMV infection. PLoS Pathog *9*, e1003266.

CHAPTER 2

MYC-induced reprogramming of glutamine catabolism supports optimal virus replication

ABSTRACT

Viruses rewire host cell glucose and glutamine metabolism to meet the bioenergetic and biosynthetic demands of viral propagation. However, the mechanism by which viruses reprogram glutamine metabolism and the metabolic fate of glutamine during adenovirus infection have remained elusive. Here, we show MYC activation is necessary for adenovirus-induced upregulation of host cell glutamine utilization and increased expression of glutamine transporters and glutamine catabolism enzymes. Adenovirus-induced MYC activation promotes increased glutamine uptake, increased use of glutamine in reductive carboxylation, and increased use of glutamine in generating hexosamine pathway intermediates and specific amino acids. We identify glutaminase (GLS) as a critical enzyme for optimal adenovirus replication and demonstrate that GLS inhibition decreases replication of adenovirus, herpes simplex virus 1, and influenza A in cultured primary cells. Our findings show that adenovirus-induced reprogramming of glutamine metabolism through MYC activation promotes optimal progeny virion generation and suggest that GLS inhibitors may be useful therapeutically to reduce replication of diverse viruses.

INTRODUCTION

Glutamine is a critical nutrient for cellular biosynthetic processes. Many cancer cells rely on increased glutamine metabolism for growth and use glutamine as a source of carbon and nitrogen atoms for synthesis of lipids, nucleotides, and certain amino acids(DeBerardinis et al., 2007; Yang et al., 2009), as well as a cellular exchange factor for uptake of essential amino acids(Nicklin et al., 2009). Similar to cancer cells, viruses require increased anabolic metabolism to support proliferation(Munger et al., 2008; Thai et al., 2014; Vastag et al., 2011), and therefore may also depend on increased glutamine metabolism for replication. Consistently, glutamine deprivation decreases human cytomegalovirus (HCMV) replication in human foreskin fibroblasts – HCMV--infected cells reportedly use glutamine to fuel ATP production and anaplerosis in the TCA cycle(Chambers et al., 2010). However, whether glutamine uptake is important for replication of other viruses, how glutamine metabolism is regulated during viral infection, and whether pharmacological inhibition of glutamine metabolism can affect replication of diverse viruses have remained unknown.

We recently reported that the gene product of adenovirus E4ORF1 enhances host cell anabolic glucose metabolism during virus replication through MYC activation(Thai et al., 2014). E4ORF1 binds to nuclear MYC and enhances MYC-induced transcription of specific glycolytic target genes. A D68A point mutation in E4ORF1 abrogates binding to and activation of MYC, and a mutant adenovirus(Vastag et al., 2011) containing the D68A point mutation in E4ORF1 (AD ORF1 D68A) that is deficient in MYC activation exhibits impaired reprogramming of glucose metabolism and virus replication in primary lung epithelial cells. Since MYC enhances glutamine metabolism in cancer cells in part through promoting increased expression of GLS(Gao et al., 2009) and the glutamine transporters ASCT2 and SN2(Wise et al., 2008), we hypothesized that E4ORF1-induced MYC activation may enhance glutamine metabolism during adenovirus infection through modulation of GLS and glutamine transporter levels. Here, we characterize changes in glutamine metabolism in primary lung epithelial cells after infection with a wild-type (WT) strain of adenovirus 5 (AD). Additionally, we compare AD WT infection to AD ORF1 D68A

infection to assess effects of adenovirus-mediated MYC activation on regulation of glutamine metabolism during infection.

RESULTS

MYC regulates glutamine consumption during adenovirus infection

To determine whether adenovirus infection alters host cell glutamine metabolism, we measured glutamine consumption rates of primary normal human bronchial epithelial cells (NHBE) at multiple time points after AD WT infection. AD WT infection causes increased glutamine consumption rates at early time points post infection (Figure 1A). Our data suggest that the adenovirus-induced increase in glutamine consumption is MYC-dependent since cells infected with a mutant adenovirus deficient in MYC activation, AD ORF1 D68A(Thai et al., 2014), do not exhibit increased glutamine consumption rates at early time points post infection (Figure 1A). Furthermore, short hairpin RNA (shRNA)-mediated knockdown of MYC impairs the ability of AD WT to enhance glutamine consumption in NHBE cells (Figure 1B, Supplementary Figure 5a).

Since MYC regulates cancer cell glutamine metabolism in part through suppression of miR-23a and miR-23b, which are microRNAs that target the GLS 3'-UTR and thereby decrease GLS expression(Gao et al., 2009), we tested whether MYC modulates miR-23a/b and GLS levels during adenovirus infection of NHBE cells. We found that AD WT infection causes reduced expression of both miR-23a and miR-23b as early as ninety minutes post infection (Figure 1C). AD ORF1 D68A infection, however, has no effect on miR-23a levels, and decreases miR-23b levels to a lesser extent than AD WT infection of NHBE cells (Figure 1C). Consistently, AD WT infection leads to a larger increase in GLS protein levels, including GLS splice variants KGA (full length GLS) and GAC (shortened splice variant)(Wise et al., 2008), than AD ORF1 D68A infection of NHBE cells (Figure 1D; Supplementary Figure 5b). Since MYC also drives glutamine metabolism by activating expression of genes involved in glutamine uptake, including SLC7A5 and SLC1A5, which encode the glutamine transporters LAT1 and ASCT2, respectively(Hensley et al., 2013), we measured expression of these transporters during adenovirus infection. We

found that AD WT, but not AD ORF1 D68A, infection increases transcription of LAT1 and ASCT2 in MCF10A cells (Supplementary Figure 1A). Additionally, AD WT, but not AD ORF1 D68A, modestly increases ASCT2 protein levels in NHBE cells (Figure 1D; Supplementary Figure 5b). Together, our data support MYC activation-dependent regulation of glutamine metabolism during adenovirus infection through repression of miR-23 leading to upregulation of GLS, as well as MYC-dependent upregulation of the glutamine transporters, ASCT2 and LAT1.

Adenovirus infection alters host cell glutamine utilization

To characterize MYC-induced changes in glutamine metabolism during adenovirus infection, NHBE cells were labeled with U-$^{13}C_5$-glutamine and mock infected or infected at an MOI of 1 with AD WT or AD ORF1 D68A. 24 hours post labeling and infection, metabolites were extracted and analyzed by liquid chromatography tandem mass spectrometry (LC-MS/MS). AD WT infection, but not AD ORF1 D68A infection (MYC activation-deficient), increases the percentage of intracellular M5 isotopologue-labeled (five carbon-labeled) glutamate relative to mock-infected cells, consistent with a MYC activation-dependent increase in GLS-catalyzed conversion of glutamine to glutamate during adenovirus infection (Supplementary Figure 1B and 1C). AD WT infection, but not AD ORF1 D68A infection, also increases the percentage of M5-labeled alpha-ketoglutarate (Supplementary Figure 1B and 1C). Typically, activity of the oxidative citric acid cycle results in elevated levels of M4-labeled TCA cycle intermediates in cells labeled with U-$^{13}C_5$-glutamine (Supplementary Figure 1B). However, AD WT infection of NHBE cells causes a decrease in M4-labeled fumarate, malate, aspartate, and citrate (Supplementary Figure 1C and 1D). Instead, AD WT infection, but not AD ORF1 D68A infection, increases the levels of M5-labeled citrate, M3-labeled fumarate, M3-labeled malate, and M3-labeled aspartate (Figure 2A, 2B, Supplementary Figure 1D). This labeling pattern of TCA cycle intermediates from U-$^{13}C_5$-glutamine metabolism suggests a MYC-dependent increase in reductive carboxylation upon adenovirus infection(Metallo et al., 2011).

To determine whether transcription of enzymes involved in reductive carboxylation is increased upon adenovirus infection, we performed real-time quantitative PCR on several enzymes that have been shown to mediate reductive glutamine metabolism(Gameiro et al., 2013a; Metallo et al., 2011; Mullen et al., 2011). We detect increased transcript levels of isocitrate dehydrogenases 1 and 2 (*IDH1 and IDH2*), nicotinamide nucleotide transhydrogenase (*NNT*), pyruvate dehydrogenase kinase isoenzyme 1 (*PDK1*), and glutamic-oxaloacetic transaminase 2 (*GOT2*) in host cells at eight hours post infection with AD WT, but not in cells infected with AD ORF1 D68A (Supplementary Figure 1E). This data supports a model whereby adenovirus-induced MYC activation increases host cell reductive glutamine metabolism through transcriptional upregulation of enzymes involved in reductive carboxylation during infection (Supplementary Figure 2).

Since glutamine is used by cells to generate non-essential amino acids and import essential and non-essential amino acids, we assessed the impact of adenovirus infection on abundance and labeling patterns of intracellular amino acid pools in NHBE cells labeled with U-$^{13}C_5$-glutamine and infected with AD WT or AD ORF1 D68A. In addition to the previously described increased percentage of intracellular M5-labeled glutamate (Figure 2C and Supplementary Figure 1C), AD WT infection, but not AD ORF1 D68A infection, also causes elevated M5-labeled proline, M3-labeled asparagine, and M3-labeled aspartate (Figure 2C). Notably, AD WT infection also causes increased intracellular levels of essential and non-essential amino acids in NHBE cells more so than AD ORF1 D68A infection, with the exception of asparagine (Figure 2D). The elevated asparagine levels in AD ORF1 D68A-infected cells may reflect differential regulation or use of asparagine versus the other amino acids in adenovirus-infected cells. Consistent with the increased intracellular levels of most amino acids, we found that transcript levels of *ASCT2* and *LAT1*, and protein levels of ASCT2, transporters that utilize glutamine as an exchange factor for amino acid uptake(Nicklin et al., 2009), are significantly elevated in AD WT infected cells, but not AD ORF1 D68A infected cells (Figure 1D and

Supplementary Figure 1A), suggesting MYC-dependent regulation of glutamine exchange for amino acid uptake.

Since glutamine can contribute to the hexosamine biosynthesis pathway through providing a nitrogen atom for conversion of fructose-6-phosphate to glucosamine-6-phosphate, and through providing carbon atoms for conversion of glucosamine-6-phosphate to GlcNAc-6-phosphate through production of acetyl-CoA from citrate, we examined the levels and labeling pattern of hexosamine pathway intermediates in NHBE cells labeled with U-$^{13}C_5$-glutamine and infected with AD WT or AD ORF1 D68A using LC-MS/MS. AD WT infection, but not AD ORF1 D68A infection, causes increased levels of M2-labeled GlcNAc-6P/GlcNAc-1P and M2-labeled UDP-GlcNAc (Figure 2E). AD WT infection also causes increased intracellular pool sizes of hexosamine pathway intermediates (Figure 2F), and increases in transcript levels of hexosamine biosynthesis pathway enzymes including hexokinase 2 (HK2)(Thai et al., 2014), glutamine fructose-6-phosphate amidotransferase 1 (GFAT1), encoded by the *GFPT1* gene, and N-acetylglucosamine kinase (NAGK) significantly more than AD ORF1 D68A infection (Supplementary Figure 3A). These findings suggest MYC-dependent changes in hexosamine biosynthesis during adenovirus infection.

GLS activity promotes optimal adenovirus replication

Because we observed increased glutamine utilization during adenovirus infection, we hypothesized that glutamine consumption may be essential for optimal adenovirus replication. To test this hypothesis, we assessed the impact of exogenous glutamine deprivation on adenovirus replication in primary NHBE cells. As shown in Figure 3A, AD WT replication in the absence of glutamine was reduced 60-fold compared to replication in the presence of 2.5 mM glutamine. Since we observed increased GLS activity in AD WT-infected cells, as judged by increased conversion of $^{13}C_5$-glutamine to $^{13}C_5$-glutamate (Figure 2C), we hypothesized that GLS activity may be important for adenovirus replication. To test this hypothesis, we first diminished GLS activity in adenovirus-infected primary NHBE cells by shRNA-mediated knockdown of GLS

(Figure 3B; Supplementary Figure 5c). GLS knockdown reduces the glutamine consumption rates of mock-infected and AD WT-infected cells (Figure 3B; Supplementary Figure 5c) and reduces AD WT replication 25-fold relative to AD WT replication in cells expressing a scrambled shRNA control (Figure 3C). These data suggest that glutamine consumption and conversion of glutamine to glutamate through GLS activity contribute to optimal adenovirus replication in primary NHBE cells.

Since GLS knockdown decreased adenovirus replication, we hypothesized that pharmacological inhibition of GLS may also limit progeny virion generation. Previous studies in vaccinia virus (VACV), a member of the *Poxviridae* family, showed that treatment of VACV-infected cells with bis-2-(5-phenylacetamido-1,3,4-thiadiazol-2-yl)ethyl sulfide (BPTES), a small-molecule GLS inhibitor, decreased viral yields in a manner similar to cells deprived of glutamine(Fontaine et al., 2014). However, clinical use of BPTES is limited due to moderate potency, poor metabolic stability, and low solubility(Gross et al., 2014). Another small molecule GLS inhibitor, CB-839, is currently undergoing phase I evaluation for treatment of patients with solid tumors and hematological malignancies, and unlike BPTES, is orally bioavailable with low nanomolar potency against both splice isoforms of GLS. CB-839 has previously been shown to decrease proliferation of triple-negative breast cancer cell lines and xenograft models, consistent with stronger reliance of these cells on extracellular glutamine for growth compared to other breast cancer cell lines(Gross et al., 2014). Therefore we tested the impact of CB-839 on glutamine consumption rate and adenovirus replication in NHBE cells. As shown in Figure 3D, treatment of NHBE cells with 1.0 μM CB-839 dramatically reduces cellular glutamine consumption rate and blocks the increased glutamine consumption rate conferred by adenovirus infection. Importantly, CB-839 treatment significantly decreases AD WT replication by 80-fold relative to AD WT replication in DMSO-treated cells (Figure 3E). These data suggest that CB-839 effectively reduces adenovirus replication in primary NHBE cells.

GLS inhibition limits HSV-1 and influenza A replication

Since glutamine is an important nutrient for biosynthesis, and increased glutamine consumption and GLS activity promote optimal adenovirus replication, we hypothesized that glutamine uptake and GLS activity may be important for replication of additional clinically relevant viruses. Herpes simplex virus 1 (HSV-1) is a highly contagious enveloped double-stranded DNA virus that causes recurrent disease worldwide, most commonly leading to oral lesions, or “cold sores”, as well as ocular and neurological manifestations in infected individuals. While the guanosine analogue acyclovir and related compounds constitute first-line treatment against HSV-1 infection, additional combination therapeutics are needed to treat drug-resistant infections and improve efficacy, especially in high-risk patients(James and Prichard, 2014). Influenza A is an enveloped, segmented, single-stranded RNA virus that causes acute respiratory illness and fatality in severe cases. New strains of influenza A can emerge to infect humans, which sometimes cause pandemics. While select antivirals can be used to treat influenza A virus infection, inherent rapid sequence changes during replication exacerbate the problem of drug resistance, necessitating continuous efforts to develop new drugs. Previous studies have characterized the effects of HSV-1(Vastag et al., 2011) and influenza A(Ritter et al., 2010) infection on host cell glucose metabolism, however it remains unknown whether these viruses promote increased host cell glutamine consumption or require increased glutamine utilization for optimal replication. We therefore assessed the effect of HSV-1 and influenza A infection on host cell glutamine consumption and the impact of GLS inhibition on replication of HSV-1 and influenza A in cultured primary cells.

To determine the impact of HSV-1 infection on host cell glutamine consumption, we measured glutamine consumption rate of DMSO-treated human foreskin fibroblasts (HFF) 24 hours after mock-infection or infection with HSV-1 at an MOI of 1. As shown in Figure 4A, HSV-1 infection significantly increases the glutamine consumption rate of HFF cells. Treatment of HFF cells with 1.25 μM CB-839 dramatically reduces the cellular glutamine consumption rate and prevents the HSV-1-induced increase in glutamine consumption (Figure 4A). Importantly, treatment of HFF cells with either 1.25 μM CB-839 or glutamine withdrawal significantly reduces

HSV-1 replication and lowers viral yields relative to DMSO treatment in the presence of 4 mM glutamine (Figure 4B). These results suggest that glutamine consumption and GLS activity are important for optimal HSV-1 replication in human foreskin fibroblasts.

To assess the impact of influenza A infection on host cell glutamine consumption, we measured glutamine consumption rate of DMSO-treated primary NHBE cells 24 hours after mock-infection or infection with influenza A at an MOI of 1. Influenza A infection significantly increases the glutamine consumption rate of NHBE cells relative to mock-infected cells (Figure 4C). Treatment of NHBE cells with 1.0 μM CB-839 effectively reduces the glutamine consumption rate and prevents the influenza A-induced increase in cellular glutamine uptake (Figure 4C). Importantly, similar to results obtained with adenovirus (Figure 3E) and HSV-1 (Figure 4B), treatment of NHBE cells with 1.0 μM CB-839 significantly reduces decreases replication of influenza A virus compared to DMSO treatment. These results show that GLS activity is important for optimal influenza A virus replication in primary NHBE cells, and together suggest that pharmacological inhibition of GLS can reduce replication of diverse viruses.

DISCUSSION

This study demonstrates that MYC-dependent rewiring of host cell glutamine metabolism during adenovirus infection promotes virus replication. These findings are consistent with previous studies showing a critical role for MYC-dependent regulation of glutamine metabolism in growth of cancer cells(Dang et al., 2009; Gao et al., 2009; Wise et al., 2008), activated T lymphocytes(Wang et al., 2011), and recently, during latent infection by Kaposi's Sarcoma-Associated Herpesvirus of host endothelial cells(Sanchez et al., 2015). Our data suggests that adenovirus E4ORF1 activation of MYC reprograms host cell glutamine metabolism through transcriptional suppression of miR-23a, upregulation of the glutamine transporters SLC7A5/ASCT2 and SLC1A5/LAT1, and upregulation of enzymes involved in reductive carboxylation and the hexosamine biosynthesis pathway. The specific contribution of each of these components to the altered glutamine metabolism observed during adenovirus infection and

viral replication requires further investigation. Importantly, we found that MYC-dependent upregulation of glutamine consumption and GLS activity are necessary for optimal adenovirus replication in primary lung epithelial cells, and that GLS activity is required for optimal replication of HSV-1 and influenza A as well. Whether HSV-1, influenza A, or other viruses also rely on MYC activation to promote reprogramming of glutamine metabolism during infection remains to be determined.

Although previous studies have reported a critical role for increased glutamine consumption and the anaplerotic use of glutamine in host cells infected by HCMV or VACV(Chambers et al., 2010; Fontaine et al., 2014), our results tracing the fate of glutamine carbons during adenovirus infection and using a MYC activation-deficient mutant virus have implicated the MYC-directed use of glutamine in additional metabolic pathways, some of which have not been previously characterized in virus-infected cells and are not canonically known to be regulated by MYC. For instance, we detected a MYC activation-dependent increase in reductive glutamine carboxylation in adenovirus-¬infected cells (Figure 2B and Supplementary Figure 2). Consistently, we found MYC activation-dependent upregulation of enzymes involved in reductive carboxylation, including isocitrate dehydrogenase 1 (IDH1), isocitrate dehydrogenase 2 (IDH2), nicotinamide nucleotide transhydrogenase (NNT), and pyruvate dehydrogenase kinase 1 (PDK1) in adenovirus-infected cells (Supplementary Figure 1E and 2). In cancer cells, reductive glutamine metabolism is thought to support growth through providing a source of citrate used for macromolecule synthesis, including for acetyl-CoA production for lipid synthesis in the context of hypoxia(Metallo et al., 2011; Wise et al., 2011) or mitochondrial dysfunction(Mullen et al., 2011). The precise functional significance and potential advantages for adenovirus replication provided by enhanced reductive glutamine metabolism remains to be determined. Additionally, while HIF has been implicated in regulating reductive glutamine carboxylation in hypoxic cancer cells(Gameiro et al., 2013b), our findings are consistent with E4ORF1-induced MYC activation enhancing reductive glutamine carboxylation during adenovirus infection. Whether MYC directly or indirectly modulates reductive carboxylation in other pathophysiological contexts merits further

investigation. Additionally, since adenovirus infection decreases host cell respiration(Thai et al., 2014), it will be interesting to determine whether decreased oxygen consumption is linked to the increased reductive carboxylation observed during adenovirus infection.

Another metabolic pathway found to be altered in a MYC activation-dependent manner during adenovirus infection is the hexosamine biosynthesis pathway (Figure 2E, 2F, and Supplementary Figure 3). The hexosamine biosynthesis pathway plays a key role in N-linked glycosylation of growth factor receptors to promote their cell surface localization and permit initiation of cell signaling pathways downstream of growth factors(Hensley et al., 2013; Lau et al., 2007; Wellen et al., 2010). Additionally, UDP-GlcNAc generated by the hexosamine biosynthesis pathway is used as the sugar nucleotide donor for O-GlcNAc modification of proteins, a highly abundant post-translational modification with emerging roles in regulation of cell signaling and metabolism(Bond and Hanover, 2015). For instance, O-GlcNAc modification of the glycolytic enzyme, phosphofructokinase 1, increases enzymatic activity, yielding increased glucose flux through the pentose phosphate pathway in cancer cells(Yi et al., 2012), and could contribute to the increased glycolytic flux observed in adenovirus-infected cells(Thai et al., 2014). Consistent with the increased levels and glutamine carbon labeling of hexosamine biosynthesis pathway intermediates detected in adenovirus-infected cells (Figure 2E and 2F), we found that adenovirus infection leads to a MYC-dependent increase in transcript levels of enzymes in the hexosamine biosynthesis pathway, GFAT1 and NAGK (Supplementary Figure 3). Interestingly, Hepatitis B virus infection also promotes elevated GFAT1 expression and increased hexosamine biosynthesis in hepatoma cells, and GFAT1 inhibition reduces HBV replication(Li et al., 2015). Whether and how GFAT activity and hexosamine biosynthesis contribute to adenovirus replication remains unknown, but our findings support future studies examining potential adenovirus-induced alterations in cellular N-linked glycosylation patterns and/or O-GlcNAc protein modifications.

In addition to changes in reductive carboxylation and hexosamine biosynthesis, we also detect MYC-dependent changes in amino acid metabolism in adenovirus-infected cells. We found increased conversion of glutamine to aspartate, asparagine, and proline post adenovirus infection

(Figure 2C and Supplementary Figure 2). The increased labeling of aspartate and asparagine from U-^{13}C-Gln in AD WT-infected cells is likely due to MYC-dependent routing of glutamine through reductive carboxylation and stimulation of asparagine synthetase activity. The increased labeling of proline from glutamine suggests MYC-induced stimulation of the proline biosynthesis pathway during adenovirus infection. Consistently, in cancer cells MYC promotes enhanced proline biosynthesis from glutamine in part by transcriptional upregulation of pyrroline-5-carboxylate synthase and pyrroline-5-carboxylate reductase 1(Liu et al., 2012), and pyrroline-5-carboxylate reductase 1 has been found to be important for optimal growth of breast cancer cell lines(Possemato et al., 2011). In activated T cells, MYC promotes increased proline biosynthesis from glutamine to support production of polyamines(Wang et al., 2011). Preliminary results suggest increased mRNA expression of proline dehydrogenase (PRODH), an enzyme involved in proline conversion to ornithine, and ornithine decarboxylase (ODC), the rate-limiting enzyme of polyamine synthesis in AD WT- versus mock-infected cells (Supplementary Figure 4). Whether the levels of proline biosynthesis and/or polyamine biosynthesis enzymes are altered in a MYC-dependent manner in adenovirus-infected cells remains to be tested. Interestingly, we also detected a MYC-dependent increase in intracellular amino acid pool sizes along with a MYC-dependent increase in LAT1 and ASCT2 transcript levels during adenovirus infection, consistent with MYC-dependent regulation of use of glutamine for amino acid uptake(Nicklin et al., 2009). The specific contribution of each of these metabolic events to anabolic metabolism during adenovirus infection and viral replication is yet unknown.

Our study shows that CB-839 treatment reduces viral replication of adenovirus, HSV-1, and influenza A in cultured primary cells. This observation highlights the importance of GLS activity in the *in vitro* propagation of a diverse set of viruses and reveals that, in principle, inhibition of glutamine metabolism could be exploited therapeutically to decrease viral replication. While disease caused by adenovirus infection is usually self-limiting and less pathogenic than infection by other viruses, cases of severe adenovirus infections have been rising over the past several decades, specifically in immunocompromised hosts (Lenaerts et al.,

2008). Limited anti-adenoviral agents are currently available that are efficacious with minimal toxicity. Our proof-of-principle results demonstrate that CB-839-mediated inhibition of GLS activity could potentially be useful to combat adenovirus infection as well as infection by other pathogenic viruses that rely on GLS activity for viral propagation. For HSV-1 and influenza A infections, where antiviral medications are currently available, GLS inhibition by CB-839 may be useful in combination with current standard of care, particularly in resistant cases. However, further studies are needed to determine whether CB-839 can beneficially limit replication of adenovirus, HSV-1 or influenza A *in vivo*. Nonetheless, our results demonstrate the interface between viral and cancer metabolism in upregulation of common metabolic pathways supporting increased proliferation of virions and daughter cells, respectively. Our results suggest that not only can viruses be used to reveal critical targets for cancer metabolism, but that drugs in development to target cancer metabolism may also be useful as antivirals.

METHODS

Cell protein extract preparation and immunoblot assays

MCF10A cells were obtained from American Type Culture Collection (ATCC) and the laboratory of Dr. Frank McCormick (UCSF) and cultured in Dulbecco's modified Eagle's medium and F12 (DMEM:F12) containing 5% Horse Serum, 50U mL^{-1} Penicillin-Streptomycin, 10 µg mL^{-1} insulin, 0.5 µg mL^{-1} hydrocortisone, 20 ng ml^{-1} EGF, 10 µg mL^{-1} cholera toxin. NBHE cells were obtained from Lonza and cultured in BEGM BulletKit (Lonza). Cells were lysed in either M-PER Mammalian Protein Extraction Reagent (Thermo) with 4 µg mL^{-1} aprotinin, 4 µg mL^{-1} leupeptin, 4 µg mL^{-1} pepstatin, 1mM PMSF, 1mM Na_3VO_4, and 5mM NaF or NP40 buffer containing 50 mM Tris pH 7.5, 1 mM EDTA, 150 mM NaCl, 1% Nonidet P-40, 4 µg ml^{-1} aprotinin, 4 µg ml^{-1} leupeptin , 4 µg ml^{-1} pepstatin, 1 mM PMSF, 1 mM Na_3VO_4, and 5 mM NaF. Nuclear and cytoplasmic fractions were prepared using NE-PER extraction reagents (Thermo). Western blot analysis was carried out according to standard methods. Protein concentrations of cell extracts were determined by the Bradford assay. The following commercial antibodies were used as probes: FLAG (Abcam;

1:1000), GLS (Abcam, AB156876; 1:1000 for Fig. 1D; Abcam, AB60709; 1:1000 for Fig. 3B), ASCT2 (Cell Signaling, 1:1000), MYC (Cell Signaling; 1:1000), β-Tubulin (Sigma; 1:5000).

Viruses

H5wt300 (AD5 WT) was kindly provided by the laboratory of Dr. Frank McCormick. AD D68A was derived by subcloning the E4 region into pBluescript (SpeI-BamHI fragment), then performing site-directed mutagenesis, and subsequently recloning back into pAd5. The mutant viruses were propagated on the W162 cell line, which contain and express the E4 region. Infection times of host cells are indicated in the figures at 37°C with 10 PFU/cell.

Measurement of glutamine consumption rates

Cellular glutamine consumption rates were measured using a Nova Biomedical Bioprofile Basic Analyzer. Briefly, cells were seeded in 10 cm plates at 70% confluency to ensure the measurements would be taken when the cells were subconfluent. 24 hours post seeding, the media was refreshed for all cells, and media was added to 10cm plate with no cells as a blank control. After 24 hr incubation, 1 ml of media was removed from each sample and the blank control, and media samples were analyzed in the Nova Bioprofile analyzer. Cell number was determined using a Coulter particle analyzer.

Metabolite extraction and metabolomics analysis

Cells were incubated in medium containing 2.5 mM U-$^{13}C_5$-glutamine for 24 h. The following day, NHBE cells were rinsed with cold 150 mM ammonium acetate (NH_4AcO). Cells were carefully scraped off in 800 µL of 50% ice cold methanol. An internal standard of 10 nmol norvaline was added to the cell suspension, followed by 400 µL of cold chloroform. The aqueous layer was transferred to a glass vial and the metabolites dried under vacuum. Metabolites were resuspended in 50 µL 70% ACN and 5 µL of this solution used for the mass spectrometer-based analysis. The analysis was performed on a Q Exactive (Thermo Scientific) coupled to an UltiMate

3000RSLC (Thermo Scientific) UHPLC system. Mobile phase A was 5 mM NH4AcO, pH 9.9, B) was ACN, and the separation achieved on a Luna 3u NH2 100A (150 x 2.0 mm) (Phenomenex) column. The flow was kept at 200 µL min^{-1}, and the gradient was from 15% A to 95% A in 18 min, followed by an isocratic step for 9 min and re-equilibration for 7 min. Metabolites we detected and quantified as area under the curve (AUC) based on retention time and accurate mass (≤ 3ppm) using the TraceFinder 3.1 (Thermo Scientific) software. Relative amounts of metabolites between various conditions, as well as percentage of labeling were calculated and depicted in bar graphs.

Quantitative real-time PCR

RNA was purified with Qiagen RNeasy Kit. 1 µg of total RNA was used to synthesize cDNA using the iScript cDNA Synthesis Kit (Bio-Rad) as per manufacturer's instructions. Quantitative PCR (qPCR) was conducted on the Roche LightCycler 480 using SYBR Green I Master Mix (Roche) and 0.5 µmol L^{-1} primers. Relative expression values are normalized to control gene (RPL32 or RPLP0) and expressed in terms of linear relative mRNA values. The following primer sequences were used:

5'-AGAATGTACTTGCCAAGGCG-3' and 5'-CACCATGGTTCTGGTCTCCT-3' for *Asct2*,

5'-GGCCTTCATCGCAGTACATC-3' and 5'-ACGCTGTAGCAGTTCACGG-3' for *Lat1*,

5'-CTTTTGGGTTCCGTCACTTG-3' and 5'-GTCGTCATGCTTATGGGGAT-3' for *Idh1*,

5'-TGAACTGCCAGATAATACGGG-3' and 5'-CTGACAGCCCCCACCTC-3' for *Idh2*,

5'-CACATTAAGCTGACCAGGCA-3' and 5'-AGCTCAATACCCCATTGCTG-3' for *Nnt*,

5'-GGAGGTCTCAACACGAGGTC-3' and 5'-CGCTGGGTAATGAGGATTTG-3' for *Pdk1*,

5'-AGGGGAGGGTTGGAATACAT-3' and 5'-AATGTTTGCCTCTGCCAATC-3' for *Got2*,

5'-TCGTCTCGTTCGAGGAACAT-3' and 5'-CACCGAAGCTCGTGTGTG-3' for *Gfpt1*, and

5'-AGGGGTGGATCCTCTGGTA-3' and 5'-GGCATCGGTGGTGATTAAGT-3' for *Nagk*.

Adenovirus assays

In glutamine withdrawal samples, NHBE cells were plated at subconfluency and media was switched to DMEM/F12 media with or without glutamine/pyruvate 24 hours prior to adenovirus infection. In drug treatment samples, cells were pre-treated with 1.0 μM CB-839 (obtained from Calithera Biosciences, Inc.) or DMSO for 3 hours prior to adenovirus infection. Cells were infected with adenovirus at a multiplicity of infection (MOI) of 1 for 72 hours. Cells from the entire plate were harvested by pipetting up and down, collected in a conical tube, and spun down at 3,000 rpm for 10 minutes. The pellet was resuspended with 100 μL 10 mM Tris pH 7.4. Cells were lysed by freezing, thawing, and vortexing vigorously. Supernatant was saved as virus stocks for virus titration assays. Infectious virus titer was measured using the 50% Tissue Culture Infective Dose (TCID50). This endpoint dilution assay quantifies the amount of virus required to produce a cytopathic effect (CPE) in 50% of inoculated tissue culture cells. In 96 well plates, HeLa cells were plated at 2,500 cells well^{-1} and subsequently infected with 10-fold dilutions of virus stocks. Dilutions of virus stocks were added to cells in replicates of 10, and CPE was manually observed and recorded for each virus dilution 5 days post infection. Results were used to mathematically calculate a TCID50 result.

Herpes simplex 1 assays

HSV-1 strain 17+ stock was generated by infecting Vero cells at an MOI of 0.05 PFU cell^{-1}. Human foreskin fibroblast cells (HFF) and Vero cells were cultured in complete Dulbecco modification of Eagle medium (DMEM) containing 10% fetal bovine serum, supplemented with penicillin and streptomycin. HFF cells were pre-treated with 1.25 μM CB-839 for 3 hours, and then infected with HSV-1 virus at an MOI of 0.01 with or without the presence of 1.25 μM CB¬839 or, in the case for glutamine withdrawal, DMEM media without L-glutamine and without pyruvate. Supernatant containing the virus was harvested 72 hours post-infection and titered by plaque assay. Plaque assay was performed in monolayers of Vero cells overlaid with 1% methylcellulose.

Influenza A assays

NHBE cells were plated at subconfluency. Cells were pre-treated with 1.0 μM CB-839 for 3 hours or DMSO control, and then infected with influenza virus (H1N1/WSN/33) at an MOI of 1 with or without the presence of 1.0 μM CB-839. Supernatant containing the virus was collected 24 hours post infection and TCID50 were assayed with A549 cells.

Micro RNA analysis

Micro RNAs were quantified using the qScript microRNA cDNA synthesis kit (Quanta Biosciences). Briefly, enriched miRNA was prepared from 100 mm plates of subconfluent NHBE cells mock infected, or infected with Ad WT or Ad D68A at the indicated times using Qiagen miRNeasy Mini Kit (Qiagen). miRNAs were first polyadenylated in a poly(A) polymerase reaction, and then reverse transcribed into cDNA with oligo-dT adapter primers using the first-strand cDNA synthesis reaction mixture. Real-time SYBR Green qRT-PCR was performed using 200 nM of each PerfeCTA microRNA Assay primer (hsa-miR23a-3p and hsa¬miR23b-3p) and PerfeCTA Universal Primer. Quantitative PCR (qPCR) was conducted on the Roche LightCycler 480. Relative values were normalized against the small nucleolar RNA SNORD43, and values were compared against mock-infected samples.

Statistical analysis

All data are presented as +/-standard deviation. As noted in figure legends, data were analyzed by two-sample equal variance Student's *t*-test with two-tailed analysis.

ACKNOWLEDGEMENTS

We would like to thank Susan Demo and Frank Parlati from Calithera Biosciences, Inc. for helpful discussions and comments on the manuscript. We thank Carolina Espindola for technical assistance. We thank Milica Momcilovic and David B. Shackelford for their technical assistance and feedback in addressing reviewers' concerns. S.K.T. is a pre-doctoral fellow supported by the UCLA Tumor Immunology Training Grant (USHHS Ruth L. Kirschstein Institutional National

Research Service Award # T32 CA009056) and is funded by an NIH NIGMS training grant, GM08042, and the Medical Scientist Training Program. H.R.C. is funded by an NIH Director's New Innovator Award (DP2 OD008454-01).

AUTHOR CONTRIBUTIONS

Min Thai, Shivani K. Thaker, and Heather R. Christofk designed the studies and wrote the paper. Min Thai and Shivani K. Thaker performed the experiments. Jun Feng and Yushen Du performed HSV-1 and Influenza A experiments with Ting Ting Wu's guidance. Daniel Braas performed LC-MS and data analysis on metabolite samples in conjunction with Thomas G. Graeber. Hailiang Hu advised on miRNA experiments.

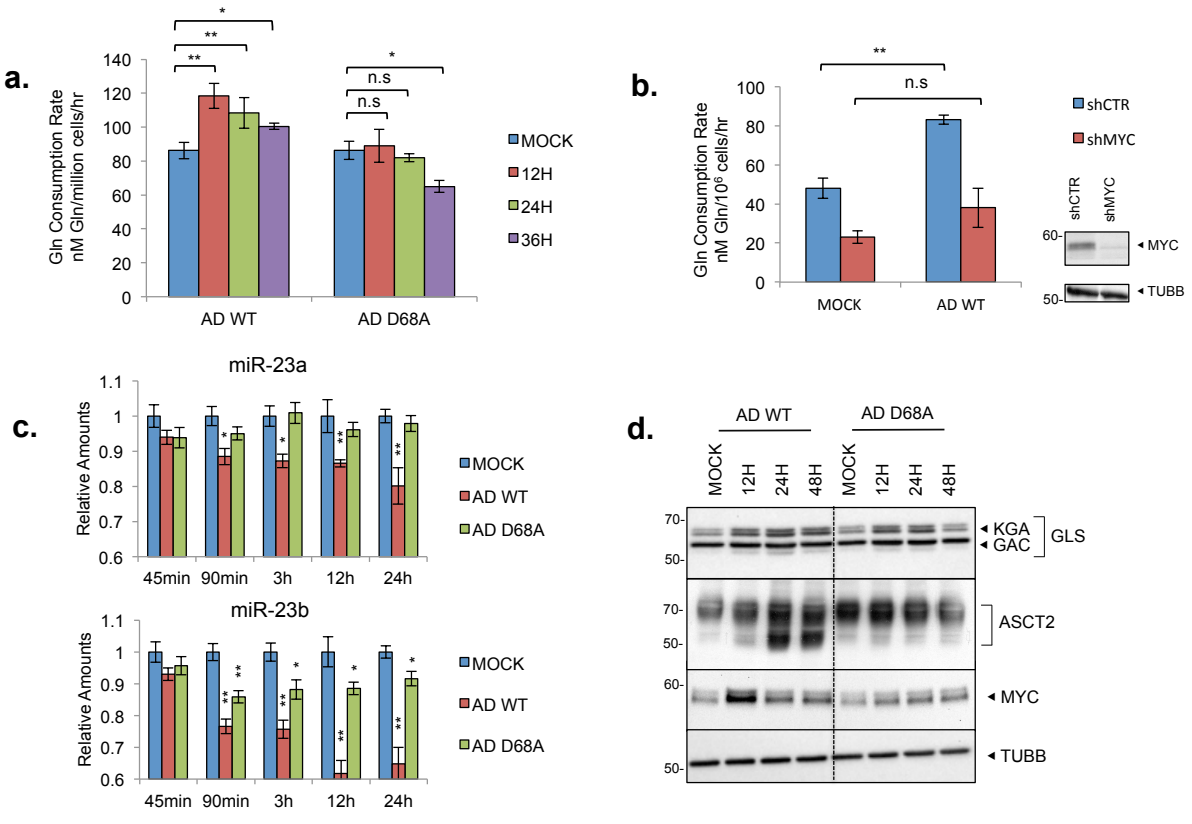

Figure 1. MYC regulates glutamine consumption during adenovirus infection. (**a**) NHBE (normal human bronchial epithelial) cells were either mock infected, infected with AD WT (wild-type strain of adenovirus 5), or infected with AD ORF1 D68A, and cellular glutamine consumption rates were measured at the indicated time points. (**b**) left, Glutamine consumption rates of NHBE cells stably expressing scrambled shRNA (shCTR, blue bars) or MYC shRNA (shMYC, red bars) 24 hours post mock infection or infection with AD WT (left). Right, Immunoblotting depicting MYC levels in NHBE cells stably expressing scrambled shRNA (shCTR) or MYC shRNA (shMYC). Tubulin antibody (TUBB) was used to control for loading. (**c**) Relative miR-23a and mir-23b levels in NHBE cells mock infected, infected with AD WT, or infected with AD ORF1 D68A at the indicated time points post infection. (**d**) Immunoblotting of lysates from NHBE cells infected with AD WT or AD ORF1 D68A at the indicated times post infection. Whole cell lysates were probed with antibodies towards GLS (glutaminase) and ASCT2 (sodium-dependent neutral amino acid transporter type 2) . KGA is the full length GLS and GAC is the shortened splice variant[29]. Nuclear

lysates were probed with an antibody towards MYC. Tubulin antibody (TUBB) was used to control for loading in the whole cell lysates. For (**a**)-(**c**), error bars denote standard deviation ($n = 3$), *$p < 0.05$; **$p < 0.01$. Student's *t*-test.

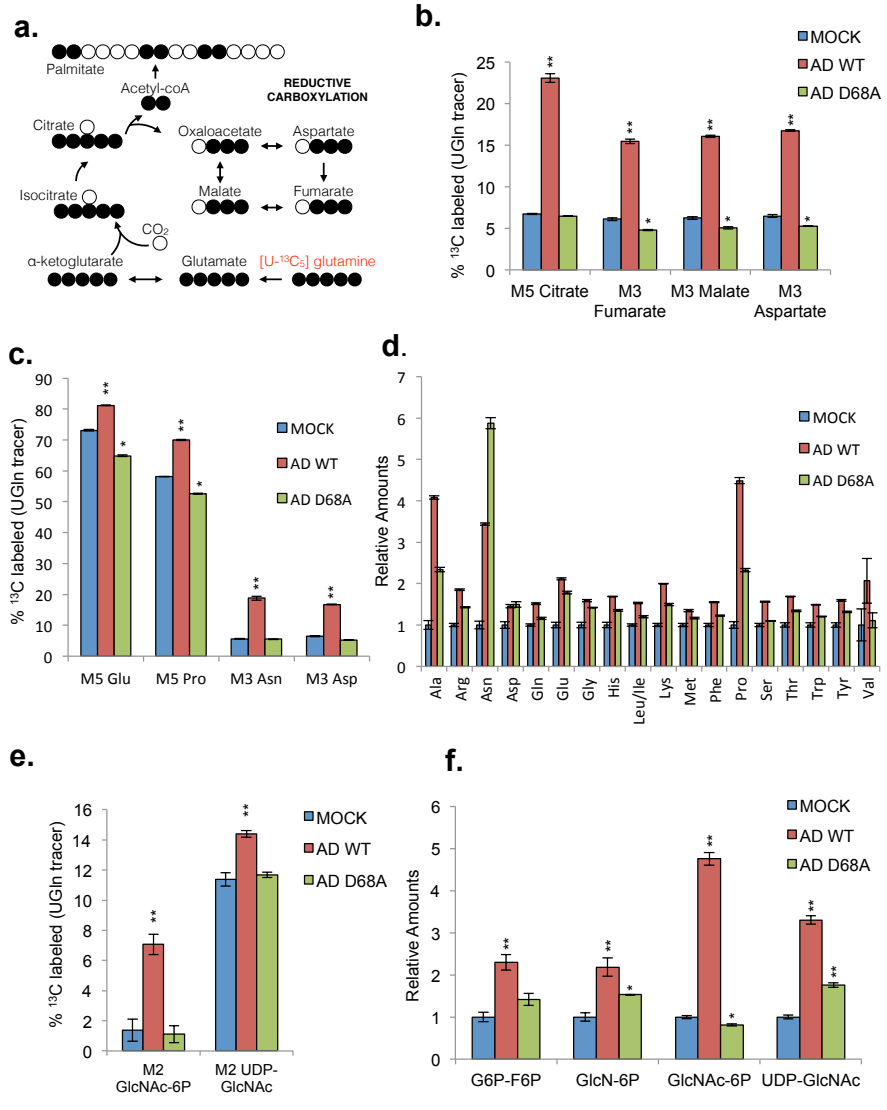

Figure 2. Adenovirus infection alters host cell glutamine utilization in a MYC activation-dependent manner. NHBE cells were labeled with U-^{13}C-glutamine and mock infected or infected with AD WT or AD ORF1 D68A at an MOI of 1. 24 hours post infection, intracellular metabolites were extracted and analyzed by LC-MS/MS. (**a**) Schematic tracing the fate of ^{13}C atoms from U-$^{13}C_5$-glutamine in reductive carboxylation. (**b**) Percentage of ^{13}C-labeled isotopomers of intermediates in reductive carboxylation. (**c**) Percentage of ^{13}C-labeled isotopomers of amino acids. (**d**) Relative levels of non-essential and essential amino acids. (**e**) Percentage of ^{13}C-labeled M2 isotopomers of intermediates in the hexosamine biosynthesis

pathway. (**f**) Relative levels of hexosamine biosynthesis pathway intermediates. For (**b**)-(**f**), error bars denote standard deviation (n = 3), *p < 0.05; **p < 0.01. Student's t-test.

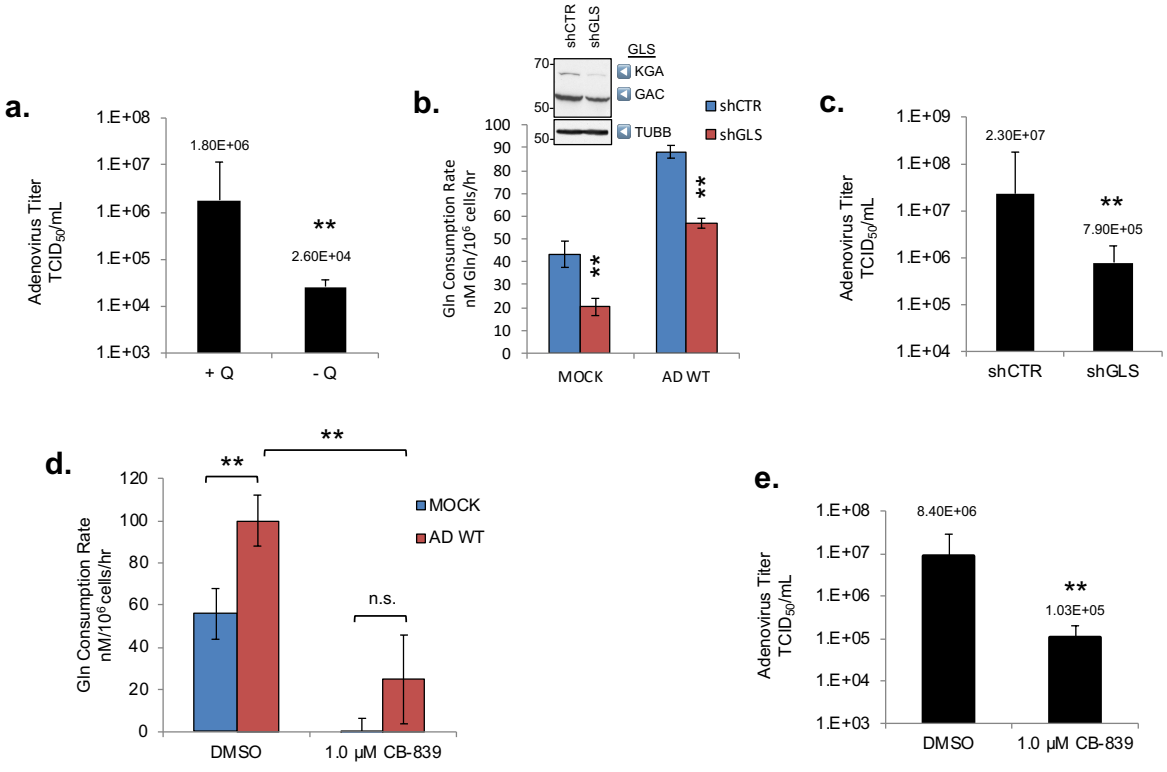

Figure 3. Glutamine consumption and GLS activity are important for optimal adenovirus replication. (**a**) NHBE cells were infected with AD WT at an MOI of 1 in the presence (+ Q) or absence (-Q) of 2.5 mM glutamine. At 24 hours post infection, progeny virus was harvested and infectious virus titer was measured using a TCID50 endpoint dilution plaque assay. (**b**) bottom, Glutamine consumption rates of NHBE cells stably expressing scrambled shRNA (shCTR, blue bars) or GLS shRNA (shGLS, red bars) 24 hours post mock infection or infection with AD WT (bottom). top, Immunoblotting depicting levels of GLS splice isoforms KGA and GAC in NHBE cells stably expressing scrambled shRNA (shCTR) or GLS shRNA (shGLS). (**c**) Progeny virus was collected from NHBE cells stably expressing shCTRL or shGLS 24 hours post infection with AD WT, and adenovirus titers were determined as in (**a**). (**d**) NHBE cells were treated with 1.0 μM CB-839 or DMSO, and either mock-infected or infected with AD WT. Glutamine consumption rates were measured 24 hours post treatment and infection. (**e**) Progeny virus was harvested from NHBE cells treated with DMSO or 1.0 μM CB-839 24 hours post infection with AD WT, and

adenovirus titers were determined as described in (a). For (**a**)-(**e**), error bars denote standard deviation (n = 3), **p < 0.01. Student's t-test.

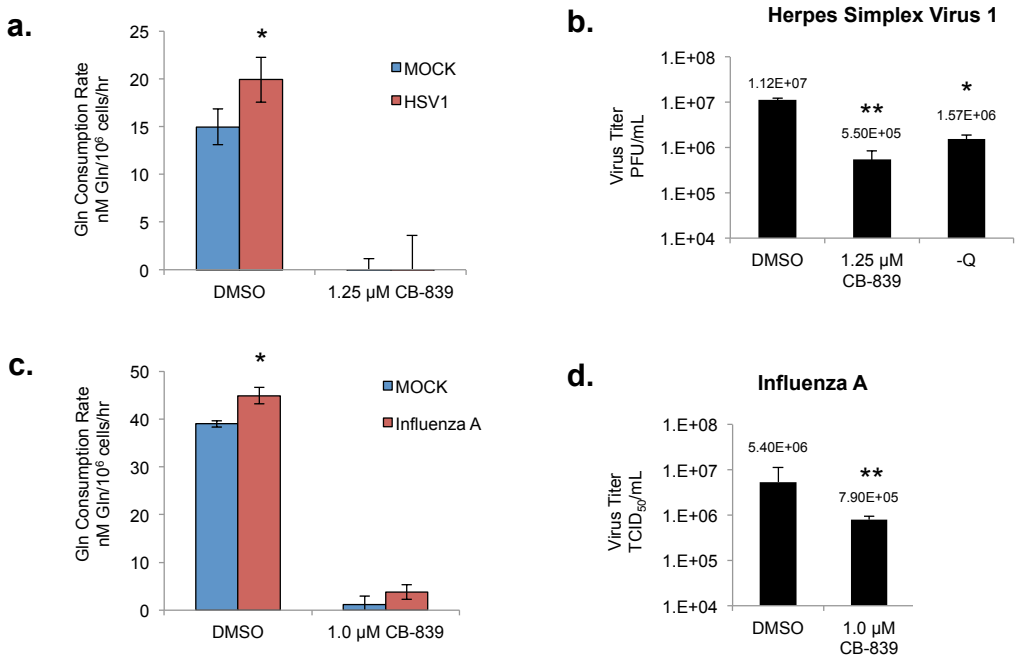

Figure 4. Glutaminase inhibition limits HSV-1 and influenza A replication. (**a**) Glutamine consumption rates of primary human foreskin fibroblasts (HFF) mock infected or infected with HSV-1 (herpes simplex virus 1) at an MOI of 1 for 24 hours in the presence of DMSO or 1.25 μM CB-839. (**b**) Infectious viral titer (measured by plaque assay) of supernatant from HFF cells infected with HSV-1 at an MOI of 0.01 for 72 hours in the presence of DMSO, 1.25 μM CB¬839, or in the absence of exogenous glutamine (-Q). (**c**) Glutamine consumption rates of NHBE cells mock infected or infected with influenza A virus at an MOI of 1 for 24 hours in the presence of DMSO or 1.0 μM CB-839. (**d**) Infectious viral titer (measured using a TCID50 endpoint dilution assay) of the supernatant from NHBE cells infected with influenza A at an MOI of 1 for 24 hours in the presence of DMSO or 1.0 μM CB-839. For (**a**)-(**d**), error bars denote standard deviation (*n* = 3), *p < 0.05; **p < 0.01. Student's *t*-test.

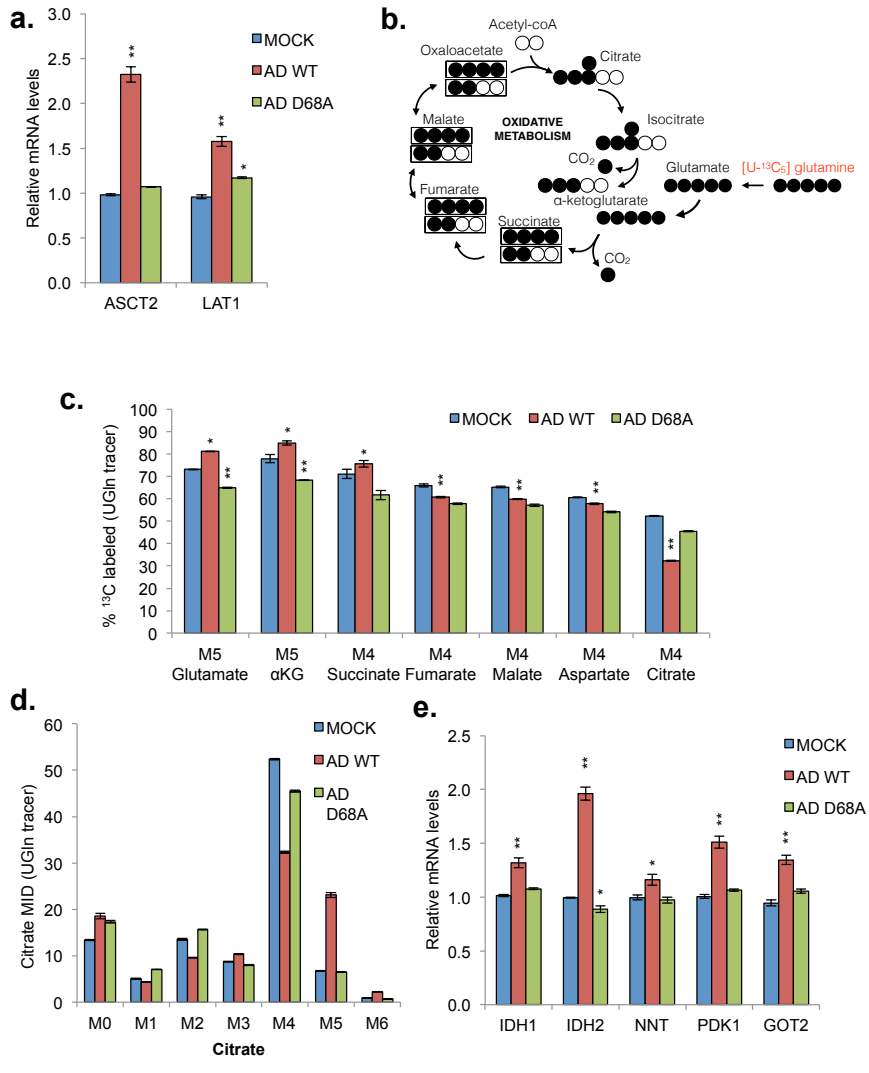

Supplementary Figure 1. (**a**) qRT-PCR was performed on RNA collected from MCF10A cells 8 hours post infection with AD WT or AD ORF1 D68A virus. Relative levels of ASCT2 and LAT1 are shown. For (b)-(e), NHBE cells were labeled with U-^{13}C-glutamine (UGln tracer) and mock infected or infected with AD WT or AD ORF1 D68A at an MOI of 1. 24 hours post infection, intracellular metabolites were extracted and analyzed by LC-MS/MS. (**b**) Schematic tracing the fate of ^{13}C atoms from U-$^{13}C_5$-glutamine in oxidative metabolism in the TCA cycle. (**c**) Percentage of ^{13}C-labeled isotopomers of intermediates in oxidative TCA cycle metabolism. (**d**) Citrate mass isotopomer distribution (MID) resulting from U-^{13}C-glutamine labeling. (**e**) qRT-PCR was performed as described in (**a**), and relative levels of transcripts involved in reductive carboxylation are shown.

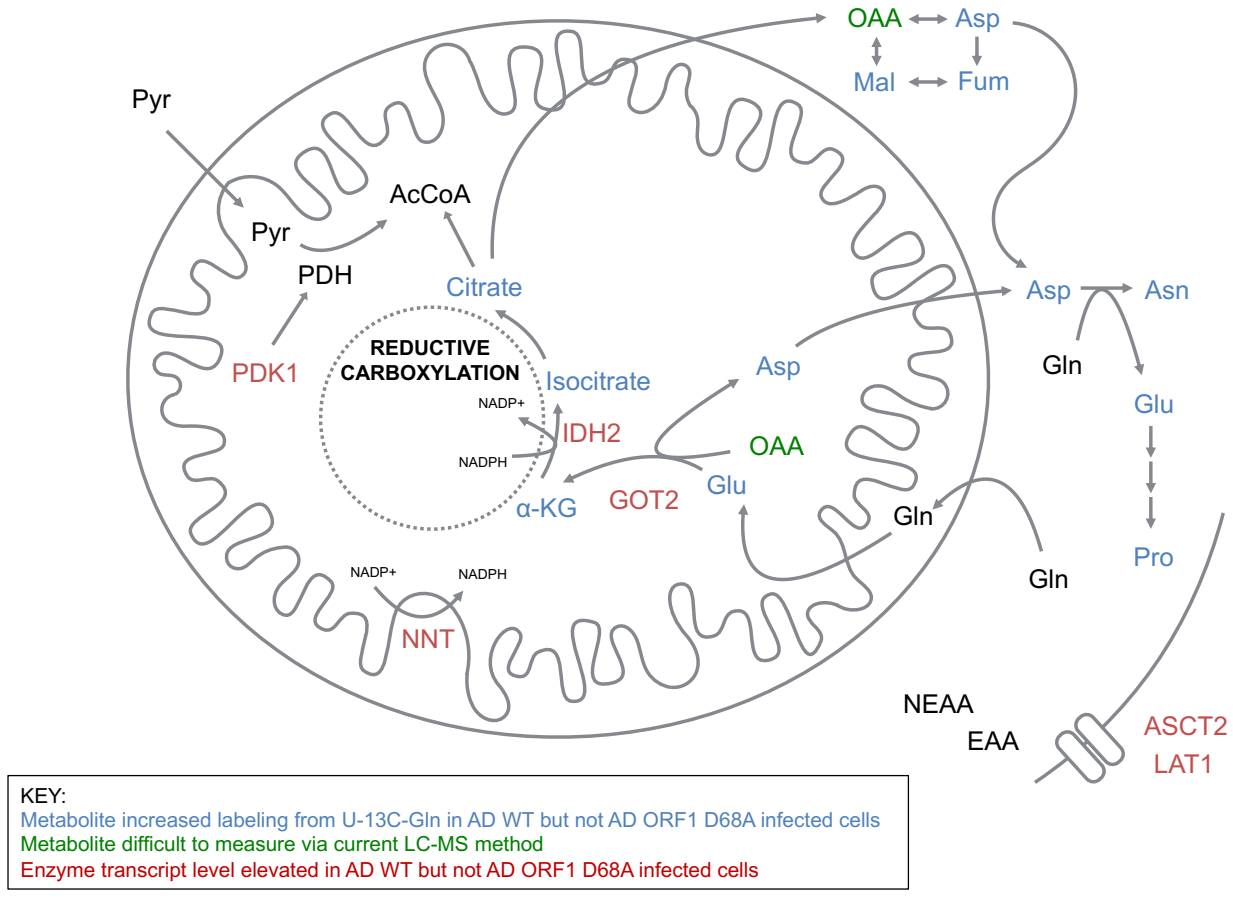

Supplementary Figure 2. Schematic of reductive glutamine carboxylation and glutamine-associated amino acid metabolism events summarizing the MYC-dependent changes observed in adenovirus-infected cells.

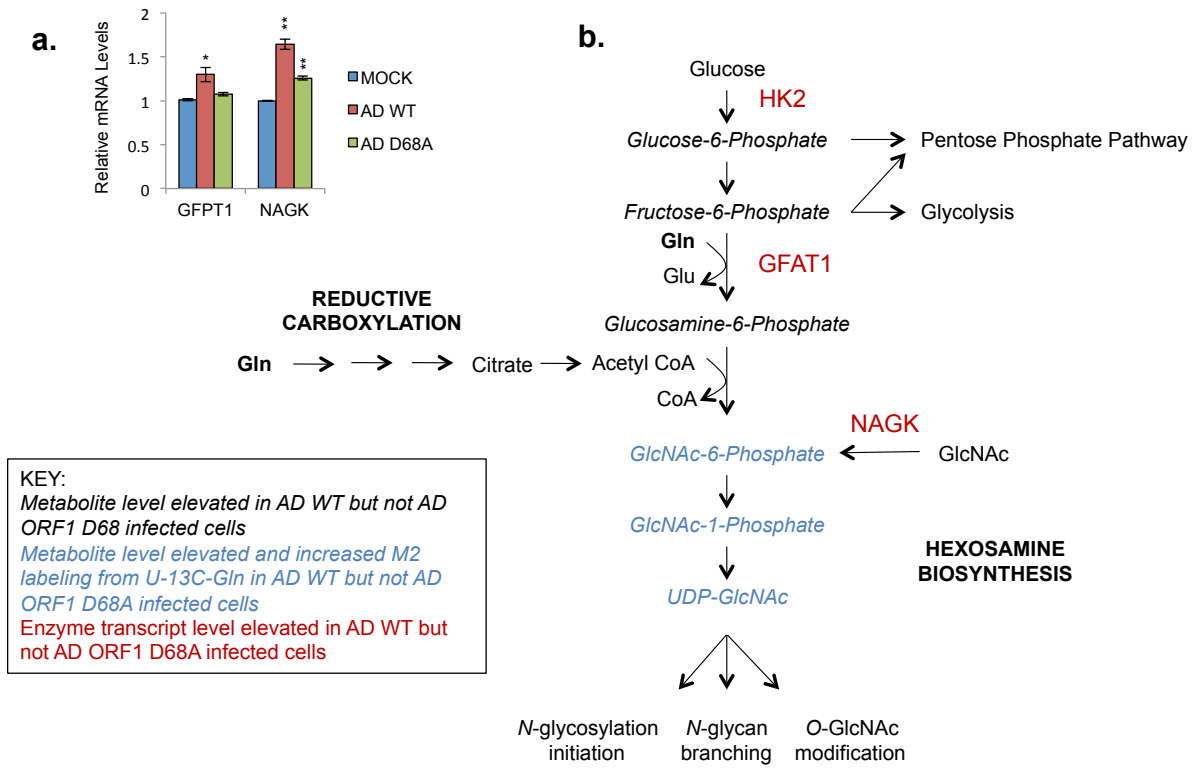

Supplementary Figure 3. (**a**) qRT-PCR was performed on RNA collected from MCF10A cells 8 hours post infection with AD WT or AD ORF1 D68A virus. Relative levels of GFPT1 (glutamine fructose-6-phosphate amidotransferase 1) and NAGK (N-acetylglucosamine kinase) are shown. (**b**) Schematic of the hexosamine biosynthesis pathway summarizing the MYC-dependent changes observed in adenovirus-infected cells.

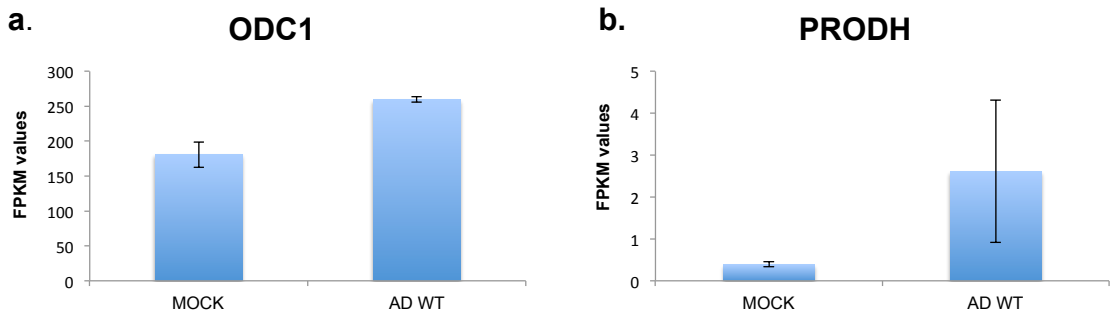

Supplementary Figure 4. Preliminary RNA-sequencing data comparing uninfected NHBE cells (MOCK) versus cells infected for 8 hours with AD WT (AD WT). The fragments per kilobase of transcript per million mapped (FPKM) values indicate that RNA levels of (**a**) ornithine decarboxylase (ODC1) and (**b**) proline dehydrogenase (PRODH) are increased at 8 hours post-AD WT infection.

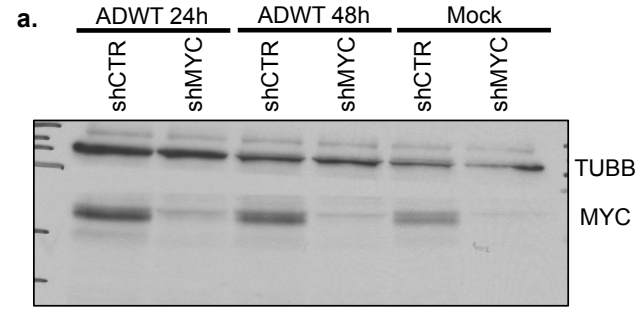

Figure 1b

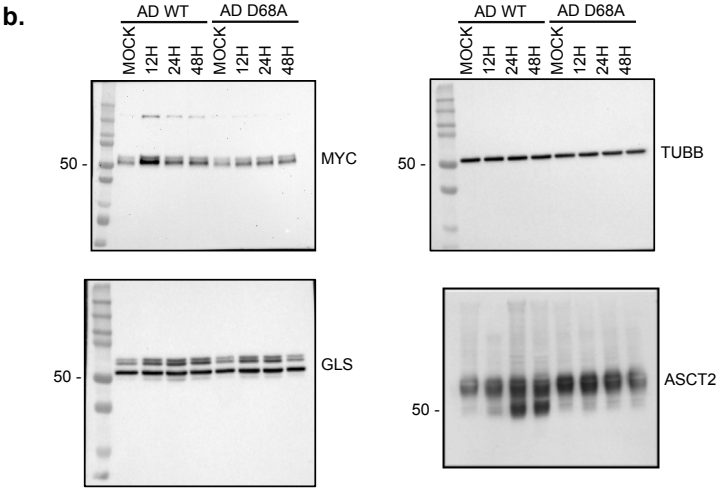

Figure 1d

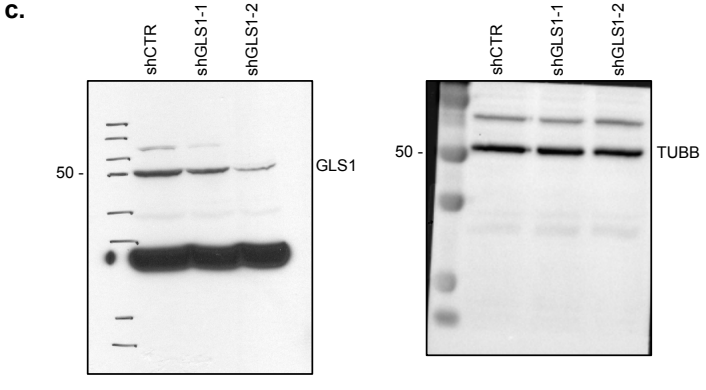

Figure 3b

Supplementary Figure 5. Uncropped Western Blot images presented in this manuscript. Figure labeling corresponds to the figure in the main manuscript.

REFERENCES

Bond, M.R., and Hanover, J.A. (2015). A little sugar goes a long way: the cell biology of O-GlcNAc. J Cell Biol *208*, 869-880.

Chambers, J.W., Maguire, T.G., and Alwine, J.C. (2010). Glutamine metabolism is essential for human cytomegalovirus infection. Journal of virology *84*, 1867-1873.

Dang, C.V., Le, A., and Gao, P. (2009). MYC-induced cancer cell energy metabolism and therapeutic opportunities. Clin Cancer Res *15*, 6479-6483.

DeBerardinis, R.J., Mancuso, A., Daikhin, E., Nissim, I., Yudkoff, M., Wehrli, S., and Thompson, C.B. (2007). Beyond aerobic glycolysis: transformed cells can engage in glutamine metabolism that exceeds the requirement for protein and nucleotide synthesis. Proc Natl Acad Sci U S A *104*, 19345-19350.

Fontaine, K.A., Camarda, R., and Lagunoff, M. (2014). Vaccinia virus requires glutamine but not glucose for efficient replication. Journal of virology *88*, 4366-4374.

Gameiro, P.A., Laviolette, L.A., Kelleher, J.K., Iliopoulos, O., and Stephanopoulos, G. (2013a). Cofactor balance by nicotinamide nucleotide transhydrogenase (NNT) coordinates reductive carboxylation and glucose catabolism in the tricarboxylic acid (TCA) cycle. J Biol Chem *288*, 12967-12977.

Gameiro, P.A., Yang, J., Metelo, A.M., Perez-Carro, R., Baker, R., Wang, Z., Arreola, A., Rathmell, W.K., Olumi, A., Lopez-Larrubia, P., et al. (2013b). In vivo HIF-mediated reductive carboxylation is regulated by citrate levels and sensitizes VHL-deficient cells to glutamine deprivation. Cell Metab *17*, 372-385.

Gao, P., Tchernyshyov, I., Chang, T.C., Lee, Y.S., Kita, K., Ochi, T., Zeller, K.I., De Marzo, A.M., Van Eyk, J.E., Mendell, J.T., et al. (2009). c-Myc suppression of miR-23a/b enhances mitochondrial glutaminase expression and glutamine metabolism. Nature *458*, 762-765.

Gross, M.I., Demo, S.D., Dennison, J.B., Chen, L., Chernov-Rogan, T., Goyal, B., Janes, J.R., Laidig, G.J., Lewis, E.R., Li, J., et al. (2014). Antitumor activity of the glutaminase inhibitor CB-839 in triple-negative breast cancer. Molecular cancer therapeutics *13*, 890-901.

Hensley, C.T., Wasti, A.T., and DeBerardinis, R.J. (2013). Glutamine and cancer: cell biology, physiology, and clinical opportunities. J Clin Invest *123*, 3678-3684.

James, S.H., and Prichard, M.N. (2014). Current and future therapies for herpes simplex virus infections: mechanism of action and drug resistance. Curr Opin Virol *8*, 54-61.

Lau, K.S., Partridge, E.A., Grigorian, A., Silvescu, C.I., Reinhold, V.N., Demetriou, M., and Dennis, J.W. (2007). Complex N-glycan number and degree of branching cooperate to regulate cell proliferation and differentiation. Cell *129*, 123-134.

Lenaerts, L., De Clercq, E., and Naesens, L. (2008). Clinical features and treatment of adenovirus infections. Rev Med Virol *18*, 357-374.

Li, H., Zhu, W., Zhang, L., Lei, H., Wu, X., Guo, L., Chen, X., Wang, Y., and Tang, H. (2015). The metabolic responses to hepatitis B virus infection shed new light on pathogenesis and targets for treatment. Sci Rep *5*, 8421.

Liu, W., Le, A., Hancock, C., Lane, A.N., Dang, C.V., Fan, T.W., and Phang, J.M. (2012). Reprogramming of proline and glutamine metabolism contributes to the proliferative and metabolic responses regulated by oncogenic transcription factor c-MYC. Proc Natl Acad Sci U S A *109*, 8983-8988.

Metallo, C.M., Gameiro, P.A., Bell, E.L., Mattaini, K.R., Yang, J., Hiller, K., Jewell, C.M., Johnson, Z.R., Irvine, D.J., Guarente, L., et al. (2011). Reductive glutamine metabolism by IDH1 mediates lipogenesis under hypoxia. Nature *481*, 380-384.

Mullen, A.R., Wheaton, W.W., Jin, E.S., Chen, P.H., Sullivan, L.B., Cheng, T., Yang, Y., Linehan, W.M., Chandel, N.S., and DeBerardinis, R.J. (2011). Reductive carboxylation supports growth in tumour cells with defective mitochondria. Nature *481*, 385-388.

Munger, J., Bennett, B.D., Parikh, A., Feng, X.J., McArdle, J., Rabitz, H.A., Shenk, T., and Rabinowitz, J.D. (2008). Systems-level metabolic flux profiling identifies fatty acid synthesis as a target for antiviral therapy. Nat Biotechnol *26*, 1179-1186.

Nicklin, P., Bergman, P., Zhang, B., Triantafellow, E., Wang, H., Nyfeler, B., Yang, H., Hild, M., Kung, C., Wilson, C., et al. (2009). Bidirectional transport of amino acids regulates mTOR and autophagy. Cell *136*, 521-534.

Possemato, R., Marks, K.M., Shaul, Y.D., Pacold, M.E., Kim, D., Birsoy, K., Sethumadhavan, S., Woo, H.K., Jang, H.G., Jha, A.K., et al. (2011). Functional genomics reveal that the serine synthesis pathway is essential in breast cancer. Nature *476*, 346-350.

Ritter, J.B., Wahl, A.S., Freund, S., Genzel, Y., and Reichl, U. (2010). Metabolic effects of influenza virus infection in cultured animal cells: Intra- and extracellular metabolite profiling. BMC Syst Biol *4*, 61.

Sanchez, E.L., Carroll, P.A., Thalhofer, A.B., and Lagunoff, M. (2015). Latent KSHV Infected Endothelial Cells Are Glutamine Addicted and Require Glutaminolysis for Survival. PLoS Pathog *11*, e1005052.

Thai, M., Graham, N.A., Braas, D., Nehil, M., Komisopoulou, E., Kurdistani, S.K., McCormick, F., Graeber, T.G., and Christofk, H.R. (2014). Adenovirus E4ORF1-induced MYC activation promotes host cell anabolic glucose metabolism and virus replication. Cell Metab *19*, 694-701.

Vastag, L., Koyuncu, E., Grady, S.L., Shenk, T.E., and Rabinowitz, J.D. (2011). Divergent effects of human cytomegalovirus and herpes simplex virus-1 on cellular metabolism. PLoS Pathog *7*, e1002124.

Wang, R., Dillon, C.P., Shi, L.Z., Milasta, S., Carter, R., Finkelstein, D., McCormick, L.L., Fitzgerald, P., Chi, H., Munger, J., et al. (2011). The transcription factor Myc controls metabolic reprogramming upon T lymphocyte activation. Immunity *35*, 871-882.

Wellen, K.E., Lu, C., Mancuso, A., Lemons, J.M., Ryczko, M., Dennis, J.W., Rabinowitz, J.D., Coller, H.A., and Thompson, C.B. (2010). The hexosamine biosynthetic pathway couples growth factor-induced glutamine uptake to glucose metabolism. Genes Dev *24*, 2784-2799.

Wise, D.R., DeBerardinis, R.J., Mancuso, A., Sayed, N., Zhang, X.Y., Pfeiffer, H.K., Nissim, I., Daikhin, E., Yudkoff, M., McMahon, S.B., et al. (2008). Myc regulates a transcriptional program that stimulates mitochondrial glutaminolysis and leads to glutamine addiction. Proc Natl Acad Sci U S A *105*, 18782-18787.

Wise, D.R., Ward, P.S., Shay, J.E., Cross, J.R., Gruber, J.J., Sachdeva, U.M., Platt, J.M., DeMatteo, R.G., Simon, M.C., and Thompson, C.B. (2011). Hypoxia promotes isocitrate dehydrogenase-dependent carboxylation of alpha-ketoglutarate to citrate to support cell growth and viability. Proc Natl Acad Sci U S A *108*, 19611-19616.

Yang, C., Sudderth, J., Dang, T., Bachoo, R.M., McDonald, J.G., and DeBerardinis, R.J. (2009). Glioblastoma cells require glutamate dehydrogenase to survive impairments of glucose metabolism or Akt signaling. Cancer Res *69*, 7986-7993.

Yi, W., Clark, P.M., Mason, D.E., Keenan, M.C., Hill, C., Goddard, W.A., 3rd, Peters, E.C., Driggers, E.M., and Hsieh-Wilson, L.C. (2012). Phosphofructokinase 1 glycosylation regulates cell growth and metabolism. Science *337*, 975-980.

CHAPTER 3

Ketohexokinase is an important metabolic enzyme for lung tumor growth

SUMMARY

Cancer cells and viruses reprogram cell metabolism towards increased nutrient uptake and anabolism. Unlike cancer cells, viruses undergo intense selection for efficiency, only upregulating metabolic nodes critical for their rapid replication. Viruses are therefore powerful tools to identify essential metabolic pathways in cancer cells. One of the most highly upregulated metabolic genes during adenovirus infection is ketohexokinase (KHK), which phosphorylates fructose to fructose 1-phosphate. We show KHK knockdown impairs optimal adenovirus replication. KHK is elevated across many patient cancers, including lung cancer. Here, we show that KHK is important for growth of cultured lung cancer cells and lung tumor growth *in vivo*. Lung tumor xenograft growth is impaired by KHK knockout and rescued by simultaneous overexpression of both splice variants, KHK-A and KHK-C. We further provide evidence that the polyol pathway, which converts intracellular glucose to fructose, supports cancer growth: we show that polyol pathway activity is increased in lung tumor xenografts relative to healthy lung and that KHK promotes nucleotide biosynthesis and cancer cell proliferation in the absence of exogenous fructose *in vitro*. Our data suggests that KHK and the polyol pathway promote anabolism in part by allowing cancer cells to evade negative feedback on PFK. Notably, essential fructosuria, a genetic condition in which individuals lack KHK activity, is asymptomatic. We hypothesize that targeting KHK, which is important for tumor growth but dispensable in healthy tissue, may effectively blunt tumor growth with limited systemic toxicities.

INTRODUCTION

Like cancer cells, viruses reprogram the metabolism of infected cells to promote anabolism and generate macromolecules for replication. However, while cancer cells have mutations and alterations in a wide array of metabolic enzymes, DNA viruses like adenovirus efficiently and selectively upregulate only the most critical enzymes important for anabolism. Therefore, we hypothesize that identifying which metabolic enzymes are specifically increased during adenovirus infection may provide insight into metabolic enzymes also important for anabolism in cancer. Using this approach, we find that an enzyme involved in fructose metabolism, ketohexokinase (KHK) is one of the most upregulated enzymes during adenovirus infection.

KHK catalyzes the ATP-dependent phosphorylation of fructose to fructose-1-phosphate (F1P). F1P can then be hydrolyzed to dihydroxyacetone phosphate (DHAP) and glyceraldehyde by the enzyme aldolase B. KHK has been studied primarily in the context of metabolic syndrome. Mice genetically lacking KHK are resistant to glucose- and fructose-induced fatty liver disease (Ishimoto et al., 2012; Lanaspa et al., 2013). Although fructose metabolism has not yet been carefully studied in cancer, recent studies found elevated levels of KHK in precancerous colon lesions relative to paired normal tissue (Uzozie et al., 2014) and KHK was identified through as an essential cell growth mediator in mutant *Kras* colon cancer lines (Rana et al., 2017). While fructose can be taken up by cells, here, we find that lung cancer cells can endogenously generate fructose from glucose via the polyol pathway, which includes the enzymes aldolase reductase (AKR1B1) and sorbitol dehydrogenase (SORD).

Whether fructose metabolism, KHK, and/or the polyol pathway contribute to lung cancer growth is currently unknown. We find that knockdown and knockout of KHK in cultured lung cancer cells reduces growth compared to control cells and that KHK KO xenografts grow at a slower rate than KHK WT xenografts. Notably, KHK knockdown leads to decreased glucose incorporation into nucleotides. Our model for how KHK promotes lung tumor growth is through

evasion of negative feedback on PFK. KHK is an attractive cancer metabolism drug target since KHK deficiency is a clinically benign condition. Patients with mutations in the KHK gene have a condition called essential fructosuria – they cannot metabolize fructose leading to its excretion in the urine, however they are asymptomatic. This suggests that targeting KHK may not cause adverse effects on normal tissues and would be well-tolerated in patients.

RESULTS

Adenovirus infection upregulates ketohexokinase.

To determine whether KHK is upregulated during adenovirus infection, primary normal human bronchial epithelial (NHBE) cells were mock-infected or infected with wild-type adenovirus (ADWT) and RNA was harvested after 8 hours. An early time point was picked to characterize changes prior to ADWT-induced lytic cell death. Compared to mock-infected cells, ADWT-infected MCF10A cells have significant elevation of KHK mRNA levels (Figure 1A). ADWT infection of MCF10A cells also leads to increased KHK protein levels (Figure 1B).

To determine whether KHK is important for adenovirus replication, non-transformed human breast epithelial MCF10A cells expressing shRNAs against KHK or a scrambled control were infected by ADWT and virus titer was determined by plaque assay. Adenovirus titer was reduced in KHK knockdown cells compared to virus generated in scrambled control cells (Figure 1C). Taken together, these data suggest that KHK mRNA and protein levels are elevated during adenovirus infection and that KHK is important for optimal adenovirus replication.

Ketohexokinase and the polyol pathway are important for growth *in vitro*.

Since KHK is important for optimal virus replication, we hypothesized that KHK may play an important role in anabolism in cancers. We next wanted to assess whether KHK mRNA levels are upregulated across different tumor types. TCGA data shows that several tumor types in which KHK mRNA levels are elevated compared to normal tissue include lung adenocarcinoma

(LUAD), breast cancer (BRCA), lung squamous cell carcinoma (LUSC) and colon adenocarcinoma (COAD) (Figure 2A). To assess the impact of KHK on cancer proliferation, we knocked down KHK in different cancer cell lines including the A549 lung adenocarcinoma cell line. A549 cells expressing shRNAs against KHK grow at a slower rate than cells expressing a scrambled control (Figure 2B). Additionally, A549 cells with CRISPR-mediated knockout of KHK grow at a slower rate than control cells (Figure 2C, 2D). KHK has two splice variants that differ by a mutually exclusive splicing event of Exon 3 (ref). Re-expression of KHK-A or KHK-C in KHK KO A549 cells leads to a slight increase in growth rate of cells compared to KHK KO cells (Figure 2E).

While KHK conversion of fructose to fructose 1-phosphate is likely important *in vivo* where fructose is abundant in the diet, we were surprised that cancer cells are sensitive to knockdown or knockout of an enzyme involved in fructose metabolism or that adenovirus upregulates an enzyme that metabolizes fructose during infection when there is no fructose present in the cell culture media. In certain contexts including hyperglycemia, glucose can be converted endogenously through the polyol pathway to fructose via the intermediary metabolite sorbitol (Hannou et al., 2018). Therefore, we hypothesized that glucose may be converted to fructose via the polyol pathway in our cultured cancer cells (Figure 2F). To determine whether glucose is converted to fructose, A549 cells were labeled with U-$^{13}C_6$-glucose and intracellular metabolites were extracted after 24 hours. Nearly a hundred percent of the sorbitol, fructose, and fructose 1-phosphate detected in the samples is labeled by U-$^{13}C_6$-glucose suggesting that fructose is generated to glucose in these cells with subsequent conversion to fructose 1-phosphate by KHK (Figure 2G). Consistently, knockdown of KHK increases relative amounts of intracellular sorbitol and decreases the relative amounts of fructose 1-phosphate compared to control cells (Figures 2H and 2I). Taken together, this data suggests that some intracellular glucose is converted to fructose through the polyol pathway and is metabolized by KHK in A549 cells.

To determine whether the polyol pathway is active *in vivo*, xenografts were generated using the RH2 lung squamous cancer cell line in SCID mice. We first compared KHK expression in normal mouse lung tissue versus tumor xenografts. Tumor xenografts have higher KHK protein levels than paired normal lung tissue from the same mouse. Since KHK is expressed highly in the liver, mouse liver tissue was used as a positive control and has high levels of KHK protein (Figure 2M). Mice were infused with U-$^{13}C_6$-glucose and metabolites from normal mouse lung and tumor xenografts were extracted. Tumor xenograft tissues have increased amounts of U-$^{13}C_6$-glucose labeling of fructose compared to normal mouse lung tissue (Figure 2J). Additionally, nearly all of the fructose labeled by U-$^{13}C_6$-glucose represents the M+6 isotopomer, supporting its derivation from glucose (Figure 2K). Both normal lung and xenograft tissue have equivalent intracellular labeling by U-$^{13}C_6$-glucose, suggesting that the difference in glucose labeling of fructose is not due simply to differences in percent labeling of glucose in both tissues (Figure 2L). Taken together, our data suggest that the polyol pathway may be active *in vivo*.

Ketohexokinase promotes anabolism.

We next wanted to determine how KHK contributes to anabolism. We traced A549 cells with U-$^{13}C_6$-glucose and measured glucose incorporation into different metabolites. KHK knockdown by two shRNAs results in decreased glucose incorporation into both the M+2 and M+4 intermediates of the TCA cycle intermediate citrate compared to scrambled control cells (Figure 3A). KHK knockdown also leads to decreased glucose incorporation into the M+2 isotopomers of other TCA metabolites including alpha-ketoglutarate, fumarate, and malate compared to scrambled control cells (Figure 3B). Together, these data suggest that KHK knockdown decreases glucose entry into the TCA cycle.

To determine whether glutamine uptake was altered with KHK knockdown, we also labeled A549 cells with U-$^{13}C_5$-glutamine. Compared to the scrambled control cells, KHK knockdown cells have reduced M+4 labeling of citrate by U-$^{13}C_5$-glutamine but have elevated

M+5 citrate levels (Supplementary Figure 1A). Additionally, the M+3 isotopomers of aspartate, fumarate, and malate from U-$^{13}C_5$-glutamine are elevated in the KHK knockdown cells compared to the scrambled control cells (Supplementary Figure 1B). These data indicate that KHK knockdown leads to increased reductive carboxylation in A549 cells.

Interestingly, KHK knockdown leads to a striking reduction of U-$^{13}C_6$-glucose labeling of nucleotides, and this phenotype is seen in both purines and pyrimidines (Figure 3E). We reasoned that it may be possible for glucose-derived fructose to enter the pentose phosphate pathway through its conversion to glyceraldehyde 3-phosphate and subsequent conversion by transketolase into ribose 5-phosphate and erythrose 4-phosphate. Since it is difficult to distinguish between glucose-derived fructose contribution to nucleotides versus glucose contribution to nucleotides through the pentose phosphate pathway, we cultured A549 cells in U-$^{13}C_6$-fructose and measured labelled fructose incorporation into different metabolites. Fructose labels several metabolites of lower glycolysis including nearly half of the intracellular 3-phosphoglycerate and close to 20 percent lactate (Figure 3D). Fructose also labels a large amount of sorbitol in the cells as well (Figure 3D). As expected, fructose can also label TCA cycle intermediates including about 17.5 percent of citrate and others (Figure 3E). Interestingly, U-$^{13}C_6$-fructose in these cells also labels nucleotides and intermediates of the pentose phosphate pathway important for generating nucleotides. Metabolites in the pentose phosphate pathway and nucleotides including ribose 5-phosphate/ribulose 5-phosphate, septulose 7-phosphate, UMP, AMP are all labeled by fructose (Figure 3F-I, Supplementary Figure 3C). Interestingly, the M+3 isotopomer is labeled by U-$^{13}C_6$-fructose (Figures 3G-3I). The labeling pattern observed is consistent with fructose conversion to G3P and subsequent conversion into pentose phosphate pathway metabolites and/or nucleotides (Figure 3L).

Glucose conversion via the polyol pathway and metabolism by KHK into fructose 1-phosphate followed by conversion to downstream steps of glycolysis bypasses a major negative regulatory step in glycolysis by phosphofructokinase (PFK). PFK is subject to negative feedback

by citrate and ATP (Lyssiotis and Cantley, 2013). Therefore, we reasoned that KHK knockout impairs the cell's ability to maintain flow of glucose into glycolysis and downstream pathways including the TCA cycle and pentose phosphate pathway through conversion from G3P. The enzyme PFKFB3 converts fructose 1,6-bisphosphate into fructose 2,6-bisphosphate which is a potent activator of PFK (Okar et al., 2001). To determine whether KHK KO prevents cancer cells from evading negative feedback on PFK, we overexpressed PFKFB3 in control vector cells and in KHK KO cells to see whether activation of PFK rescues growth of the KHK KO cells. Interestingly, PFKFB3 overexpression of KHK KO cells restored the growth rate to levels of the vector control cells with wild-type KHK (Figure 3J, 3L). Our results suggest that KHK conversion of fructose to fructose 1-phosphate contributes to cancer cell growth through bypassing regulation of glycolysis by PFK and that metabolism of fructose by KHK may contribute to nucleotide synthesis.

Ketohexokinase promotes optimal growth of lung tumors *in vivo*.

We next wanted to determine the effects of KHK KO on tumor growth in *vivo.* Therefore, we injected SCID mice with control A549 cells expressing wild-type KHK versus A549 cells with KHK KO and measured tumor size of the xenografts. About 3 weeks after injection, KHK KO tumors were significantly smaller than control tumors, suggesting that KHK is important for optimal growth of the tumors (Figure 4A).

To determine whether overexpression of KHK in the KHK KO cells could restore growth of the knockout cells, we overexpressed vector, KHK-A, KHK-C, or KHK-A and KHK-C together in A549 KHK KO cells and injected into SCID mice to form tumor xenografts. Preliminary data suggests that overexpression of KHK-A or overexpression of KHK-A and KHK-C together in KHK KO xenografts increasing tumor growth when compared to growth of control KHK KO or KHK-C overexpressing tumors (Figure 4B). This data supports the idea that KHK contributes to tumor growth.

DISCUSSION

In this study, we use adenovirus infection as an approach to determine important metabolic enzymes for proliferation and identify KHK as an important metabolic enzyme for anabolism. KHK is upregulated both during virus infection and in certain cancers, and we show that reducing KHK levels decreases optimal virus infection as well as reduces growth of cultured lung cancer cells and lung tumor xenografts *in vivo*. We show that glucose can be converted to fructose in cultured lung cancer cells and potentially lung tumors *in vivo*. Knockdown of KHK in cultured lung cancer cells reduces the fractional contribution of glucose towards TCA cycle intermediates and most notably, into nucleotides. Interestingly, fructose can be incorporated into pentose phosphate pathway intermediates and nucleotides in cultured lung cancer cells. Our model for how KHK and the polyol pathway promote growth is through evasion of negative feedback on PFK. Consistently, we show that overexpression of PFKFB3 to promote PFK activity is sufficient to rescue the growth defects conferred by KHK knockout.

We show that overexpression of both KHK splice variants, KHK-A and KHK-C, together in cells lacking KHK increases tumor growth compared to KHK deficient cells. Further studies examining the potential differences between KHK-A and KHK-C in promoting cancer growth will be interesting to pursue. A previous study has described a switch from expression of KHK-C to KHK-A in hepatocellular carcinoma (HCC) cells, which they observe promotes growth of HCC cells (Li et al., 2016). Interestingly, KHK-C is thought to be the more active form of KHK in terms of its affinity and ability to metabolize fructose. However, it remains unknown whether each splice variant contributes to anabolism differently in the context of lung tumors and whether one KHK isoform or the other is preferentially utilized by lung tumors.

Whether fructose contributes to lung tumor growth also remains to be explored. Previous studies have suggested increased expression of GLUT5, a putative fructose transporter, in neoplastic primary human breast tissue (Zamora-Leon et al., 1996) and clear renal cell carcinoma (Medina Villaamil et al., 2011). Enhanced fructose uptake and utilization has been

found to contribute to growth of acute myeloid leukemia (AML) cell lines, glioma cells (Su et al., 2018), pancreatic cancer (Liu et al., 2010), and most recently, $APC^{-/-}$ colorectal carcinoma (Goncalves et al,, 2019). A recent study reported that a majority of dietary fructose is cleared by the small intestine, and the overflow by the liver (Jang et al., 2018). It remains to be determined whether or not dietary fructose enters the systemic circulation in order for lung tumors to have access to the fructose.

Our study demonstrates that KHK is an important enzyme in adenovirus infection and for growth of lung tumors, in part through its metabolism of fructose that is endogenously produced via glucose through the polyol pathway. Because of its limited systemic toxicities, targeting KHK in lung tumors may serve as an attractive therapeutic approach in the future.

ACKNOWLEDGMENTS

We thank Dr. Minh Thai and Lisa Situ for their technical assistance. S.K.T. is a pre-doctoral fellow supported by an NIH NIGMS training grant (GM008042), UCLA Virology and Gene Therapy Training Grant (T32AI060567), and UCLA Tumor Immunology Training Grant (USHHS Ruth L. Kirschstein Institutional National Research Service Award #T32 CA009056).

AUTHOR CONTRIBUTIONS

S.K.T. and H.R.C. designed the study. S.K.T. and H.R.C. wrote the manuscript. S.K.T., M.M., E.S., N.Z., and D.B. performed experiments. T.S. and Z.M. performed computational analysis. X.L. generated reagents to help test our model. D.S., S.K., and A.B. provided guidance. H.R.C. supervised the project.

DECLARATION OF INTERESTS

The authors declare no competing interests.

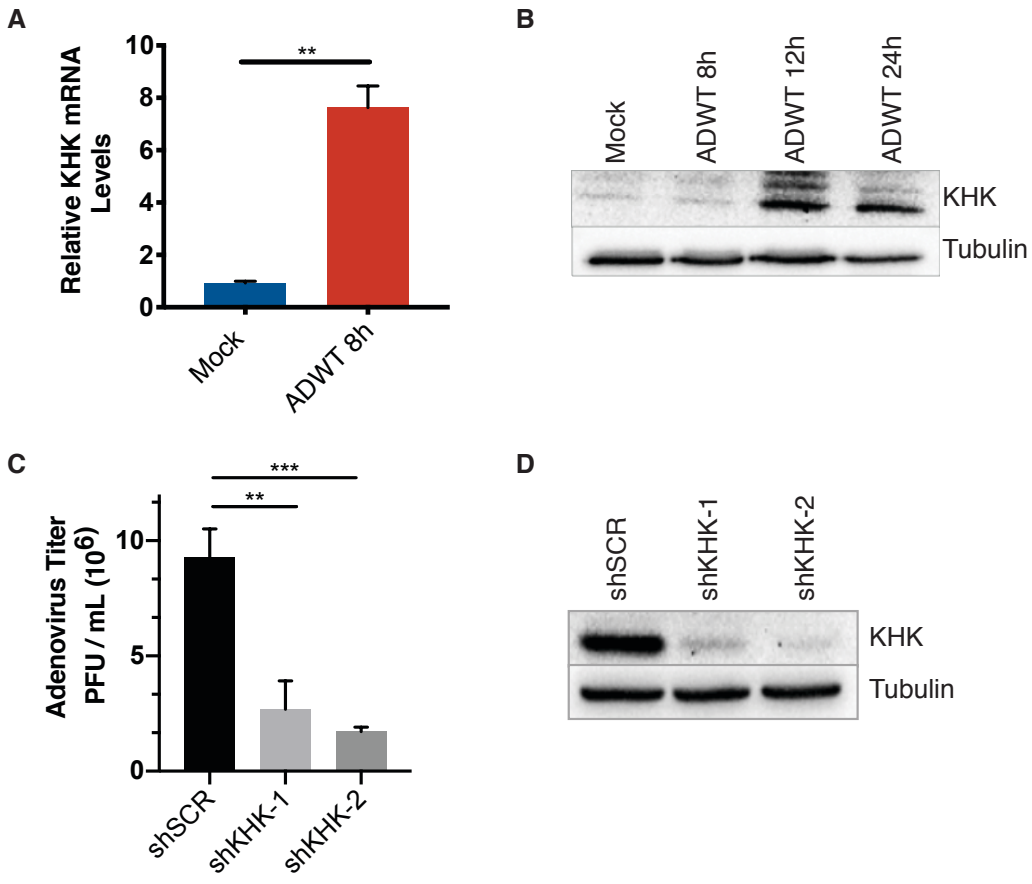

Figure 1. Adenovirus infection upregulates ketohexokinase. (A) NHBE cells were mock-infected or infected with ADWT at an MOI of 10 and mRNA levels of KHK were measured by qPCR 8 hours post-infection. mRNA levels are normalized relative to mock-infected cells. (B) NHBE cells were mock-infected or infected with AD WT at an MOI of 10 for 6, 12, and 24 hours. KHK immunoblots from lysates collected at the indicated time points. Tubulin was used as a loading control. (C) MCF10A cells stably expressing shSCR, shKHK-1, or shKHK-2 were infected with ADWT and virus produced was collected after 24 hours post-infection. Viral titers were determined using plaque assays. *p*-values were calculated using Student's *t*-test and error bars indicate s.d. (n=3), $*p < 0.05$, $**p < 0.01$, $***p < 0.005$.

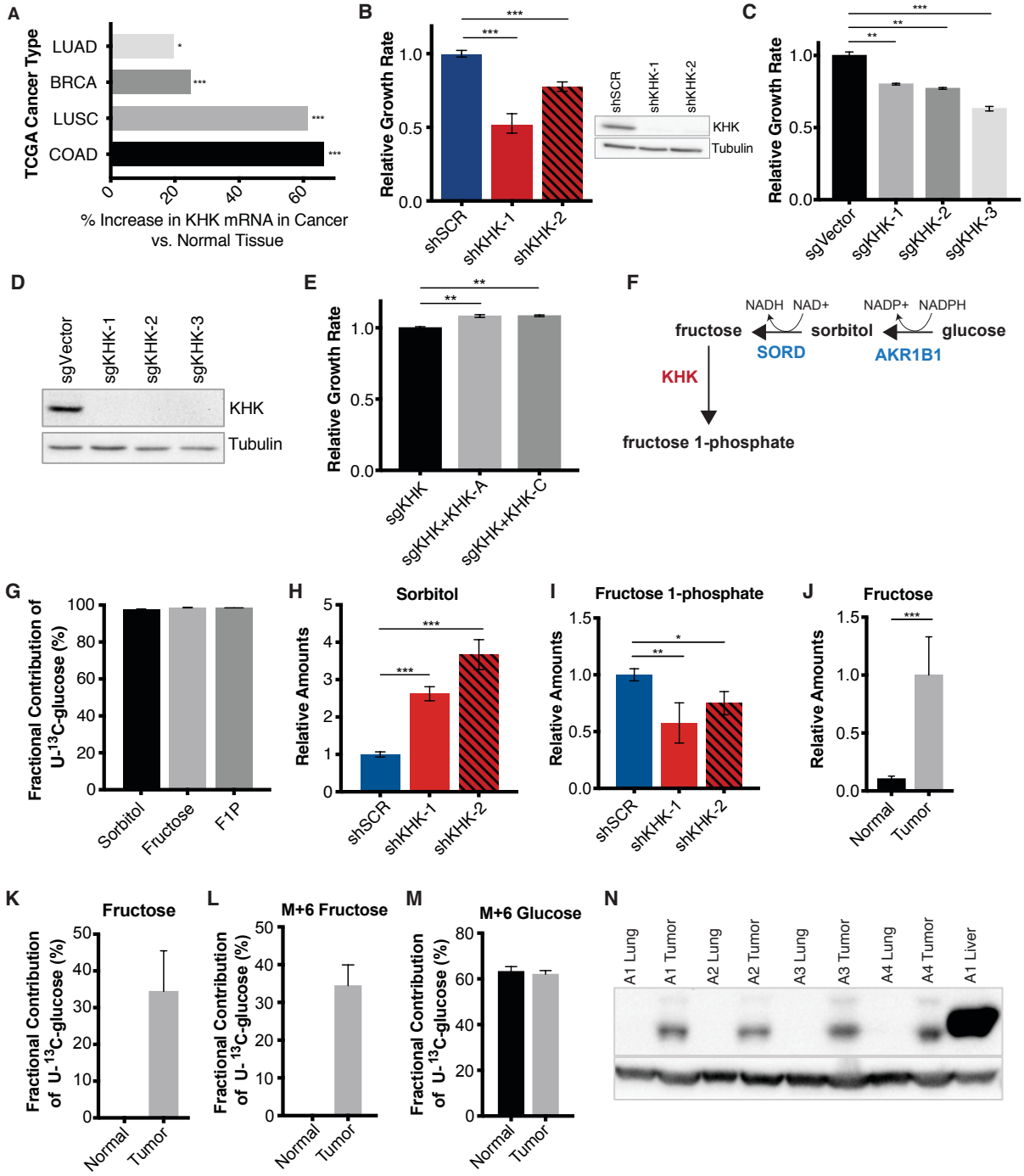
A
TCGA Cancer Type
LUAD
BRCA
LUSC
COAD
0
20
40
60
% Increase in KHK mRNA in Cancer vs. Normal Tissue
B
Relative Growth Rate
shSCR
shKHK-1
shKHK-2
KHK
Tubulin
C
Relative Growth Rate
sgVector
sgKHK-1
sgKHK-2
sgKHK-3
D
sgVector
sgKHK-1
sgKHK-2
sgKHK-3
KHK
Tubulin
E
Relative Growth Rate
sgKHK
sgKHK+KHK-A
sgKHK+KHK-C
F
NADH
NAD+
NADP+
NADPH
fructose
sorbitol
glucose
SORD
AKR1B1
KHK
fructose 1-phosphate
G
Fractional Contribution of U-13C-glucose (%)
Sorbitol
Fructose
F1P
H
Sorbitol
Relative Amounts
shSCR
shKHK-1
shKHK-2
I
Fructose 1-phosphate
Relative Amounts
shSCR
shKHK-1
shKHK-2
J
Fructose
Relative Amounts
Normal
Tumor
K
Fructose
Fractional Contribution of U-13C-glucose (%)
Normal
Tumor
L
M+6 Fructose
Fractional Contribution of U-13C-glucose (%)
Normal
Tumor
M
M+6 Glucose
Fractional Contribution of U-13C-glucose (%)
Normal
Tumor
N
A1 Lung
A1 Tumor
A2 Lung
A2 Tumor
A3 Lung
A3 Tumor
A4 Lung
A4 Tumor
A1 Liver

Figure 2. Ketohexokinase and the polyol pathway are important for growth *in vitro*.

(A) KHK mRNA levels in tumor versus normal tissue was determined from the TCGA database. Differences are expressed as the percent increase in tumor versus normal tissues. (B) The relative growth rates of A549 cells stably expressing a scrambled shRNA or two different shRNAs against KHK were measured over 72 hours. immunoblots on lysates from the indicated cells were performed to determine KHK levels. Tubulin was used as a loading control. (C) A549 KHK KO were generated using three different CRISPR sgRNAs. The growth rate of three different A549 KHK KO clones were calculated compared to an empty vector control over 72 hours. (D) KHK immunoblot from lysates from generated from A549 cells in (C). Tubulin was used as a loading control. (E) Relative growth rates of A549 KHK KO cells and KHK KO cells re-expressing KHK-A or KHK-C over 72 hours. (F) Schematic of the polyol pathway, showing conversion of glucose to fructose, and the KHK reaction. (G) Metabolites were extracted from A549 cells cultured in U-$^{13}C_6$-glucose for 24 hours and quantified via LC-MS. Fractional contribution of U-$^{13}C_6$-glucose into different metabolites of the polyol pathway and fructose metabolism are displayed. (H) Metabolites were collected from A549 cells stably expressing a scrambled shRNA or shRNA against KHK after 24 hours and quantified by LC-MS. The relative amounts of sorbitol and fructose 1-phosphate (I) are displayed. (J) Metabolites from RH2 tumor xenografts and normal mouse lung tissue were extracted and quantified via LC-MS. The relative amounts of fructose are displayed. (K) SCID mice were infused with U-$^{13}C_6$-glucose for 120 minutes (100mg/25kg) and metabolites were extracted and analyzed via LC-MS. The fractional contribution of U-$^{13}C_6$-glucose to fructose was determined. (L) M+6 isotopomer labeling of fructose by glucose from (K). (M) Percent labeling of tissue glucose by U-$^{13}C_6$-glucose tracer. (N) KHK immunoblots of normal mouse lung tissue, RH2 tumor xenografts, and normal mouse liver tissue. Normal mouse liver tissue was used as a positive control for KHK staining. Tubulin was used as a loading control.

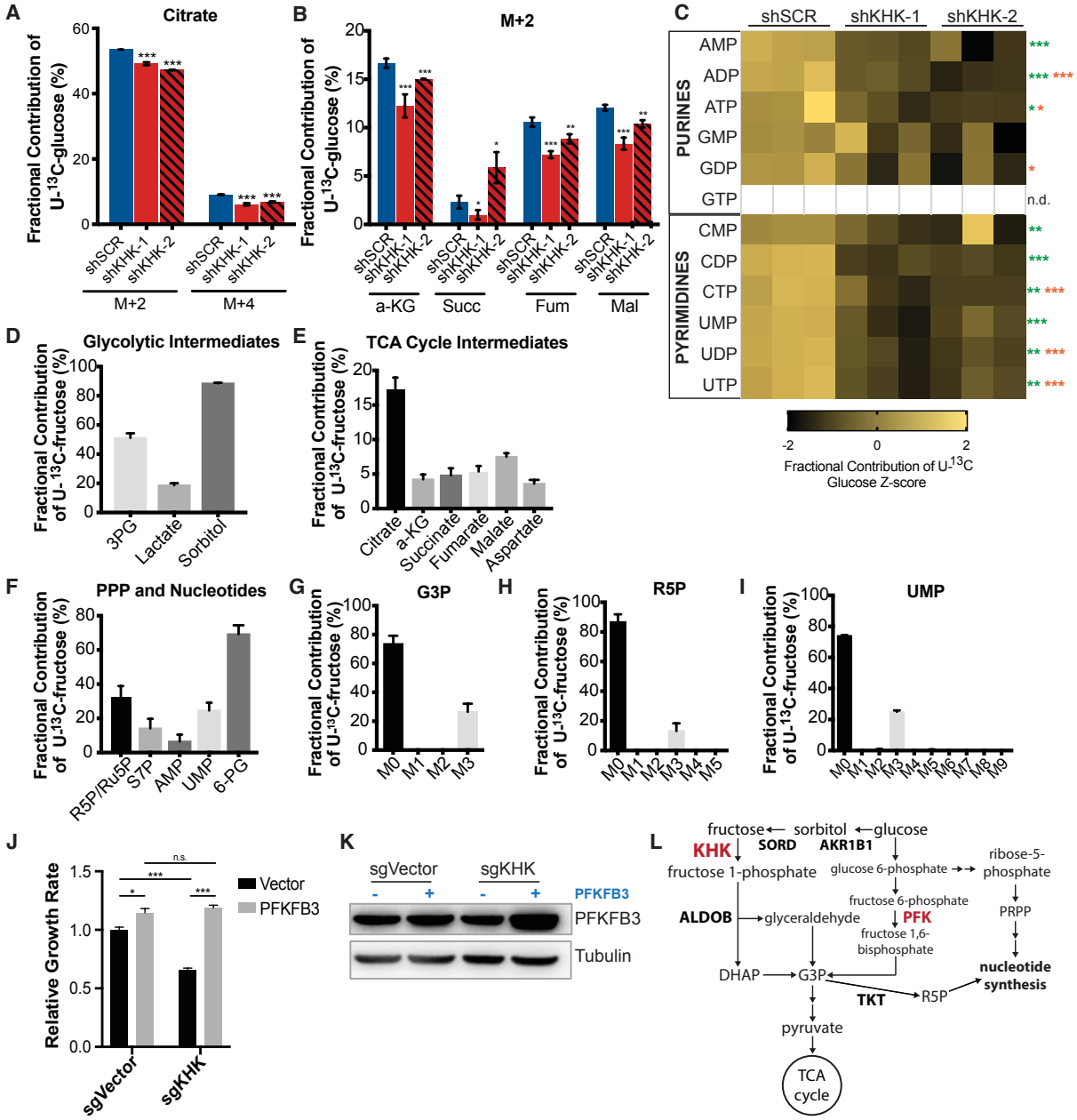
A
Citrate
Fractional Contribution of U-13C-glucose (%)
shSCR
shKHK-1
shKHK-2
M+2
M+4
B
M+2
a-KG
Succ
Fum
Mal
C
shSCR
shKHK-1
shKHK-2
PURINES
AMP
ADP
ATP
GMP
GDP
GTP
n.d.
PYRIMIDINES
CMP
CDP
CTP
UMP
UDP
UTP
Fractional Contribution of U-13C Glucose Z-score
D
Glycolytic Intermediates
Fractional Contribution of U-13C-fructose (%)
3PG
Lactate
Sorbitol
E
TCA Cycle Intermediates
Citrate
a-KG
Succinate
Fumarate
Malate
Aspartate
F
PPP and Nucleotides
R5P/Ru5P
S7P
AMP
UMP
6-PG
G
G3P
M0
M1
M2
M3
H
R5P
M0
M1
M2
M3
M4
M5
I
UMP
M0
M1
M2
M3
M4
M5
M6
M7
M8
M9
J
Relative Growth Rate
n.s.
Vector
PFKFB3
sgVector
sgKHK
K
sgVector
sgKHK
PFKFB3
Tubulin
L
fructose
sorbitol
glucose
KHK
SORD
AKR1B1
fructose 1-phosphate
glucose 6-phosphate
ribose-5-phosphate
fructose 6-phosphate
ALDOB
glyceraldehyde
PFK
PRPP
fructose 1,6-bisphosphate
DHAP
G3P
TKT
R5P
nucleotide synthesis
pyruvate
TCA cycle
K
sgVector + Ctrl
sgVector + PFKFB3
sgKHK + Ctrl
sgKHK + PFKFB3

Figure 3. Ketohexokinase promotes anabolism.

(A) Metabolites were extracted from A549 cells stably expressing a scrambled control, shKHK-1 or 2 and cultured in U-$^{13}C_6$-glucose for 24 hours and quantified via LC-MS. Fractional contribution of U-$^{13}C_6$-glucose into the M+2 and M+4 isotopomers of citrate are quantified. (B) M+2 isotopomer distribution of U-$^{13}C_6$-glucose incorporation into various TCA cycle metabolites from cells in (A). (C) A549 cells stably expressing a scrambled control, or shRNAs against KHK were labeled with U-^{13}C glucose and metabolites were extracted 24 hours later and analyzed via LC-MS. Z-scores of the fractional contribution of U-$^{13}C_6$-glucose into are displayed in the heatmaps. (D) A549 cells were labeled for 24 hours with U-$^{13}C_6$-fructose and extracted metabolites were analyzed via LC-MS to determine fractional contribution into glycolytic intermediates. (E) Metabolites were extracted from A549 cells were labeled for 24 hours with U-$^{13}C_6$-fructose and analyzed via LC-MS to determine fractional contribution into TCA cycle intermediates. (F) A549 cells were labeled for 24 hours with U-$^{13}C_6$-fructose and extracted metabolites were analyzed via LC-MS to determine fractional contribution into pentose phosphate pathway intermediates and nucleotides. (G) Metabolites from A549 labeled for 24 hours with U-$^{13}C_6$-fructose were analyzed via LC-MS to determine fractional contribution of U-$^{13}C_6$-fructose into isotopomers of G3P, (H) R5P, and (I) IMP. (J) A549 sgVector or sgKHK cells with stable overexpression of a vector control (black) or PFKFB3 (gray). Relative growth rates were measured over 48 hours. (K) PFKFB3 immunoblot from A549 cells in (J). Tubulin was used as a loading control. (L) Model of KHK activity and evasion of negative feedback by PFK. TKT can allow G3P entry into the PPP. (K) Light microscope images of A549 cells in (J).

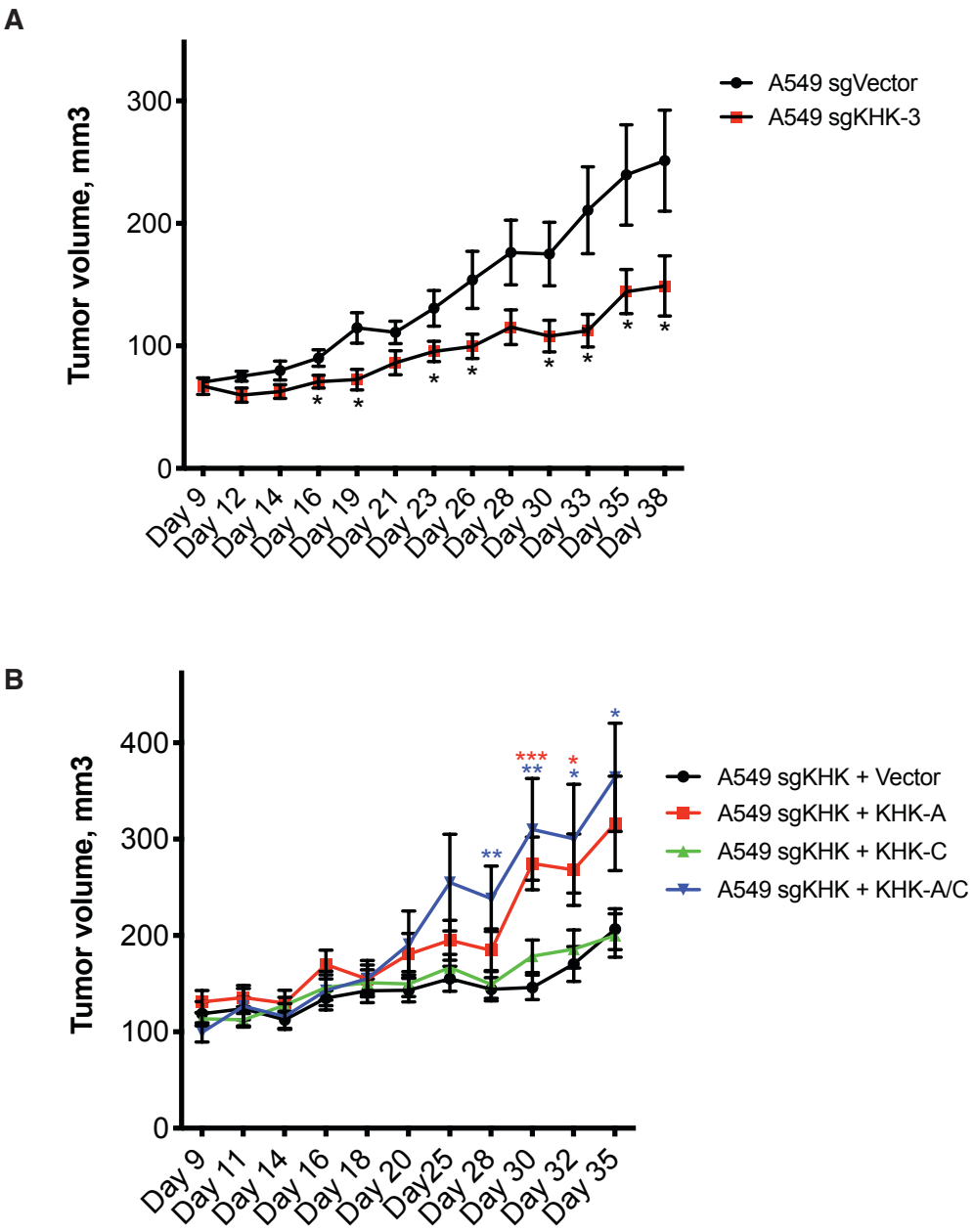

Figure 4. Ketohexokinase promotes optimal growth of lung tumors *in vivo*. (A) Tumor volume was measured by calipers for xenografts derived from A549 sgVector or sgKHK cells over 38 days. (B) Tumor volume was measured by calipers for xenografts derived from A549 cells that were either sgKHK or sgKHK re-expressing KHK-A and KHK-C cells over 35 days.

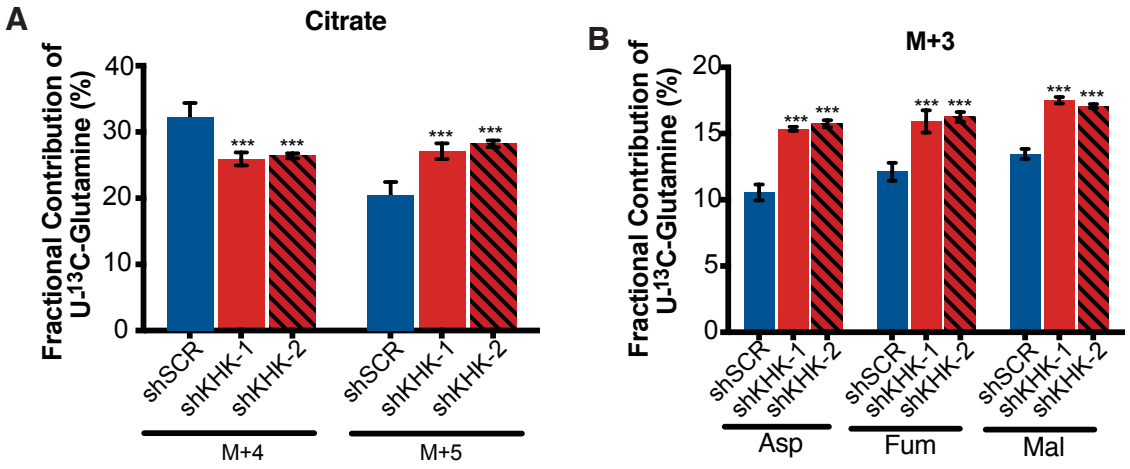

Supplementary Figure 3. *related to Figure 3.* (A) A549 cells were labeled with U-13C5-glutamine and fractional contribution into M+2 and M+4 citrate isotopomers was measured.

CONTACT FOR REAGENT AND RESOURCE SHARING

Further information and requests for resources and reagents should be directed to and will be fulfilled by the Lead Contact, Heather Christofk (hchristofk@mednet.ucla.edu).

EXPERIMENTAL MODEL AND SUBJECT DETAILS

MCF10A, A549, and 293T cells were obtained from the ATCC. 293T cells were cultured in DMEM high glucose medium supplemented with 10% fetal bovine serum and 1% penicillin/streptomycin. MCF10A cells were cultured in DMEM/F12 media supplemented with 5% horse serum, 1% penicillin/streptomycin, EGF (20ng/mL), hydrocortisone (0.5mg/mL), cholera toxin (100ng/mL), and insulin (10ug/mL). A549 cells were cultured in RPMI media supplemented with 10% FBS and 1% penicillin/streptomycin. NHBE cells were obtained from Lonza and cultured in BEGM Bronchial Epithelial Cell Growth Medium (Lonza). All cells were maintained at 37^{o}C with 5% CO_2.

METHOD DETAILS

Intracellular metabolite extraction and analysis

Cells were seeded in six-well plates and metabolites were extracted at 70–80% confluence. Cells were washed with ice-cold 150 mM ammonium acetate (pH 7.3) and scraped off the plate in 800 µl ice-cold 50% methanol. 10 nmol norvaline was added as an internal standard, followed by 400 µl chloroform. Following vigorous vortexing, samples were centrifuged at maximum speed, the aqueous layer was transferred to a glass vial and the metabolites were dried under an EZ-2Elite evaporator. Metabolites were resuspended in 50 µl 70% acetonitrile (ACN) and 5 µl of this solution used for the mass spectrometer-based analysis. The analysis was performed on a Q Exactive (Thermo Scientific) in polarity-switching mode with positive

voltage 4.0 kV and negative voltage 4.0 kV. The mass spectrometer was coupled to an UltiMate 3000RSLC (Thermo Scientific) UHPLC system. Mobile phase A was 5 mM NH_4AcO, pH 9.9, B was ACN and the separation achieved on a Luna 3 mm NH2 100 A (150 × 2.0 mm) (Phenomenex) column. The flow was 200 µl min^{-1}, and the gradient ran from 15% A to 95% A in 18 min, followed by an isocratic step for 9 min and re-equilibration for 7 min. Metabolites were detected and quantified as area under the curve based on retention time and accurate mass (≤3 p.p.m.) using the TraceFinder 3.1 (Thermo Scientific) software. Relative amounts of metabolites between various conditions, as well as percentage of labelling, were calculated and corrected for naturally occurring ^{13}C abundance.

Western Blotting

Cells were lysed in 50 mM Tris pH 7.4, 1% NP-40, 0.25% sodium deoxycholate, 1 mM EDTA, 150 mM NaCl, 1 mM Na_3VO_4, 20 mM NaF, 1mM PMSF, 2 µg ml^{-1} aprotinin, 2 µg ml^{-1} leupeptin and 0.7 µg ml^{-1} pepstatin. Protein concentrations of cell extracts were determined by the Bradford assay. Western blot analysis was carried out as previously described (Thai et al., 2015). The following antibodies were used as probes: Actin (Abcam),

Mice

Mice were housed in pathogen-free facilities at University of California Los Angeles (UCLA). All experimental procedures performed on mice were approved by the UCLA Animal Research Committee (ARC). Female SCID mice between the ages of 6-12 weeks old were used for xenograft studies with established human cell lines.

***In vivo* Tracing with $^{13}C_6$-Glucose**

Experiments were conducted as described previously (Momcilovic et al., 2018). Mice were fasted for 6 hr prior to infusions. Infusions with $^{13}C_6$-glucose (Cambridge Isotope Laboratories, CLM-1396-PK) were performed via tail vein catheters for 120 min. $^{13}C_6$-glucose was infused at

100 mg/kg/min. Mice were kept under 2% isoflurane on warm pads for the entire duration of the infusion. At the end of the infusion, mice were terminally anesthetized with 100% isoflurane and tissues were dissected within 3-5 min and serum was collected. Tissues and serum were snap frozen in liquid nitrogen and stored at -80°C.

QUANTIFICATION AND STATISTICAL ANALYSIS

All numerical data were calculated and plotted with mean +/- s.d. Results were analyzed by ANOVA for multiple group comparisons and unpaired Student's *t* test. Differences were considered statistically significant when $p<0.05$ (*) or $p<0.01$ (**) or $p<0.005$ (***).

REFERENCES

Hannou, S.A., Haslam, D.E., McKeown, N.M., and Herman, M.A. (2018). Fructose metabolism and metabolic disease. J Clin Invest *128*, 545-555.

Ishimoto, T., Lanaspa, M.A., Le, M.T., Garcia, G.E., Diggle, C.P., Maclean, P.S., Jackman, M.R., Asipu, A., Roncal-Jimenez, C.A., Kosugi, T., et al. (2012). Opposing effects of fructokinase C and A isoforms on fructose-induced metabolic syndrome in mice. Proc Natl Acad Sci U S A *109*, 4320-4325.

Jang, C., Hui, S., Lu, W., Cowan, A.J., Morscher, R.J., Lee, G., Liu, W., Tesz, G.J., Birnbaum, M.J., and Rabinowitz, J.D. (2018). The Small Intestine Converts Dietary Fructose into Glucose and Organic Acids. Cell Metab *27*, 351-361 e353.

Lanaspa, M.A., Ishimoto, T., Li, N., Cicerchi, C., Orlicky, D.J., Ruzycki, P., Rivard, C., Inaba, S., Roncal-Jimenez, C.A., Bales, E.S., et al. (2013). Endogenous fructose production and metabolism in the liver contributes to the development of metabolic syndrome. Nat Commun *4*, 2434.

Li, X., Qian, X., Peng, L.X., Jiang, Y., Hawke, D.H., Zheng, Y., Xia, Y., Lee, J.H., Cote, G., Wang, H., et al. (2016). A splicing switch from ketohexokinase-C to ketohexokinase-A drives hepatocellular carcinoma formation. Nature cell biology *18*, 561-571.

Liu, H., Huang, D., McArthur, D.L., Boros, L.G., Nissen, N., and Heaney, A.P. (2010). Fructose induces transketolase flux to promote pancreatic cancer growth. Cancer Res *70*, 6368-6376.

Lyssiotis, C.A., and Cantley, L.C. (2013). Metabolic syndrome: F stands for fructose and fat. Nature *502*, 181-182.

Medina Villaamil, V., Aparicio Gallego, G., Valbuena Rubira, L., Garcia Campelo, R., Valladares-Ayerbes, M., Grande Pulido, E., Victoria Bolos, M., Santamarina Cainzos, I., and Anton Aparicio, L.M. (2011). Fructose transporter GLUT5 expression in clear renal cell carcinoma. Oncol Rep *25*, 315-323.

Momcilovic, M., Bailey, S.T., Lee, J.T., Fishbein, M.C., Braas, D., Go, J., Graeber, T.G., Parlati, F., Demo, S., Li, R., et al. (2018). The GSK3 Signaling Axis Regulates Adaptive Glutamine Metabolism in Lung Squamous Cell Carcinoma. Cancer Cell *33*, 905-921 e905.

Okar, D.A., Manzano, A., Navarro-Sabate, A., Riera, L., Bartrons, R., and Lange, A.J. (2001). PFK-2/FBPase-2: maker and breaker of the essential biofactor fructose-2,6-bisphosphate. Trends in biochemical sciences *26*, 30-35.

Rana, T.M., Yau, E.H., Kummetha, I.R., Lichinchi, G., Tang, R., and Zhang, Y. (2017). Genome-wide CRISPR screen for essential cell growth mediators in mutant KRAS colorectal cancers. Cancer Res.

Su, C., Li, H., and Gao, W. (2018). GLUT5 increases fructose utilization and promotes tumor progression in glioma. Biochemical and biophysical research communications *500*, 462-469.

Thai, M., Thaker, S.K., Feng, J., Du, Y., Hu, H., Ting Wu, T., Graeber, T.G., Braas, D., and Christofk, H.R. (2015). MYC-induced reprogramming of glutamine catabolism supports optimal virus replication. Nat Commun *6*, 8873.

Uzozie, A., Nanni, P., Staiano, T., Grossmann, J., Barkow-Oesterreicher, S., Shay, J.W., Tiwari, A., Buffoli, F., Laczko, E., and Marra, G. (2014). Sorbitol dehydrogenase overexpression and other aspects of dysregulated protein expression in human precancerous colorectal neoplasms: a quantitative proteomics study. Mol Cell Proteomics *13*, 1198-1218.

Zamora-Leon, S.P., Golde, D.W., Concha, II, Rivas, C.I., Delgado-Lopez, F., Baselga, J., Nualart, F., and Vera, J.C. (1996). Expression of the fructose transporter GLUT5 in human breast cancer. Proc Natl Acad Sci U S A *93*, 1847-1852.

CHAPTER 4

Differential metabolic reprogramming by Zika virus promotes cell death in human versus mosquito cells

ABSTRACT

Zika virus is a pathogen that poses serious consequences including congenital microcephaly. Although many viruses reprogram host cell metabolism, whether Zika virus alters cellular metabolism and the functional consequences of Zika-induced metabolic changes remain unknown. Here we show that Zika virus infection differentially reprograms glucose metabolism in human versus C6/36 mosquito cells by increasing glucose use in the tricarboxylic acid cycle in human cells, versus increasing glucose use in the pentose phosphate pathway in mosquito cells. Infection of human cells selectively depletes nucleotide triphosphate levels, leading to elevated AMP/ATP ratios, AMP-activated protein kinase (AMPK) phosphorylation, and caspase-mediated cell death. AMPK is also phosphorylated in Zika virus-infected mouse brain. Inhibiting AMPK in human cells decreases Zika virus-mediated cell death, whereas activating AMPK in mosquito cells promotes Zika virus-mediated cell death. These findings suggest the differential metabolic reprogramming during Zika virus infection of human versus mosquito cells determines whether cell death occurs.

INTRODUCTION

Zika virus (ZIKV), a member of the *Flaviviridae* family, is an emerging public health concern. Though the virus was first isolated in 1947, several outbreaks have occurred since that time, most notably in Brazil, the Americas, and parts of Asia and Africa beginning in 2015, leading the World Health Organization to declare ZIKV as a global public health emergency in 2016(Baud et al., 2017). While ZIKV infection typically leads to mild clinical symptoms, the virus can also cause a range of more severe symptoms including Guillain-Barré in adults and devastating outcomes including microcephaly and congenital brain defects in fetuses of infected mothers(de Oliveira et al., 2017).

Studies over the past two years have begun to examine the mechanisms underlying ZIKV tropism and pathology. As an arthropod-borne virus, the urban transmission cycle of ZIKV involves replication in both mosquito vectors as well as humans (Petersen et al., 2016; Saiz et al., 2016). In humans, ZIKV shows broad tropism including neuronal cell types, placental cells, cells of the reproductive tract, endothelial cells, and ocular tissue (Miner and Diamond, 2017). ZIKV infection of fetal neural stem cells and neuronal progenitor cells leads to caspase-mediated cell death and resulting neurodevelopmental deficits (Liang et al., 2016; Tang et al., 2016). Additionally, ZIKV has been shown to infect peripheral neurons and induce apoptotic cell death (Oh et al., 2017). While ZIKV pathogenesis may be in part be due to death of infected cells, the mechanism by which apoptosis occurs during ZIKV infection is currently unknown. Unlike ZIKV-infected human cells, mosquito vectors infected with flaviviruses are viral reservoirs for their lifespans without experiencing any adverse health effects (Daep et al., 2014). The molecular mechanisms underlying the differential fate observed between ZIKV-infected host human cells and vector mosquito cells remain unknown.

Like proliferating cells, viruses require sufficient nutrients to satisfy the metabolic needs of replication (Munger et al., 2008; Thai et al., 2014). Lack of sufficient nutrients can have adverse effects, including energetic stress and cell death. Diverse viruses rewire the metabolism of

infected host cells to meet the biosynthetic needs of virus replication, and our group and others have shown that modulating host cell metabolism can alter virus replication (Sanchez et al., 2017; Thai et al., 2014; Thai et al., 2015). Currently, whether and how ZIKV alters host cell metabolism during infection is unknown. Here, we characterize ZIKV reprogramming of host cell glucose metabolism in both human and C6/36 mosquito cells. We show that the differential effects on nucleotide levels during infection of human versus C6/36 mosquito cells selectively leads to activation of AMPK signaling and contributes to cell death observed in human but not C6/36 mosquito cells during ZIKV infection.

RESULTS

Zika virus infection alters glucose consumption in human foreskin fibroblasts.

To determine whether Zika virus infection leads to changes in glucose metabolism, we infected a non-transformed human foreskin fibroblast cell line (HFF-1) with ZIKV strain PRVABC-59 and measured changes in glucose consumption and lactate production by host cells at different time points following infection. HFF-1 cells were used because they have been shown to be permissive to ZIKV infection, and ZIKV has been found to replicate in cells of the male reproductive tract (Hamel et al., 2015). ZIKV infection of HFF-1 cells significantly increases glucose consumption of infected cells compared to mock-infected cells 1.5 to 2-fold at 24, 36, and 48 hours post-infection. ZIKV-infection of HFF-1 cells also increases the relative lactate production of infected cells relative to mock cells at 36 and 48 hours post-infection (Figure 1A). These findings suggest that ZIKV infection promotes increased glucose utilization and glycolysis in host cells. Infection of HFF-1 cells with UV-inactivated ZIKV does not induce the same increases in glucose consumption and lactate production, indicating that the observed metabolic changes are due to active reprogramming by the virus and not the host cell response to the virus (Figure S1A).

To characterize ZIKV-induced changes in glucose metabolism during infection, HFF-1 cells were labelled with U-$^{13}C_6$-glucose and mock-infected or infected with ZIKV for 18, 24, and

36 hours. Extracted intracellular metabolites and U-$^{13}C_6$-glucose incorporation into different metabolites were measured and analyzed by liquid chromatography mass spectrometry (LC-MS). ZIKV infection increases fractional U-$^{13}C_6$-glucose incorporation into certain glycolytic intermediates compared to mock-infected cells (Figure S1B). Notably, ZIKV infection robustly increases fractional contribution of U-$^{13}C_6$-glucose into nearly all TCA cycle intermediates at all time points post-ZIKV infection compared to mock-infected cells (Figure 1B). Additionally, ZIKV infection generally promotes increased U-$^{13}C_6$-glucose incorporation into different amino acids at 18, 24, and 36 hours post-ZIKV infection (Figure 1C). Taken together, these data suggest that ZIKV infection of human foreskin fibroblast cells promotes increased glucose utilization in the TCA cycle and for amino acid generation.

Zika virus infection differentially impacts survival and glucose metabolism of human versus C6/36 mosquito cells.

ZIKV is primarily transmitted by *Aedes* species of mosquitoes (Ciota et al., 2017; Grard et al., 2014). Therefore, we assessed ZIKV infection of *Aedes albopictus* mosquito (C6/36) cells as compared with infection of HFF-1 human cells. ZIKV effectively infects both human HFF-1 cells and C6/36 cells, as can be visualized by flavivirus envelope protein immunostaining (Figure 2A). ZIKV infection of HFF-1 cells leads to increased cell death and decreased number of cells over a period of 48 hours, as visualized by reduced DAPI staining at later time points (Figure 2A). In contrast, ZIKV effectively infects C6/36 cells without promoting cell death or decreasing cell number, as visualized by little change in DAPI staining over 48 hours (Figure 2A). To better characterize ZIKV replication in both cell types, cell-free supernatant was harvested from infected HFF-1 and C6/36 cells and virus titers were determined and quantified. ZIKV infection of both HFF-1 and C6/36 cells leads to increased viral titers from 6 to 30 hours post-infection. However, after 30 hours, infected HFF-1 cells have decreased viral titer levels compared to earlier time points due to increased cell death, whereas the viral titers of infected C6/36 cells continues to

elevate with increasing time points (Figure 2B). Our findings that Zika virus infection promotes death of cultured HFF-1 but not C6/36 cells are similar to previous studies showing that Sindbis virus promotes cell death of mammalian cells but maintains persistent, non-lytic viral replication in mosquito cells (Karpf and Brown, 1998; O'Neill et al., 2015).

In order to better understand the differences in ZIKV replication in human and mosquito cells, we examined whether there were underlying metabolic differences between ZIKV infection of HFF-1 versus C6/36 cells. We again labeled both HFF-1 and C6/36 cells with U-$^{13}C_6$-glucose and determined relative levels of and glucose incorporation into different metabolites. ZIKV infection of C6/36 mosquito cells significantly elevates glucose contribution to glycolytic intermediates 24 hours post-infection (Figure 2C). In contrast to infection of HFF-1 cells, ZIKV infection of C6/36 cells trends towards decreased glucose contribution to TCA cycle intermediates (Figure 2D). Additionally, glucose contribution to pentose phosphate pathway intermediates increases during ZIKV infection of C6/36 cells 24 hours post-infection (Figure 2E). In contrast, ZIKV infection of HFF-1 cells leads either to no change or decreased glucose incorporation into pentose phosphate pathway intermediates at 24 hours post-infection (Figure 2F). Overall, ZIKV infection of C6/36 mosquito cells increases glucose contribution to glycolytic and pentose phosphate intermediates and decreases glucose contribution to TCA cycle intermediates, whereas infection of human HFF-1 cells promotes increased glucose contribution to TCA cycle intermediates and amino acids and decreased contribution to nucleotides (Figure 2G). These findings suggest that Zika virus promotes differential glucose utilization in human versus C6/36 mosquito cells.

Zika virus infection selectively depletes nucleotide triphosphate levels in human but not C6/36 mosquito cells.

Since we observed decreased glucose incorporation into pentose phosphate pathway intermediates in ZIKV-infected HFF-1 cells but not in C6/36 cells, we examined whether ZIKV

infection leads to different nucleotide levels in human versus C6/36 mosquito cells. ZIKV infection of HFF-1 cells results in increased relative levels of nucleotide mono- and diphosphates but selective depletion of the relative amounts of nucleotide triphosphate levels, particularly ATP and UTP, 24 and 36 hours following infection (Figure 3A, left). Conversely, ZIKV infection of C6/36 cells leads to increased relative levels of most nucleotide mono-, di- and triphosphates at 24 hours post-infection and decreased relative amounts of all nucleotides at 36 hours post-infection (Figure 3A, right). Because of the decrease in relative amounts of ATP and increased levels of ADP and AMP, ZIKV infection of HFF-1 cells leads to robustly elevated ADP/ATP and AMP/ATP ratios at 24 and 36 hours post-infection (Figure 3B). In contrast, ZIKV infection of C6/36 cells does not lead to a significant increase in the AMP/ATP ratio at 24 or 36 hours post-infection and results in only a minor increase in the ADP/ATP ratio at 36 hours post-infection (Figure 3C).

Since we observed a robust increase in the AMP/ATP and ADP/ATP ratios during ZIKV infection of HFF-1 cells, we hypothesized that this imbalance in AMP, ADP, and ATP levels may activate the serine/threonine kinase AMP-activated protein kinase (AMPK), a major sensor of energetic stress in cells (Mihaylova and Shaw, 2011). Consistently, ZIKV infection of HFF-1 cells leads to increased AMPK phosphorylation at Thr172 and elevation of the pAMPK/AMPK ratios at 24 and 36 hours post-infection (Figure 3D, left). Phosphorylation of a well-known target of AMPK signaling, pACC (Ser79) (Mihaylova and Shaw, 2011), is also elevated at the same time points post-infection (Figure S2A). ZIKV has previously been shown to promote caspase-mediated cell death of human fetal neuronal progenitor cells and mouse models of ZIKV infection(Hanners et al., 2016) (Rosenfeld et al., 2017) (Huang et al., 2016). Consistently, we observe that ZIKV infection of HFF-1 cells leads to increased cleaved caspase 3 levels 36 hours post-infection (Figure 3D).

Since ZIKV infection of HFF-1 cells depletes nucleotide triphosphate levels, we next assessed whether addition of exogenous nucleotide precursors could at least in part rescue pAMPK/AMPK levels and the cell death phenotype observed. Since ATP and UTP were most

significantly depleted, we supplemented media with 250 μM adenine and uridine during ZIKV infection and assessed effects on the pAMPK/AMPK ratio and cleaved caspase 3 levels. Adenine and uridine were added instead of ATP and UTP, since the latter are large, polar molecules that may not readily cross the plasma membrane, and purines are typically salvaged through the base (e.g. adenine) whereas pyrimidines are typically salvaged through the nucleoside (e.g. uridine). Compared to ZIKV-infected cells in regular media, infected cells in the adenine and uridine-supplemented media have reduced pAMPK/AMPK levels (Figure 3D). Interestingly, addition of 250 μM adenine and uridine also reduces levels of caspase 3 cleavage in ZIKV-infected cells 36 hours post-infection compared to cells cultured in regular media (Figure 3D). Importantly, adenine and uridine supplementation of HFF-1 cells during ZIKV infection partially rescues the decrease in relative cell number of ZIKV-infected/mock-infected cells, indicating less cell death during infection with addition of nucleotide precursors (Figure 3E). The relative increase in cell number of infected adenine and uridine supplemented cells relative to cells infected in regular media can also be observed clearly via light microscopy images (Figure S2B). These results suggest that supplementation of exogenous nucleotide precursors can reduce the pAMPK/AMPK ratio and partially rescue caspase-mediated cell death during ZIKV infection.

Zika virus infection increases AMPK phosphorylation and contributes to Zika virus-induced cell death in clinically relevant models.

We next wanted to determine whether ZIKV infection of other clinically relevant cell types and models results in similar changes in AMPK phosphorylation. Mice lacking the type I interferon (IFN) receptor (IFNAR) have been shown to be permissive to ZIKV infection and viral replication within the central nervous system, testis, uterus, and retina (Jurado et al., 2018). We subcutaneously inoculated *Ifnar1*$^{-/-}$ mice with ZIKV ($1x10^6$ pfu/mouse) and assessed pAMPK levels in the brain 7 days post-infection using immunohistochemistry (IHC). Serial sections of mock-infected mouse brain tissue are negative for ZIKV envelope protein (ENV) and have low

levels of pAMPK immunostaining (Figure 4A). ZIKV-infected mouse brain tissue stains positive for ZIKV ENV and displays elevated AMPK phosphorylation compared to mock-infected tissue as quantified across serial mouse brain tissue sections (Figure 4A).

ZIKV infection has also been linked to congenital ocular defects, including retinal abnormalities (de Paula Freitas et al., 2016). To determine whether similar activation of AMPK occurs in clinically relevant human fetal retinal pigment epithelial (hFRPE) cells, we infected the cells with ZIKV and observed co-localization of the flavivirus envelope protein and pAMPK in ZIKV-infected cells (Figure 4B, bottom). Mock-infected hFRPE cells are negative for the flavivirus envelope protein and have low levels of pAMPK staining (Figure 4B, top). ZIKV-infection of hFRPE cells at MOIs of 1, 5, and 10 leads to increasing pAMPK/AMPK ratios in a dose-dependent manner (Figure 4C). To determine whether there is a link between AMPK activation and caspase-mediated cell death in hFRPE cells, we treated mock-infected and ZIKV-infected cells with and without Compound C, a potent AMPK inhibitor, and measured cleaved caspase 3/7 activity. Compared to mock-infected cells, hFRPE cells infected with ZIKV for 48 hours show increased relative levels of cleaved caspase 3/7 activity (Figure 4D), consistent with the increased cleaved caspase 3 protein levels observed in ZIKV-infected HFF-1 cells (Figure 3D). Interestingly, treatment of ZIKV-infected hFRPE cells with 1 μM Compound C partially rescues the increased cleaved caspase 3/7 activity seen in DMSO-treated ZIKV-infected cells and 5 μM Compound C restores caspase 3/7 activity to levels seen in mock-infected cells (Figure 4D). These data suggest that AMPK is activated by ZIKV infection of human fetal retinal pigment epithelial cells and that blocking AMPK activation can decrease ZIKV-promoted cleaved caspase 3/7 activity.

Our data suggests that AMPK activation contributes to caspase-mediated cell death of ZIKV-infected human cells. In contrast, our data shows that ZIKV-infected C6/36 mosquito cells do not display robustly elevated AMP/ATP and ADP/ATP ratios, and therefore presumably do not have AMPK activation. Therefore, we wanted to determine whether increasing AMPK activity in ZIKV-infected C6/36 cells would be sufficient to promote apoptosis and decrease cell number and

viability. We therefore treated C6/36 cells with water or AICAR (5-Aminoimidazole-4-carboxamide ribonucleotide), an adenosine analog and AMPK activator(Garcia and Shaw, 2017), and measured cleaved caspase 3/7 activity and cell viability in mock- and ZIKV-infected cells. ZIKV infection of C6/36 cells over 48 hours leads to no change in cleaved caspase activity (Figure 4E), no change in cell viability (Figure 4F), and little visible change in cell number by light microscopy compared to mock-infected cells (Figure 4G). Conversely, AICAR treatment of C6/36 cells is sufficient to increase cleaved caspase 3/7 activity (Figure 4E) and decrease cell viability compared to water-treated, mock-infected cells (Figure 4F). Furthermore, AICAR treatment of ZIKV-infected C6/36 cells over a period of 48 hours post-infection greatly increases cleaved caspase 3/7 activity, decreases cell number and reduces cell viability compared to mock-infected, ZIKV-infected, and mock-infected plus AICAR treated cells (Figures 4E-G). Consistently, we found that pentose phosphate pathway inhibition in ZIKV-infected C6/36 mosquito cells, through dehydroepiandrosterone (DHEA)-mediated inhibition of glucose-6-phosphate dehydrogenase (G6PD) (Figure S3A), also increases cleaved caspase 3/7 activity (Figure S3B). Taken together, these results suggest that differences in pentose phosphate pathway activity and AMPK activation in ZIKV-infected human versus C6/36 mosquito cells may in part underlie the differences in cell death during infection.

DISCUSSION

This study is the first to characterize metabolic reprogramming during Zika virus infection and to reveal differences between ZIKV-promoted metabolic changes in human versus C6/36 mosquito cells. We show that ZIKV infection differentially promotes altered glucose utilization in human foreskin fibroblasts and C6/36 mosquito cells, with increased glucose utilization in the TCA cycle in human foreskin fibroblasts and increased glucose utilization in the pentose phosphate pathways in C6/36 mosquito cells. We observe selective depletion of nucleotide triphosphates of ZIKV-infected human cells, leading to increased AMP/ATP and ADP/ATP ratios and AMPK

activation, which contributes to the caspase-mediated cell death of human cells during infection. Consistently, we show that AMPK phosphorylation is elevated in the brain tissue from a mouse model of ZIKV infection and in clinically relevant human fetal retinal pigment epithelial cells. We also demonstrate that modulation of AMPK activity through supplementation of nucleotide precursors in human cells or pharmacological approaches in both human cells and C6/36 mosquito cells can influence whether or not cells undergo cell death during ZIKV infection.

Though previous studies have identified metabolic changes triggered by infection of other flaviviruses, ZIKV rewiring of glucose metabolism has not yet been elucidated. Another member of the *Flaviviridae* family, Dengue virus (DENV), has been shown to increase glucose consumption and GAPDH activity during infection (Allonso et al., 2015; Fontaine et al., 2015). Hepatitis C virus, a hepacivirus in the *Flaviviridae* family, has been shown to increase pyruvate dehydrogenase kinase (PDK) and hexokinase activity and increase glycolysis and fatty acid synthesis in infected cells (Diamond et al., 2010; Jung et al., 2016; Ramiere et al., 2014; Waris et al., 2007; Yang et al., 2008). However, many studies examining viral metabolic reprogramming have not examined how glucose utilization is altered during infection through metabolic tracer analysis. It is intriguing that while ZIKV infection of both HFF-1 and C6/36 cells promotes glycolysis, infection of human cells leads to increased glucose utilization to generate TCA cycle intermediates rather than pentose phosphate pathway intermediates for nucleotide synthesis. This contrasts with infection of human cells by several other viruses, including adenovirus and human cytomegalovirus (HCMV), which increase glucose utilization towards pentose phosphate pathway intermediates (Thai et al., 2014; Vastag et al., 2011). Perhaps one explanation for this difference is that double-stranded DNA viruses, like adenovirus and HCMV, require higher nucleotide generation to synthesize their larger viral genomes, which are approximately 36 kilobases (kb) and 236 kb, respectively, compared to the single-stranded ZIKV RNA genome which is only about 10.8 kb (Cunha et al., 2016; Dolan et al., 2004; Russell, 2009).

The mechanism by which Zika virus can modulate glycolysis and nucleotide levels in infected cells also remains to be determined. A previous study performed with Dengue virus showed that viral NS1 protein can modulate glycolysis by directly interacting with and increasing activity of the enzyme GAPDH (glyceraldehyde-3-phosphate dehydrogenase) (Allonso et al., 2015). The ZIKV NS1 protein shares 51-53% homology with DENV NS1 protein(Balmaseda et al., 2017). Whether ZIKV NS1 protein or another ZIKV protein can mediate the glycolytic changes observed during infection would provide insight into the precise molecular mechanism by which ZIKV can alter metabolism of host cells.

To our knowledge, no other study has shown that the underlying metabolic differences between infection of mosquito cells and human cells may in part explain differences in cell death. Here we show that relative levels of nucleotides are differentially altered during ZIKV infection of human and C6/36 mosquito cells, leading to elevation of AMP/ATP ratios, subsequent activation of AMPK, and caspase-mediated cell death in human cells but not mosquito cells. Previous studies have shown modulation of AMPK signaling in human cells during infection with other viruses. However, the role of AMPK signaling during virus infection seems to vary depending on the virus; AMPK activation has been shown by previous studies to exert both antiviral effects, as during infection by West Nile and Rift Valley Fever viruses (Jimenez de Oya et al., 2018; Moser et al., 2012), and proviral effects for DENV, HCMV, Vaccinia virus, and others (McArdle et al., 2012; Moser et al., 2010; Terry et al., 2012). Perhaps one advantage of cell death in human cells during lytic virus infection is to prevent propagation of the virus (Everett and McFadden, 1999; Upton and Chan, 2014), despite causing pathogenic consequences in some tissues. Infection of mammalian cell lines and mouse models by other flaviviruses has also been shown to induce caspase 3 cleavage. West Nile virus infection promotes caspase activation in human glioblastoma cells and mouse brain tissue (Kleinschmidt et al., 2007; Samuel et al., 2007), and Japanese encephalitis virus infection promotes caspase 3 cleavage in both human medulloblastoma and mouse neuroblastoma cells (Tsao et al., 2008; Yang et al., 2009). However, these studies have

not explored in detail the upstream causes of caspase 3 activation, and it will be interesting for future studies to explore whether altered nucleotide levels and AMPK activation lead to apoptosis during infection by these and other flaviviruses.

Our study describes key metabolic differences between ZIKV infection of human and C6/36 mosquito cells, provides a link between AMPK activation and cell death during infection, and sets the stage for further studies to examine whether metabolic reprogramming plays a role in the vector supporting ZIKV replication without impaired health *in vivo*.

LIMITATIONS OF THE STUDY

We show ZIKV-induced metabolic rewiring of multiple human cell lines and ZIKV-induced promotion of AMPK phosphorylation in human cells *in vitro* and mouse brain tissue *in vivo*. However, since our findings on ZIKV-induced metabolic rewiring of mosquito cells were derived from only one mosquito cell line, they may not be reflective of the metabolic changes conferred by ZIKV at the organismal level in mosquitoes. Studies in mosquitoes is currently limited due to limited availability of mosquito cell lines, particularly those that are permissive to ZIKV replication. Additionally, since *in vivo* tissue metabolism varies greatly from *in vitro* cell culture conditions, future studies should determine metabolic changes conferred by Zika infection in *in vivo* models of different species.

STAR METHODS

CONTACT FOR REAGENT AND RESOURCE SHARING

Further information and requests for resources and reagents should be directed to and will be fulfilled by the Lead Contact, Heather Christofk (hchristofk@mednet.ucla.edu).

EXPERIMENTAL MODEL AND SUBJECT DETAILS

Vero, Human foreskin fibroblast (HFF-1), *Aedes albopictus* C6/36, and Aedes cells were obtained from the ATCC and cultured in DMEM high glucose medium supplemented with 10% fetal bovine serum and 1% penicillin/streptomycin. Vero and HFF-1 cells were maintained at 37°C with 5% CO_2, while C6/36 cells were maintained at 28°C with 5% CO_2. Human fetal retinal pigment epithelial (FRPE) cells were kindly provided by Dr. Guoping Fan at UCLA with required informed consent described in previously published reports (Liao et al., 2010) (Liu et al., 2014). Use of this established hFRPE line for the study was approved by the Cedars-Sinai Medical Center Institutional Biosafety Committee (IBC). hFRPE cells were grown in DMEM high glucose medium supplemented with 10% fetal bovine serum and 1% penicillin/streptomycin. FRPEs were originally isolated from fetal retina (~20-week-old) using a previously published protocol (Sonoda et al., 2009) and were incubated at 37°C with 5% CO_2. Since the hFRPE line is deidentified, information on the sex of the line is unavailable.

Mice

All animal experiements in the study were approved by the Institutional Animal Care and Use Committee (IACUC). 4-6 week old male *Ifnar1*-/- (A129 or IFN-αβR-KO; strain: B6.129S2-Ifnar1tm1Agt) mice (Jackson Laboratory) were used for the *in vivo* ZIKV infection experiments. Mice were housed at Cedars-Sinai Medical Center Vivarium at 37°C with 12 hour light/dark cycles and fed autoclaved rodent chow.

METHOD DETAILS

Zika Virus Generation and Plaque Assay

Zika virus (ZIKV) Puerto Rico strain PRVABC-59 (GenBank number KU501215) was obtained through distribution from the United States Center for Disease Control and Prevention (CDC). Virus stocks were produced by collecting cell-free supernatant from infected C6/36 cell culture 6

days after infection at a multiplicity of infection (MOI) of 0.01. Virus titers were determined in duplicate by plaque assay in Vero cells as described previously (Gong et al., 2018). Briefly, 60,000 Vero cells were seeded in 12-well plates 24 hours before infection, then infected with ZIKV for 1 h with gentle shaking every 15 min and overlaid with 1% methylcellulose (Sigma). Four days later, cells were fixed and stained with 1% crystal violet in 20% ethanol, and plaques were counted to determine the titer.

Zika virus infection of HFF-1, C6/36, or FRPE cells

HFF-1, C6/36, or FRPE cells were seeded at subconfluency prior to ZIKV infection. After 24-hours, ZIKV inoculum, with a multiplicity of infection of 1 (for FRPE cells) or 3 (for HFF-1 and C6/36 cells), was formulated using the base media specified for each cell type. A total of 1 ml of viral inoculum was added to each well and the plates were incubated at 37 °C with 5% CO_2 for 2-4 hours. After the incubation period, the base media was replaced with complete media at a volume of 3 mL per well. For the uninfected (mock) group, each cell type received the specified cell-growth media that was concurrently used to prepare the viral inoculum, as described above. At the end of each timepoint, cell lysates and RNA were harvested for downstream analyses.

Measurement of Glucose Consumption Rates and Lactate Production Rates

Cellular glucose consumption and lactate production rates were measured using a Nova Biomedical BioProfile Basic Analyzer. Briefly, cells were seeded in triplicate in 6-well plates at 50% confluency to ensure that the measurements would be taken when the cells were subconfluent. Twenty-four hours post-seeding, the media was refreshed for all cells and cells were either mock-infected or infected with ZIKV at an MOI of 3. Media was also added to empty wells as a blank control. After the indicated duration of infection, 1 mL of media was removed from each sample and the blank control, and media samples were analyzed in the Nova BioProfile

Basic Analyzer. Cell numbers were determined using a Beckman Coulter particle analyzer and used to normalize the calculated rates.

Intracellular metabolite extraction and analysis

Cells were seeded in six-well plates, infected with ZIKV at a MOI of 3 for the listed duration of time, and metabolites were extracted at 70–80% confluence. Medium was replaced with medium containing the U-$^{13}C_6$-glucose at the time of infection. Cells were washed with ice-cold 150 mM ammonium acetate (pH 7.3) and scraped off the plate in 800 µl ice-cold 50% methanol. 10 nmol norvaline was added as an internal standard, followed by 400 µl chloroform. Following vigorous vortexing, samples were centrifuged at maximum speed, the aqueous layer was transferred to a glass vial and the metabolites were dried under an EZ-2Elite evaporator. Metabolites were resuspended in 50 µl 70% acetonitrile (ACN) and 5 µl of this solution used for the mass spectrometer-based analysis. The analysis was performed on a Q Exactive (Thermo Scientific) in polarity-switching mode with positive voltage 4.0 kV and negative voltage 4.0 kV. The mass spectrometer was coupled to an UltiMate 3000RSLC (Thermo Scientific) UHPLC system. Mobile phase A was 5 mM NH_4AcO, pH 9.9, B was ACN and the separation achieved on a Luna 3 mm NH2 100 A (150 × 2.0 mm) (Phenomenex) column. The flow was 200 µl min^{-1}, and the gradient ran from 15% A to 95% A in 18 min, followed by an isocratic step for 9 min and re-equilibration for 7 min. Metabolites were detected and quantified as area under the curve based on retention time and accurate mass (≤3 p.p.m.) using the TraceFinder 3.1 (Thermo Scientific) software. Relative amounts of metabolites between various conditions, as well as percentage of labelling, were calculated and corrected for naturally occurring ^{13}C abundance.

Viral Growth Analysis

C6/36 or HFF-1 cells were seeded in 12-well plates 24 hours before infection to generate a monolayer of 80% confluence. Cells were inoculated with ZIKV for 1 hour at an MOI of 3 for single step growth analysis. The inoculum was removed, the infected monolayer was rinsed with phosphate-buffered saline (PBS), and fresh medium was replenished. Cell-free virus was collected in the medium at indicated times post-infection, and viral titer was determined by plaque assay.

Immunofluorescence and Brightfield Imaging

Intracellular localization of proteins of interest was analyzed by using an immunofluorescence assay. Cells were seeded in 12-well plates 24hr prior to ZIKV infection. At the indicated times post-infection, the cells were washed with PBS, fixed with 4% paraformaldehyde for 20 minutes, permeabilized with 0.1% Triton for 15 minutes, and blocked with 5% fetal bovine serum in PBS at room temperature for 30 min. Cells were incubated with primary antibodies, including Cell Signaling Phospho-AMPKα (Thr172) (40H9) rabbit mAb #2535 (1:100) and EMD Millipore mouse anti-Flavivirus Group Antigen (MAB10216) (1:1000) for 30 minutes at room temperature and subsequently labeled with secondary antibodies coupled to Alexa Fluor 488 (Invitrogen-Molecular Probes). Cells were stained with DAPI for DNA staining and visualized using a Nikon Eclipse Ti Immunofluroscence Microscope with 30 Nikon Intenselight C-HGFI using the 63X/1.40-0.60 oil lens.

Western Blotting

Cells were lysed in 50 mM Tris pH 7.4, 1% NP-40, 0.25% sodium deoxycholate, 1 mM EDTA, 150 mM NaCl, 1 mM Na_3VO_4, 20 mM NaF, 1mM PMSF, 2 μg ml^{-1} aprotinin, 2 μg ml^{-1} leupeptin and 0.7 μg ml^{-1} pepstatin. Protein concentrations of cell extracts were determined by the Bradford assay. Western blot analysis was carried out as previously described (Thai et al., 2015). The following antibodies were used as probes: Actin (Abcam; 1:1000), Phospho-

AMPKα Thr172 (Cell Signaling #2535; 1:1000), AMPKα (Cell Signaling #2532; 1:1000), Caspase 3 (Cell Signaling #9662; 1:1000), Cleaved Caspase 3 (Asp175) 5A1E (Cell Signaling #9664; 1:1000), pACC1 (Ser79) D7D11 (Cell Signaling #11818; 1:1000), ACC1 (Cell Signaling #4190; 1:1000).

Nucleotide Rescue Experiments

Cells were seeded at subconfluency in 6-well plates. The next day, 200μM of adenine (Sigma A2786) and 200μM of uridine (Sigma U3003) were added to cell media versus an equal volume water-only control concurrently with ZIKV infection at an MOI of 3. After 48 hours incubation period, cell numbers were determined using a Beckman Coulter particle analyzer.

***In vivo* mouse model of ZIKV infection**

4-6-week old *Ifnar1*$^{-/-}$ male mice were inoculated with phosphate buffered saline (PBS) (n=5 mice) or PRVABC ZIKV (1 x10^6 pfu per mouse in a 40 μl volume) (n=5 mice) by subcutaneous route in the hind limb region under isoflurane anesthesia. Tissues were collected at 7 dpi.

Compound C Experiments

An antiviral analysis screen of Dorsomorphin (Compound C) (Abcam) in a dose-response was performed in fetal retinal pigment epithelial cells. RPE cells were seeded at a cell density of 5 x 10^3 cells per well in 96-well plates and 10 x 10^3 cells per well in 48-well plates. Sixteen hours later, cells were infected with ZIKV at an MOI of 1 or 10 for 1 hour and Compound C was added to cells to a final concentration of 1uM or 5uM. Infected cells were subjected to cell viability and apoptosis assays two days later. RNA was isolated from the same cells for quantification of the ZIKV genome.

Caspase 3/7 Assay

Caspase-Glo 3/7 Assay was performed as indicated in the manufacturer's protocol (Promega, USA). Briefly, at the 48 hours post-infection, ZIKV infected and mock-infected FRPE or C6/36 cells were incubated with the pro-luminescent caspase-3/7 substrate for 1 hour at room temperature. Following incubation, 100 µL of lysate was transferred to a white 96-well microtiter plate and the luminescence signal was read using a luminometer (Glomax Microplate Luminometer, Promega).

Mouse brain tissue immunohistochemistry

Brain tissue was incubated in 4% PFA for an hour and transferred to PBS. Tissues were then submerged in 10%, 20%, and 30% sucrose for an hour each. Tissue was then embedded in OCT (Fisher Healthcare) and incubated overnight at -80°C. Tissues were cut (6 µm thick) using a Leica cryostat microtome and mounted on Super Frost microscope slides (VWR). Sections were washed 3 times and permeabilized using blocking buffer (0.3% Triton X-100, 0.1% BSA, in 1 X PBS) for 1 hour at room temperature. For ZIKV staining, sections were incubated overnight at 4℃ with a polyclonal anti-ZIKV Envelope protein antibody (rabbit, 1:250) (GeneTex) or anti-Phospho-AMPKα (Thr172) (clone 40H9) (Rabbit, 1:150). The sections were then rinsed with 1X PBS three times and incubated with secondary antibody, Alexa Fluor-conjugated 488 or 555 antibodies (raised in rabbit, 1:1000; or mouse, 1:1000) for 1 hour at room temperature. Nucleus was stained with DAPI (4',6-Diamidino-2-Phenylindole, Dihydrochloride) (Life Technologies) at a dilution of 1:1000 in blocking buffer. Image acquisition was done using the Zeiss LSM 700 confocal microscope. The Zeiss imaging software was used with the maximum intensity projection feature to capture images. Image J's plug-in cell counter feature was used to count the positively stained cells by a double blinded approach. The mean positively-stained cells from 4 independent images were calculated.

AICAR Experiment

C6/36 cells were treated with water or 300 μM AICAR (Sigma A9978) dissolved in water and simultaneously mock-infected or infected with ZIKV at an MOI of 3. 48 hours post-infection, cells were collected and cell viability measurements using trypan blue staining or cleaved caspase 3/7 activity were determined. Light microscope images were taken with the Zeiss Axiovert.

QUANTIFICATION AND AND STATISTICAL ANALYSIS

All numerical data were calculated and plotted with mean +/- s.d. Results were analyzed using Graphpad Prism 8 software. Normality was determined by the Shapiro-Wilk test, followed by unpaired Student's *t*-test for normally distributed data. Multiple group comparisons were made by ANOVA with Student's t-test post-tests used between groups. Differences were considered statistically significant when $p<0.05$ (*) or $p<0.01$ (**) or $p<0.005$ (***). Additional statistical parameters can be found in the figure legends.

ACKNOWLEDGMENTS

We thank Dr. Guoping Fan (UCLA) for providing the human fetal retinal pigment epithelial cells used in the experiments. We thank Dr. Laura Martinez for technical assistance. S.K.T. is a pre-doctoral fellow supported by the UCLA Virology and Gene Therapy Training Grant (T32AI060567) and UCLA Tumor Immunology Training Grant (USHHS Ruth L. Kirschstein Institutional National Research Service Award #T32 CA009056). H.R.C. was supported by a Research Scholar Grant, RSG-16-111-01-MPC, from the American Cancer Society, NIH/NCI RO1 CA215185-01, and the UCLA Jonsson Comprehensive Cancer Center and Eli and Edythe Broad Center for Regenerative Medicine Ablon Scholars Program. V.A. was supported by a California Institute for Regenerative Medicine (CIRM) award DISC2-10188.

AUTHOR CONTRIBUTIONS

Shivani K. Thaker, Travis Chapa, Ren Sun, and Heather R. Christofk designed the study. Shivani K. Thaker and Heather R. Christofk wrote the manuscript. Shivani K. Thaker, Travis Chapa, Gustavo Garcia Jr., Danyang Gong, and Ernst W. Schmid performed experiments. Heather R. Christofk, Ren Sun, and Vaithilingaraga Arumugaswami supervised the project. All authors edited the manuscript.

DECLARATION OF INTERESTS

The authors declare no competing interests.

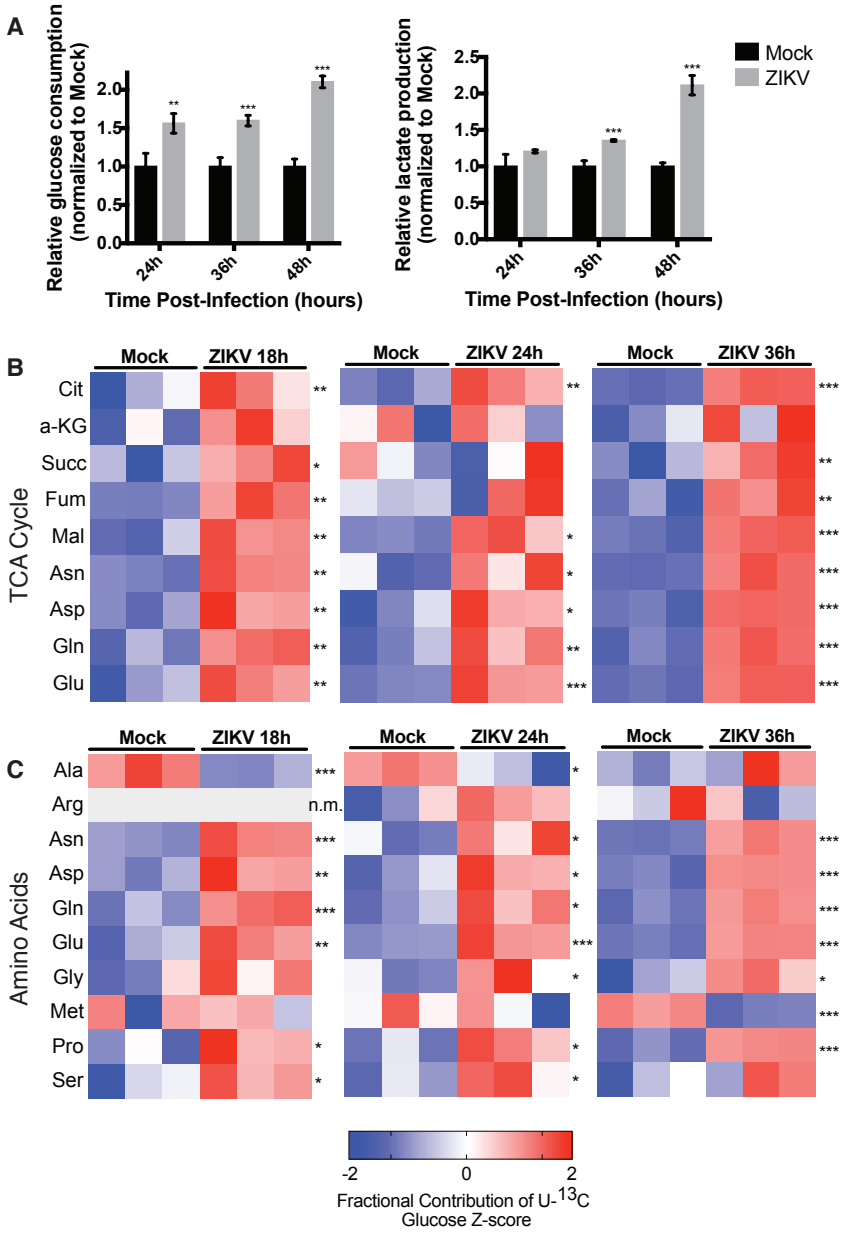

Figure 1. Zika virus infection alters glucose utilization in human foreskin fibroblasts. (A) HFF-1 cells were either mock-infected or infected by ZIKV at a MOI of 3, and glucose consumption and lactate production rates of host cells were measured at 24, 36, and 48 hours post-infection. Rates are normalized relative to mock-infected cells. Data are represented as mean +/- s.d. (B) HFF-1 cells were labeled with U-^{13}C glucose and metabolites were extracted at 18, 24, and 36 hours post-ZIKV infection and analyzed via LC-MS. Z-scores of the fractional contribution of U-

$^{13}C_6$-glucose into TCA cycle intermediates are displayed in the heatmaps. (C) Mock- and ZIKV-infected HFF-1 cells were labeled with U-$^{13}C_6$-glucose and fractional contribution of glucose into amino acids are quantified by z-scores. *n.m.* indicates that the metabolite was not measured. *p*-values were calculated using Student's *t*-test and error bars indicate s.d. (n=3), **p* < 0.05, ***p* < 0.01, ****p* < 0.005.

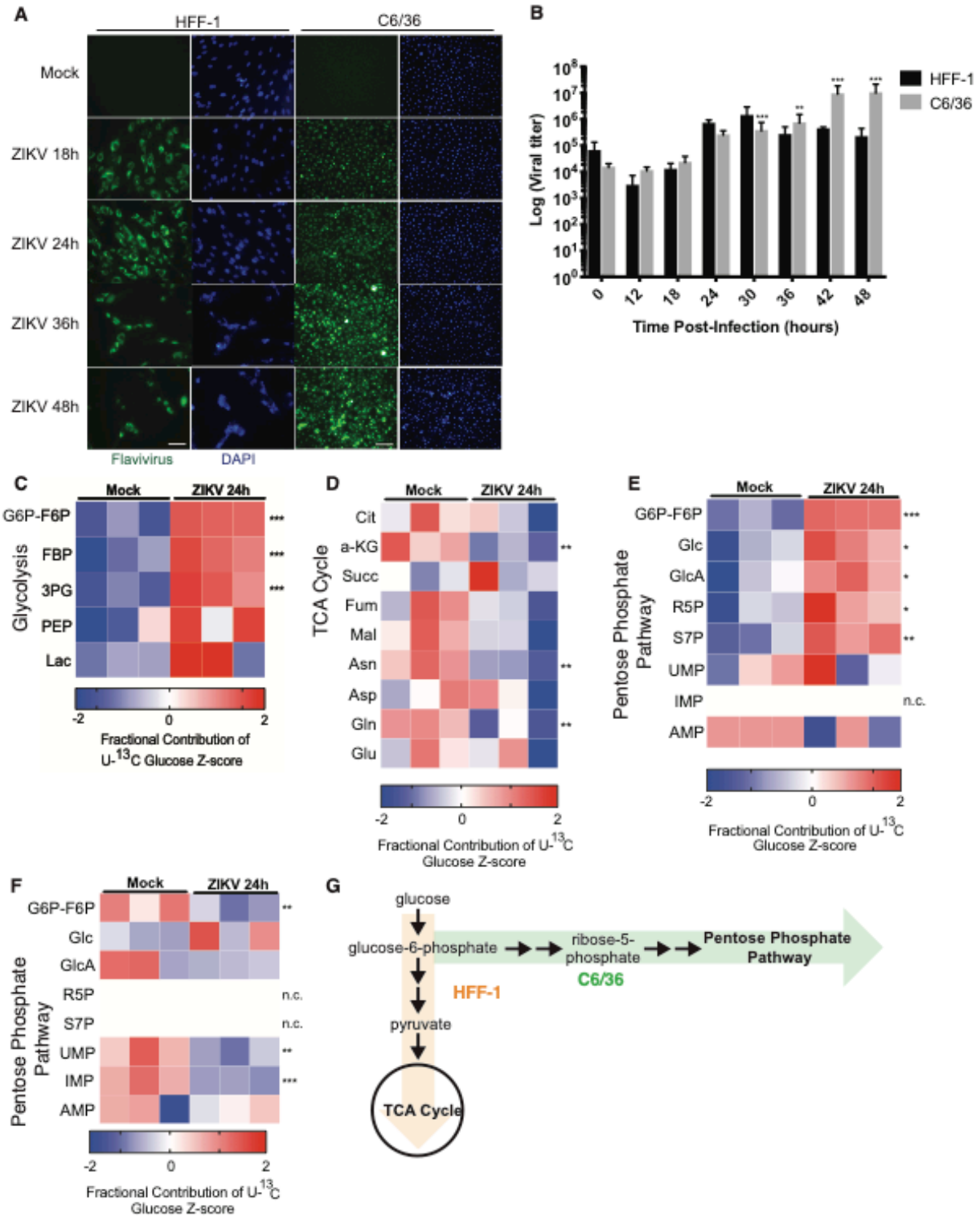
A
HFF-1
C6/36
Mock
ZIKV 18h
ZIKV 24h
ZIKV 36h
ZIKV 48h
Flavivirus
DAPI
B
Log (Viral titer)
Time Post-Infection (hours)
HFF-1
C6/36
C
Mock
ZIKV 24h
Glycolysis
G6P-F6P
FBP
3PG
PEP
Lac
Fractional Contribution of U-13C Glucose Z-score
D
TCA Cycle
Cit
a-KG
Succ
Fum
Mal
Asn
Asp
Gln
Glu
Fractional Contribution of U-13C Glucose Z-score
E
Pentose Phosphate Pathway
G6P-F6P
Glc
GlcA
R5P
S7P
UMP
IMP
AMP
n.c.
Fractional Contribution of U-13C Glucose Z-score
F
Pentose Phosphate Pathway
G6P-F6P
Glc
GlcA
R5P
S7P
UMP
IMP
AMP
n.c.
Fractional Contribution of U-13C Glucose Z-score
G
glucose
glucose-6-phosphate
ribose-5-phosphate
Pentose Phosphate Pathway
HFF-1
C6/36
pyruvate
TCA Cycle

Figure 2. Zika virus infection differentially impacts survival and glucose metabolism of human versus C6/36 mosquito cells. (A) HFF-1 and C6/36 mosquito cells were mock-infected or infected with ZIKV at an MOI of 3 and visualized via immunofluorescence by DAPI staining (blue) and Flavivirus envelope protein staining (green). Scale bar, 20 μM. (B) HFF-1 and C6/36 mosquito cells were infected with ZIKV at an MOI of 3. Cell-free supernatant was collected from infected cultures at indicated times post infection, and virus titers were determined in duplicate by plaque assay in Vero cells (n=4). (C) Mock- and ZIKV-infected C6/36 cells were labeled with U-$^{13}C_6$-glucose for 24 hours and metabolites were extracted and analyzed via LC-MS. Fractional contribution of labeled glucose into glycolytic intermediates, (D) TCA cycle intermediates, and (E) pentose phosphate pathway intermediates were quantified and displayed as z-scores. (F) HFF-1 cells were labeled with U-$^{13}C_6$-glucose and mock- or ZIKV-infected. Metabolites were extracted and analyzed via LC-MS to determine fractional contribution of glucose to pentose phosphate pathway intermediates. (G) Schematic of glucose metabolite tracing data in HFF-1 (orange) versus C6/36 cells (green). *n.c.* indicates there was no change in fractional contribution between groups measured. *p*-values were calculated using Student's *t*-test and error bars indicate s.d. (n=3), **p* < 0.05, ***p* < 0.01, ****p* < 0.005.

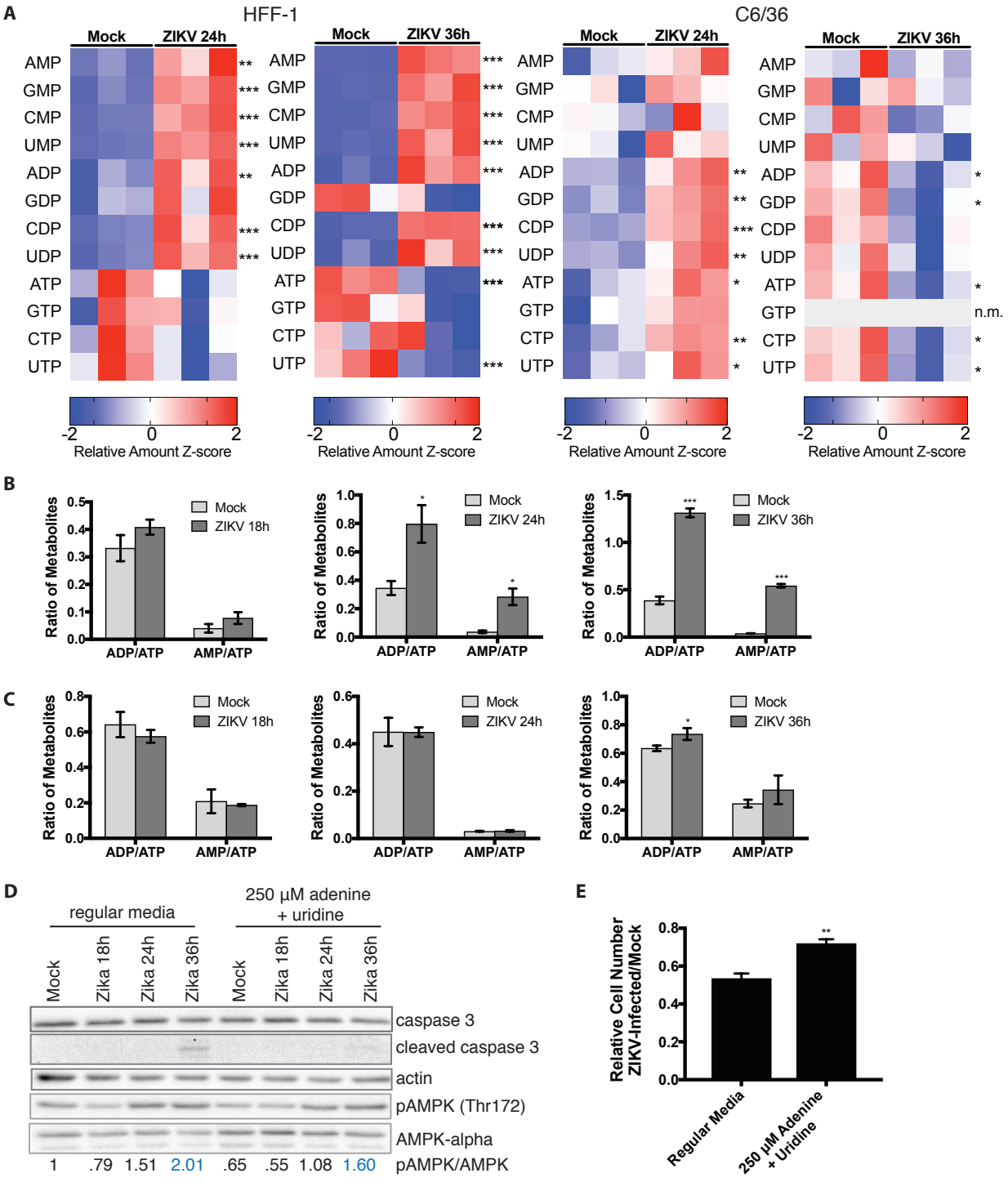
A
HFF-1
C6/36
Mock
ZIKV 24h
ZIKV 36h
AMP
GMP
CMP
UMP
ADP
GDP
CDP
UDP
ATP
GTP
CTP
UTP
n.m.
Relative Amount Z-score
B
C
Ratio of Metabolites
ADP/ATP
AMP/ATP
Mock
ZIKV 18h
ZIKV 24h
ZIKV 36h
D
regular media
250 µM adenine
+ uridine
Mock
Zika 18h
Zika 24h
Zika 36h
caspase 3
cleaved caspase 3
actin
pAMPK (Thr172)
AMPK-alpha
1 .79 1.51 2.01 .65 .55 1.08 1.60 pAMPK/AMPK
E
Relative Cell Number
ZIKV-Infected/Mock
Regular Media
250 µM Adenine
+ Uridine

Figure 3. Zika virus infection selectively depletes nucleotide triphosphates in human but not C6/36 mosquito cells. (A) Metabolites were extracted from mock- or ZIKV-infected HFF-1 (left) and C6/36 (right) cells and quantified via LC-MS. Z-scores of the relative amounts of nucleotides are displayed in the heatmaps. (B) AMP/ATP and ADP/ATP ratios in mock- versus ZIKV-infected HFF-1 cells. (C) AMP/ATP and ADP/ATP ratios from mock- versus ZIKV-infected C6/36 cells. (D) Immunoblots from lysates collected from mock- vs. ZIKV-infected HFF-1 cells at indicated time points. Cells were either cultured in normal media (left) or in media supplemented with 250 μM exogenous adenine and uridine (right). Lysates were probed for total and cleaved caspase 3 levels, pAMPK (Thr172) and AMPK-alpha levels. Actin was used as a loading control. The pAMPK/AMPK ratios are quantified at the bottom as a readout of AMPK activation. (E) HFF-1 cells were mock-infected or ZIKV-infected and cultured in regular vs. adenine and uridine-supplemented media. The relative ZIKV/mock-infected cell counts were measured and displayed in the bar graph. *n.m.* indicates that the metabolite was not measured. Data are represented as mean +/- s.d. *p*-values were calculated using Student's *t*-test and error bars indicate s.d. (n=3), $*p < 0.05$, $**p < 0 .01$, $***p < 0.005$.

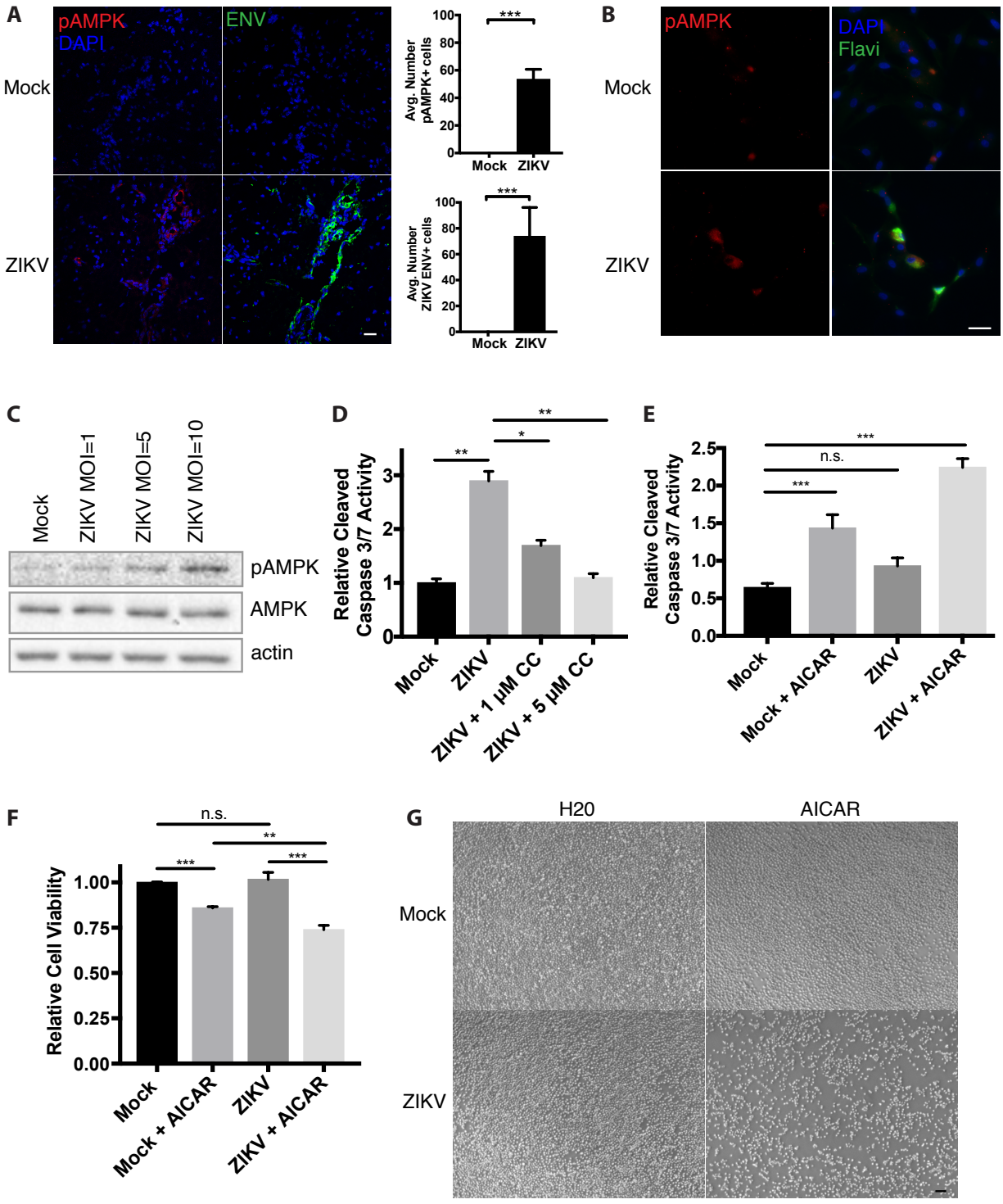
A
pAMPK
DAPI
ENV
Mock
ZIKV
Avg. Number pAMPK+ cells
Avg. Number ZIKV ENV+ cells
***
Mock
ZIKV
B
pAMPK
DAPI
Flavi
C
Mock
ZIKV MOI=1
ZIKV MOI=5
ZIKV MOI=10
pAMPK
AMPK
actin
D
Relative Cleaved Caspase 3/7 Activity
Mock
ZIKV
ZIKV + 1 μM CC
ZIKV + 5 μM CC
E
Relative Cleaved Caspase 3/7 Activity
n.s.
Mock
Mock + AICAR
ZIKV
ZIKV + AICAR
F
Relative Cell Viability
n.s.
Mock
Mock + AICAR
ZIKV
ZIKV + AICAR
G
H20
AICAR
Mock
ZIKV

Figure 4. Zika virus infection increases AMPK phosphorylation and contributes to cell death in clinically relevant models. (A) Immunohistochemistry of pAMPK, ZIKV envelope (ENV) protein, and DAPI staining of brain tissue slices from *Ifnar1*-/- mice infected subcutaneously with ZIKV. IHC staining quantification was performed using a series of 4 mouse brain tissue sections per condition and ImageJ software to count cells that stain positive for pAMPK of ZIKV ENV foci. Scale bar, 25 μM. (B) Immunofluoresence of pAMPK, Flavivirus envelope protein (Flavi), and DAPI staining of hFRPE cells 48 hours post-infection with ZIKV at a MOI of 1. Scale bar, 25 μM. (C) pAMPK and AMPK immunoblots on lysates from hFRPE cells mock-infected and infected by ZIKV at MOIs = 1, 5, 10. Actin was used as a loading control. (D) hFRPE cells were mock- and ZIKV-infected for 48 hours and relative cleaved caspase 3/7 activities were measured in cells that were DMSO-treated or treated with 1 μM and 5 μM Compound C. Data are represented as mean +/- s.d. (E) C6/36 cells were mock-infected or infected with ZIKV at a MOI of 3 and treated with water (H_20) or 300 μM AICAR (dissolved in water) for 48 hours and cleaved caspase 3/7 activity was measured 48 hours post-infection or treatment of C6/36 cells. (F) Cell viability measurements were performed using trypan blue exclusion 48 hours post-infection of treatment of C6/36 cells in (E). (G) Light microscope images of C6/36 cells mock-infected or infected with ZIKV taken at 48 hours post-infection. Scale bar, 20 μM.

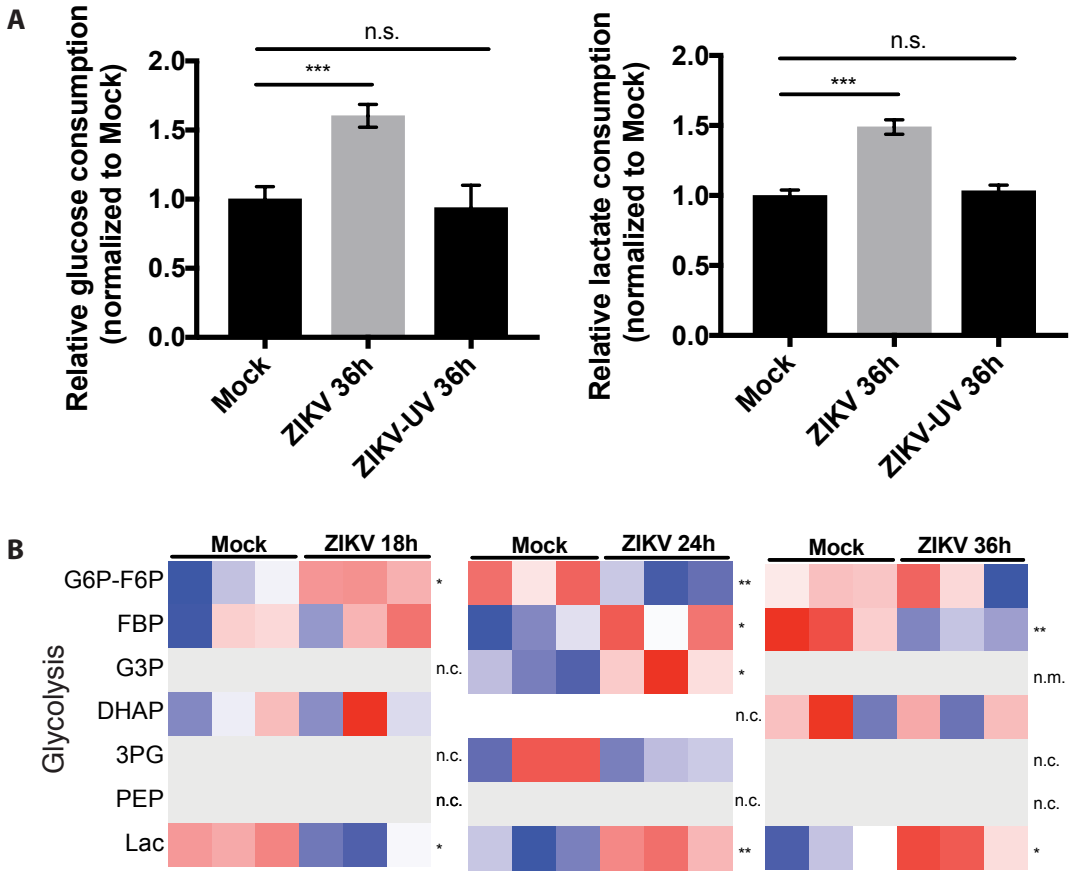

Supplementary Figure 1. Related to Figure 1. Glycolytic metabolism is actively reprogrammed by ZIKV infection. (A) HFF-1 cells were mock-infected, infected by ZIKV (MOI=3), or infected by UV-inactivated ZIKV for 36 hours and glucose consumption and lactate production were measured at 36 hours post-infection. Data are represented as mean +/- s.d. (B) HFF-1 cells were labeled with U-13C glucose and metabolites were extracted 18, 24, and 36 hours post-ZIKV infection and analyzed via LC-MS/MS to determine fractional contribution into glycolytic intermediates. n.m. indicates that the metabolite was not measured. n.c. indicates that there was no change in the fractional contribution for that metabolite between conditions.

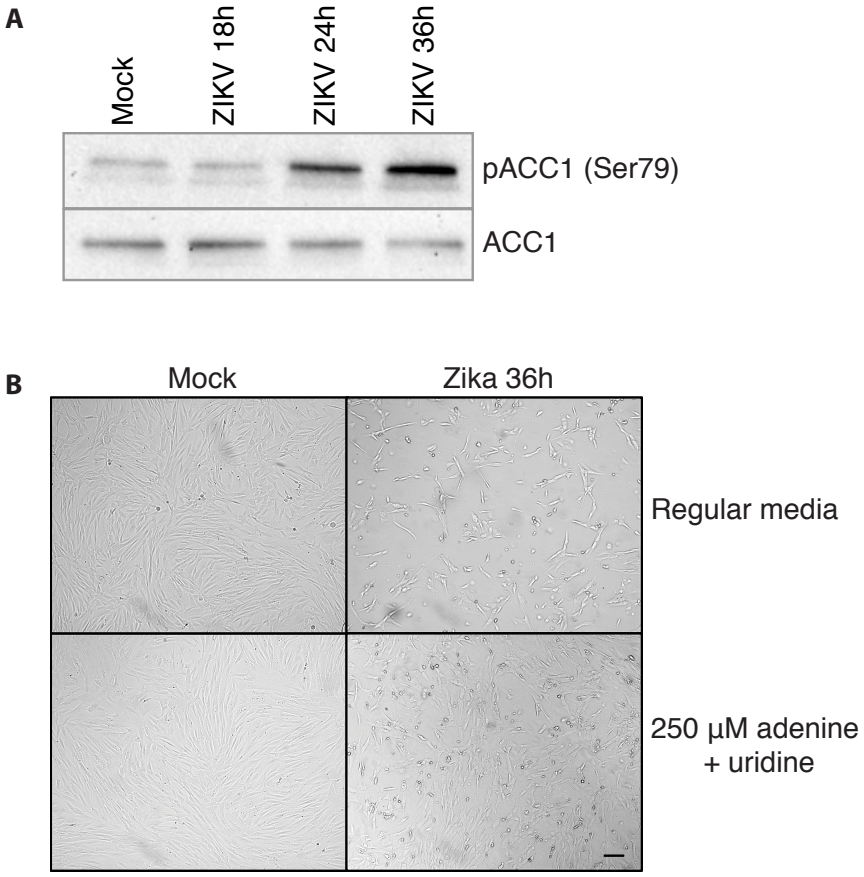

Supplementary Figure 2. Related to Figure 3. (A) HFF-1 cells mock-infected or infected with ZIKV for 18, 24, or 36 hours were lysed and Western. (B) HFF-1 cells were mock-infected or infected with ZIKV and cultured in regular media or media containing 250 μM adenine and uridine for 36 hours. Light microscopy images are shown in the figure. Scale bar, 20 μM.

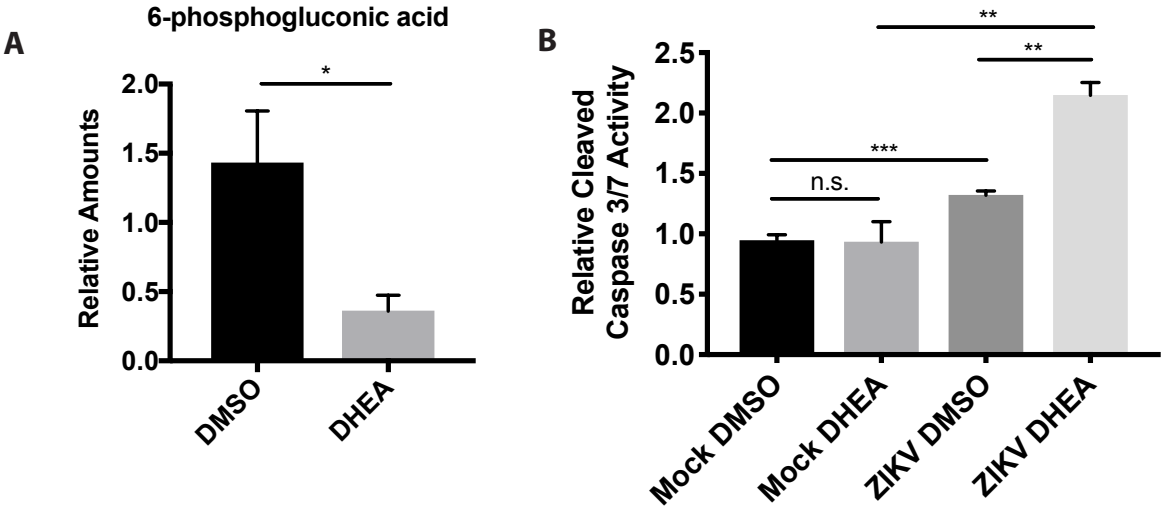

Supplementary Figure 3. Related to Figure 4. (A) C6/36 cells were treated with 50uM DHEA and 6-phosphogluconate levels were measured by LC-MS metabolomics to confirm reduction of G6PD activity. (B) Cleaved caspase 3/7 activity was measured in C6/36 cells following treatment of DMSO or with DMSO or DHEA (50uM) and mock-infection or ZIKV-infection for 48 hours. Data are represented as mean +/- s.d.

REFERENCES

Allonso, D., Andrade, I.S., Conde, J.N., Coelho, D.R., Rocha, D.C., da Silva, M.L., Ventura, G.T., Silva, E.M., and Mohana-Borges, R. (2015). Dengue Virus NS1 Protein Modulates Cellular Energy Metabolism by Increasing Glyceraldehyde-3-Phosphate Dehydrogenase Activity. Journal of virology *89*, 11871-11883.

Balmaseda, A., Stettler, K., Medialdea-Carrera, R., Collado, D., Jin, X., Zambrana, J.V., Jaconi, S., Cameroni, E., Saborio, S., Rovida, F., et al. (2017). Antibody-based assay discriminates Zika virus infection from other flaviviruses. Proc Natl Acad Sci U S A *114*, 8384-8389.

Baud, D., Gubler, D.J., Schaub, B., Lanteri, M.C., and Musso, D. (2017). An update on Zika virus infection. Lancet *390*, 2099-2109.

Ciota, A.T., Bialosuknia, S.M., Ehrbar, D.J., and Kramer, L.D. (2017). Vertical Transmission of Zika Virus by Aedes aegypti and Ae. albopictus Mosquitoes. Emerg Infect Dis *23*, 880-882.

Cunha, M.S., Esposito, D.L., Rocco, I.M., Maeda, A.Y., Vasami, F.G., Nogueira, J.S., de Souza, R.P., Suzuki, A., Addas-Carvalho, M., Barjas-Castro Mde, L., et al. (2016). First Complete Genome Sequence of Zika Virus (Flaviviridae, Flavivirus) from an Autochthonous Transmission in Brazil. Genome Announc *4*.

Daep, C.A., Munoz-Jordan, J.L., and Eugenin, E.A. (2014). Flaviviruses, an expanding threat in public health: focus on dengue, West Nile, and Japanese encephalitis virus. J Neurovirol *20*, 539-560.

de Oliveira, W.K., Carmo, E.H., Henriques, C.M., Coelho, G., Vazquez, E., Cortez-Escalante, J., Molina, J., Aldighieri, S., Espinal, M.A., and Dye, C. (2017). Zika Virus Infection and Associated Neurologic Disorders in Brazil. N Engl J Med *376*, 1591-1593.

de Paula Freitas, B., de Oliveira Dias, J.R., Prazeres, J., Sacramento, G.A., Ko, A.I., Maia, M., and Belfort, R., Jr. (2016). Ocular Findings in Infants With Microcephaly Associated With Presumed Zika Virus Congenital Infection in Salvador, Brazil. JAMA Ophthalmol.

Diamond, D.L., Syder, A.J., Jacobs, J.M., Sorensen, C.M., Walters, K.A., Proll, S.C., McDermott, J.E., Gritsenko, M.A., Zhang, Q., Zhao, R., et al. (2010). Temporal proteome and lipidome profiles reveal hepatitis C virus-associated reprogramming of hepatocellular metabolism and bioenergetics. PLoS Pathog *6*, e1000719.

Dolan, A., Cunningham, C., Hector, R.D., Hassan-Walker, A.F., Lee, L., Addison, C., Dargan, D.J., McGeoch, D.J., Gatherer, D., Emery, V.C., et al. (2004). Genetic content of wild-type human cytomegalovirus. J Gen Virol *85*, 1301-1312.

Everett, H., and McFadden, G. (1999). Apoptosis: an innate immune response to virus infection. Trends Microbiol *7*, 160-165.

Fontaine, K.A., Sanchez, E.L., Camarda, R., and Lagunoff, M. (2015). Dengue virus induces and requires glycolysis for optimal replication. Journal of virology *89*, 2358-2366.

Garcia, D., and Shaw, R.J. (2017). AMPK: Mechanisms of Cellular Energy Sensing and Restoration of Metabolic Balance. Mol Cell *66*, 789-800.

Gong, D., Zhang, T.-H., Zhao, D., Du, Y., Chapa, T.J., Shi, Y., Wang, L., Contreras, D., Zeng, G., Shi, P.-Y., et al. (2018). High-Throughput Fitness Profiling of Zika Virus E Protein Reveals Different Roles for Glycosylation during Infection of Mammalian and Mosquito Cells. iScience *1*, 97-111.

Grard, G., Caron, M., Mombo, I.M., Nkoghe, D., Mboui Ondo, S., Jiolle, D., Fontenille, D., Paupy, C., and Leroy, E.M. (2014). Zika virus in Gabon (Central Africa)--2007: a new threat from Aedes albopictus? PLoS Negl Trop Dis *8*, e2681.

Hamel, R., Dejarnac, O., Wichit, S., Ekchariyawat, P., Neyret, A., Luplertlop, N., Perera-Lecoin, M., Surasombatpattana, P., Talignani, L., Thomas, F., et al. (2015). Biology of Zika Virus Infection in Human Skin Cells. Journal of virology *89*, 8880-8896.

Hanners, N.W., Eitson, J.L., Usui, N., Richardson, R.B., Wexler, E.M., Konopka, G., and Schoggins, J.W. (2016). Western Zika Virus in Human Fetal Neural Progenitors Persists Long Term with Partial Cytopathic and Limited Immunogenic Effects. Cell Rep *15*, 2315-2322.

Huang, W.C., Abraham, R., Shim, B.S., Choe, H., and Page, D.T. (2016). Zika virus infection during the period of maximal brain growth causes microcephaly and corticospinal neuron apoptosis in wild type mice. Sci Rep *6*, 34793.

Jimenez de Oya, N., Blazquez, A.B., Casas, J., Saiz, J.C., and Martin Acebes, M.A. (2018). Direct Activation of Adenosine Monophosphate-Activated Protein Kinase (AMPK) by PF-06409577 Inhibits Flavivirus Infection through Modification of Host-Cell Lipid Metabolism. Antimicrob Agents Chemother.

Jung, G.S., Jeon, J.H., Choi, Y.K., Jang, S.Y., Park, S.Y., Kim, S.W., Byun, J.K., Kim, M.K., Lee, S., Shin, E.C., et al. (2016). Pyruvate dehydrogenase kinase regulates hepatitis C virus replication. Sci Rep *6*, 30846.

Jurado, K.A., Yockey, L.J., Wong, P.W., Lee, S., Huttner, A.J., and Iwasaki, A. (2018). Antiviral CD8 T cells induce Zika-virus-associated paralysis in mice. Nat Microbiol *3*, 141-147.

Karpf, A.R., and Brown, D.T. (1998). Comparison of Sindbis virus-induced pathology in mosquito and vertebrate cell cultures. Virology *240*, 193-201.

Kleinschmidt, M.C., Michaelis, M., Ogbomo, H., Doerr, H.W., and Cinatl, J., Jr. (2007). Inhibition of apoptosis prevents West Nile virus induced cell death. BMC Microbiol *7*, 49.

Liang, Q., Luo, Z., Zeng, J., Chen, W., Foo, S.S., Lee, S.A., Ge, J., Wang, S., Goldman, S.A., Zlokovic, B.V., et al. (2016). Zika Virus NS4A and NS4B Proteins Deregulate Akt-mTOR Signaling in Human Fetal Neural Stem Cells to Inhibit Neurogenesis and Induce Autophagy. Cell Stem Cell *19*, 663-671.

Liao, J.L., Yu, J., Huang, K., Hu, J., Diemer, T., Ma, Z., Dvash, T., Yang, X.J., Travis, G.H., Williams, D.S., et al. (2010). Molecular signature of primary retinal pigment epithelium and stem-cell-derived RPE cells. Hum Mol Genet *19*, 4229-4238.

Liu, Z., Jiang, R., Yuan, S., Wang, N., Feng, Y., Hu, G., Zhu, X., Huang, K., Ma, J., Xu, G., et al. (2014). Integrated analysis of DNA methylation and RNA transcriptome during in vitro

differentiation of human pluripotent stem cells into retinal pigment epithelial cells. PLoS One *9*, e91416.

McArdle, J., Moorman, N.J., and Munger, J. (2012). HCMV targets the metabolic stress response through activation of AMPK whose activity is important for viral replication. PLoS Pathog *8*, e1002502.

Mihaylova, M.M., and Shaw, R.J. (2011). The AMPK signalling pathway coordinates cell growth, autophagy and metabolism. Nature cell biology *13*, 1016-1023.

Miner, J.J., and Diamond, M.S. (2017). Zika Virus Pathogenesis and Tissue Tropism. Cell Host Microbe *21*, 134-142.

Moser, T.S., Jones, R.G., Thompson, C.B., Coyne, C.B., and Cherry, S. (2010). A kinome RNAi screen identified AMPK as promoting poxvirus entry through the control of actin dynamics. PLoS Pathog *6*, e1000954.

Moser, T.S., Schieffer, D., and Cherry, S. (2012). AMP-activated kinase restricts Rift Valley fever virus infection by inhibiting fatty acid synthesis. PLoS Pathog *8*, e1002661.

Munger, J., Bennett, B.D., Parikh, A., Feng, X.J., McArdle, J., Rabitz, H.A., Shenk, T., and Rabinowitz, J.D. (2008). Systems-level metabolic flux profiling identifies fatty acid synthesis as a target for antiviral therapy. Nat Biotechnol *26*, 1179-1186.

O'Neill, K., Olson, B.J., Huang, N., Unis, D., and Clem, R.J. (2015). Rapid selection against arbovirus-induced apoptosis during infection of a mosquito vector. Proc Natl Acad Sci U S A *112*, E1152-1161.

Oh, Y., Zhang, F., Wang, Y., Lee, E.M., Choi, I.Y., Lim, H., Mirakhori, F., Li, R., Huang, L., Xu, T., et al. (2017). Zika virus directly infects peripheral neurons and induces cell death. Nat Neurosci *20*, 1209-1212.

Petersen, L.R., Jamieson, D.J., and Honein, M.A. (2016). Zika Virus. N Engl J Med *375*, 294-295.

Ramiere, C., Rodriguez, J., Enache, L.S., Lotteau, V., Andre, P., and Diaz, O. (2014). Activity of hexokinase is increased by its interaction with hepatitis C virus protein NS5A. Journal of virology *88*, 3246-3254.

Rosenfeld, A.B., Doobin, D.J., Warren, A.L., Racaniello, V.R., and Vallee, R.B. (2017). Replication of early and recent Zika virus isolates throughout mouse brain development. Proc Natl Acad Sci U S A *114*, 12273-12278.

Russell, W.C. (2009). Adenoviruses: update on structure and function. J Gen Virol *90*, 1-20.

Saiz, J.C., Vazquez-Calvo, A., Blazquez, A.B., Merino-Ramos, T., Escribano-Romero, E., and Martin-Acebes, M.A. (2016). Zika Virus: the Latest Newcomer. Front Microbiol *7*, 496.

Samuel, M.A., Morrey, J.D., and Diamond, M.S. (2007). Caspase 3-dependent cell death of neurons contributes to the pathogenesis of West Nile virus encephalitis. Journal of virology *81*, 2614-2623.

Sanchez, E.L., Pulliam, T.H., Dimaio, T.A., Thalhofer, A.B., Delgado, T., and Lagunoff, M. (2017). Glycolysis, Glutaminolysis, and Fatty Acid Synthesis Are Required for Distinct Stages of Kaposi's Sarcoma-Associated Herpesvirus Lytic Replication. Journal of virology *91*.

Sonoda, S., Spee, C., Barron, E., Ryan, S.J., Kannan, R., and Hinton, D.R. (2009). A protocol for the culture and differentiation of highly polarized human retinal pigment epithelial cells. Nat Protoc *4*, 662-673.

Tang, H., Hammack, C., Ogden, S.C., Wen, Z., Qian, X., Li, Y., Yao, B., Shin, J., Zhang, F., Lee, E.M., et al. (2016). Zika Virus Infects Human Cortical Neural Progenitors and Attenuates Their Growth. Cell Stem Cell *18*, 587-590.

Terry, L.J., Vastag, L., Rabinowitz, J.D., and Shenk, T. (2012). Human kinome profiling identifies a requirement for AMP-activated protein kinase during human cytomegalovirus infection. Proc Natl Acad Sci U S A *109*, 3071-3076.

Thai, M., Graham, N.A., Braas, D., Nehil, M., Komisopoulou, E., Kurdistani, S.K., McCormick, F., Graeber, T.G., and Christofk, H.R. (2014). Adenovirus E4ORF1-induced MYC activation promotes host cell anabolic glucose metabolism and virus replication. Cell Metab *19*, 694-701.

Thai, M., Thaker, S.K., Feng, J., Du, Y., Hu, H., Ting Wu, T., Graeber, T.G., Braas, D., and Christofk, H.R. (2015). MYC-induced reprogramming of glutamine catabolism supports optimal virus replication. Nat Commun *6*, 8873.

Tsao, C.H., Su, H.L., Lin, Y.L., Yu, H.P., Kuo, S.M., Shen, C.I., Chen, C.W., and Liao, C.L. (2008). Japanese encephalitis virus infection activates caspase-8 and -9 in a FADD-independent and mitochondrion-dependent manner. J Gen Virol *89*, 1930-1941.

Upton, J.W., and Chan, F.K. (2014). Staying alive: cell death in antiviral immunity. Mol Cell *54*, 273-280.

Vastag, L., Koyuncu, E., Grady, S.L., Shenk, T.E., and Rabinowitz, J.D. (2011). Divergent effects of human cytomegalovirus and herpes simplex virus-1 on cellular metabolism. PLoS Pathog *7*, e1002124.

Waris, G., Felmlee, D.J., Negro, F., and Siddiqui, A. (2007). Hepatitis C virus induces proteolytic cleavage of sterol regulatory element binding proteins and stimulates their phosphorylation via oxidative stress. Journal of virology *81*, 8122-8130.

Yang, T.C., Shiu, S.L., Chuang, P.H., Lin, Y.J., Wan, L., Lan, Y.C., and Lin, C.W. (2009). Japanese encephalitis virus NS2B-NS3 protease induces caspase 3 activation and mitochondria-mediated apoptosis in human medulloblastoma cells. Virus Res *143*, 77-85.

Yang, W., Hood, B.L., Chadwick, S.L., Liu, S., Watkins, S.C., Luo, G., Conrads, T.P., and Wang, T. (2008). Fatty acid synthase is up-regulated during hepatitis C virus infection and regulates hepatitis C virus entry and production. Hepatology *48*, 1396-1403.

CHAPTER 5

Conclusion and Future Directions

The work in this thesis demonstrates mechanisms by which two different viruses, adenovirus and Zika virus, reprogram host cell metabolism. In addition to promoting glucose metabolism, we show that adenovirus also increases glutaminolysis in infected cells through MYC activation by viral protein E4ORF1. Glutaminase, which modulates a critical step in glutamine metabolism, is important for optimal virus replication. Metabolic changes induced by adenovirus parallel metabolic phenotypes observed in many cancer cells and we use adenovirus infection as an approach to identify important metabolic enzymes in cancer, specifically ketohexokinase. Ketohexokinase promotes lung tumor growth by allowing cancer cells to evade negative feedback on PFK and increase glucose incorporation into nucleotides and other metabolites. Finally, we show that Zika virus infection differentially alters metabolism of infected human versus mosquito cells. Zika virus specifically depletes nucleotide triphosphates in human cells, leading to caspase-mediated cell death. Several major questions emerge from this work to follow up on for future studies and are described below.

Elucidating the roles of KHK splice variants, KHK-A and KHK-C, in lung tumor growth

KHK has two splice variants, KHK-A and KHK-C, both of which are the same molecular weight and differ only in the mutually exclusive splicing event of exon 3 (Hayward and Bonthron 1998). To determine whether KHK-A and KHK-C differentially contribute to tumor growth, we are currently overexpressing each splice variant in A549 KHK KO cells and assessing growth of cultured lung cancer cell lines as well as tumor xenografts in immunocompetent SCID or NSG mice. Our preliminary data suggests that KHK-A, but not KHK-C, promotes tumor growth in KHK KO xenografts derived from A549 cells (Figure 1). We are currently repeating this experiment. Nutrient tracer studies involving U-$^{13}C_6$-glucose and U-$^{13}C_6$-fructose infusion of mice will be informative to determine how knockout of each splice variant in the xenograft affects utilization of these key nutrients *in vivo.*

Additionally, we will further assess the role of KHK in tumor initiation and tumor progression in genetically engineered mouse models (GEMMs) of cancer. With the collaboration of Dr. David Shackelford (UCLA), this will be accomplished by crossing KHK-/- mice with inducible oncogene activation or tumor suppressor loss, namely $Kras^{G12D}$;$Lkb1^{-/-}$ (KL), $Kras^{G12D}$;$p53^{-/-}$ (KP), $Lkb1^{-/-}$;$p53^{-/-}$;$PTEN^{-/-}$ (LPP), and $Kras^{G12D}$;$p53^{-/-}$;$Lkb1^{-/-}$ (KPL) mice. In addition to assessing tumor initiation and growth in the previously mentioned GEMMs, we will also cross mice containing specific deletion of KHK-A or KHK-C and perform similar analysis to determine whether tumor initiation or tumor progression are specifically affected by loss of a particular KHK splice variant.

Another potential difference between KHK-A and KHK-C may be the subcellular localization of each splice variant. We have previously performed immunohistochemistry on tissue sections from GEMMs and xenografts derived from lung cancer cell lines and have observed both nuclear and cytoplasmic staining of total KHK. It would be interesting for future studies to determine whether KHK-A and KHK-C localize to different compartments in the cell and whether this can contribute to varying effects of each splice variant.

Regulation of KHK and polyol pathway

Since the polyol pathway has been studied primarily in the context of hyperglycemia and diabetes, we are interested in determining whether altering levels of glucose can alter flux or activity of the polyol pathway. We have cultured A549 cells in different concentrations of glucose and measured metabolites, extracted RNA, and cell lysate to assay KHK levels. To look at protein levels of KHK and polyol pathway genes, we serum starved cells overnight and cultured cells in either 1, 5, 10, 20 mM glucose for 48 hours. We have some preliminary evidence that suggests that increasing glucose concentrations in the media can lead to elevated total KHK levels and levels of KHK-A and KHK-C as well as increased SORD protein levels and GLUT5 levels (Figure 2A). Our preliminary data also suggests that this change may, at least in part, be

transcriptional as KHK and SORD mRNA levels are elevated at higher glucose concentrations in the same conditions (Figure 2B). We also wanted to see how enzymes in glycolysis are affected by increasing glucose concentrations in the media. Many glycolytic enzymes remain unaffected; however, there seems to be a slight increase in PFKM levels, which is intriguing because of the connection to KHK and the polyol pathway, which help bypass negative feedback on KHK (Figure 2C).

We are interested in understanding the sensing mechanism and the transcription factor(s) responsible for the induction of KHK with increasing glucose. Fructose has been shown to induce carbohydrate-response element-binding protein (ChREBP) (Koo, Miyashita et al. 2009) and high ChREBP activity correlates with higher KHK levels (Kim, Krawczyk et al. 2016).. Preliminary assessment of the KHK promoter and promoter of other genes also reveals putative MYC binding sites. We will infect NHBE cells with a mutant adenovirus containing a D68A point mutation in the E4ORF1 gene with impaired binding and activation of MYC (Thai, Graham et al. 2014) and compare with infection by ADWT to determine whether KHK is regulated by MYC in the context of adenovirus infection. Exploring whether or not KHK is regulated by the previously described transcription factors and others will provide important insight into regulation of KHK and the polyol pathway in the context of cancer.

Post-translational regulation of KHK

In addition to transcriptional regulation of KHK, we are interested in exploring whether KHK is post-translationally modified as well. Using Scansite (MIT; https://scansite4.mit.edu/4.0/#home), we have observed that KHK has a predicted phosphorylation motif site at the Ser80 residue. Interestingly, this site is present only in the KHK-A splice isoform, and not KHK-C, based on sequence comparison between residues 71-90 (Figure 3B). Interestingly, based on the KHK-A crystal structure, the S80 residue is on the outer surface of the protein and we would predict it to

be easily accessible to kinases or external proteins (Figure 3A). Candidate kinases predicted to phosphorylate the RXXS motif at the S80 residue include AKT1 and Aurora A kinase.

We are currently examining whether KHK is phosphorylated by serum starving A549 cells and stimulating with either serum or specific growth factors (i.e IGF) to determine whether KHK immunoblots show an extra band by Western blot. Proteomic analysis will also aid in validating whether S80 or other residues of KHK-A or KHK-C can be phosphorylated or undergo other post-translational modifications. If KHK-A is indeed phosphorylated, we will next assess potential consequences on KHK activity or stability. Phosphorylation of KHK by Akt, which is downstream of PI3K signaling, would be an intriguing possibility since Akt is also known to promote glucose uptake (Kohn, Summers et al. 1996), and this could be another means to promote KHK activity to which would be consistent with increased KHK activity in higher glucose concentrations (Figure 3C).

Contributions of dietary fructose to lung tumor growth

Given our findings that fructose can contribute to generation of pentose phosphate pathway intermediates and nucleotides, we are highly interested in determining whether exogenous fructose (i.e. through diet) can impact lung tumor growth. To determine whether fructose can impact lung tumor growth in vivo, in collaboration with the Shackelford lab (UCLA), we have put mice in two groups- either regular drinking water or drinking water containing 10% or 30% fructose, which is approximately the concentration in soda. Mice were started on the control or fructose water 4 weeks prior to inducing lung tumors through inhalation of an Adeno-Cre virus that induces oncogenic activation or loss of tumor suppressors. Both $Lkb1^{-/-}$;$p53^{-/-}$;$PTEN^{-/-}$ (LPP) and $Kras^{G12D}$;$p53^{-/-}$ (KP) were used for these experiments and growth of the tumors. Growth of the KP tumors was assessed by bioluminescent imaging (BLI) mice since they express luciferase in tumor cells and BLI signal correlates with tumor size as previously described

(Shackelford, Abt et al. 2013). Tumor characteristics and grade was assessed by IHC for LPP mice.

Our preliminary data from an experiment consisting of mice with tumors driven by $Kras^{G12D};p53^{-/-}$ shows that male mice in the 30% fructose water group compared to male mice in the control water group mice have increased BLI signal and therefore increased growth over a period of 5 weeks (Figure 4). It is intriguing that we only observe this phenotype in male mice and determining whether fructose can specifically impact tumor growth in male mice would be interesting for future studies to pursue.

Mice with tumors driven by $Lkb1^{-/-};p53^{-/-};PTEN^{-/-}$ (LPP) were placed in groups with either control water, 10% fructose water, or 30% fructose water. A group of female mice were sacrificed at 24 weeks post-induction of LPP and H&E was performed. Our preliminary results with female mice indicate that mice on the control water diet have few tumors in the lung based on histology (Figure 5). However, mice on either 10% or 30% fructose water have large tumors in the lungs. The tumors formed appear to be mucinous adenocarcinomas of the lung (Cha and Shim 2017).

Taken together, our data on the effects of fructose water on tumor growth in genetically engineered mouse models suggests that fructose may affect tumor growth in specific subsets of mice, but further studies repeating these experiments with larger cohorts would be required to draw conclusions. Additionally, both studies, while providing some intriguing results, do not address whether the effects of fructose are tumor autonomous or non-autonomous, so we are working to use CRISPR to generate KHK KO lines first in primary mouse lines derived from KP tumors. We will inject KHK WT versus KHK KO mouse KP cells transthoracially and assess growth of control tumors versus KHK KO tumors with and without fructose water to determine whether the effects on KP tumor growth in males is tumor autonomous or by other non-autonomous means. A critical aspect of these experiments involves quantification of serum

fructose levels to determine whether or not most of the fructose is cleared by the small intestine and liver and whether any residual fructose enters the serum of the mice in the fructose groups.

The Role of KHK in the Cell Cycle

Our findings indicate that KHK knockdown in cells have reduced glucose incorporation into nucleotides. Additionally, we have observed that KHK knockdown cells have altered morphology and are typically larger and flatter than control cells with atypical looking nuclei (Figure 6A). Knockdown of KHK by two shRNAs leads to decreased levels of cyclin A2, cyclin B1, and cyclin E and leads to no change or an increase in levels of cyclin D1 (Figure 6B). Therefore, we were curious whether KHK plays a role in the cell cycle.

We looked at the TCGA database for genes that correlate most highly with KHK levels and observed that KHK expression correlated highly with genes associated with the cell cycle in lung squamous cell carcinoma (LUSC) (Figure 6C) and breast invasive carcinoma. Data was generated using Metascape software (http://metascape.org). While our preliminary data hints at a potential connection between the cell cycle and KHK, future studies examining whether KHK mRNA and/or protein levels fluctuate with different phases of the cell cycle and whether KHK knockout cells exhibit defects in cell cycle progression would be valuable.

Developing Novel Inhibitors for KHK

Because genetic KHK deficiency in humans, essential fructosuria, is a clinically benign condition, targeting KHK should have limited systemic toxicities. KHK serves as an attractive potential drug target for this reason since most chemotherapeutic drugs have extensive adverse effects in normal, rapidly dividing tissues as well. While several KHK inhibitors have been published with the goal of treating non-alcoholic steatohepatitis (NASH) (Huard, Ahn et al. 2017), there are currently no clinically approved KHK inhibitors used to treat patients for cancer. Therefore, we are working with in conjunction with medicinal chemist Dr. Michael Jung's lab

(UCLA) as well as the UCLA Molecular Screening Shared Resource (MSSR) to identify and develop novel KHK inhibitors. Additionally, as an alternative approach, we are working with Dr. Daniel Nomura's lab (UC Berkeley) to perform cysteine-reactive covalent ligand screening (Counihan, Wiggenhorn et al. 2018) against KHK to identify hit compounds of which we can make analogues of potential KHK inhibitors.

Determine the role of other adenovirus-induced metabolic genes in anabolism and tumor growth

We identified KHK by determining which metabolic genes were most upregulated during adenovirus infection. Both GLS and KHK are examples of metabolic enzymes that are important for optimal adenovirus replication and also important for growth of tumors (Thai, Thaker et al. 2015). Thus, further studies examining other adenovirus-induced metabolic genes (AIMGs) may lead to the discovery of novel metabolic enzymes and pathways that are important in cancer. We have generated a list of the top metabolic genes upregulated during adenovirus infection, and the top five including KHK are shown in Figure 7.

First, the impact of AIMGs on adenovirus replication can be assessed to confirm importance of the enzymes in this context. Next, AIMGs can be knocked down or knocked out in various cancer cell lines to determine whether they are important for growth. Nutrient tracer experiments using U-$^{13}C_6$-glucose and U-$^{13}C_5$-glutamine will determine potential effects of knockdown or knockout of the enzyme on utilization of key nutrients and lend insight into possible mechanisms by which the AIMGs may contribute to tumor proliferation. This approach may lead to identification of new pathways contributing to anabolism and cancer growth.

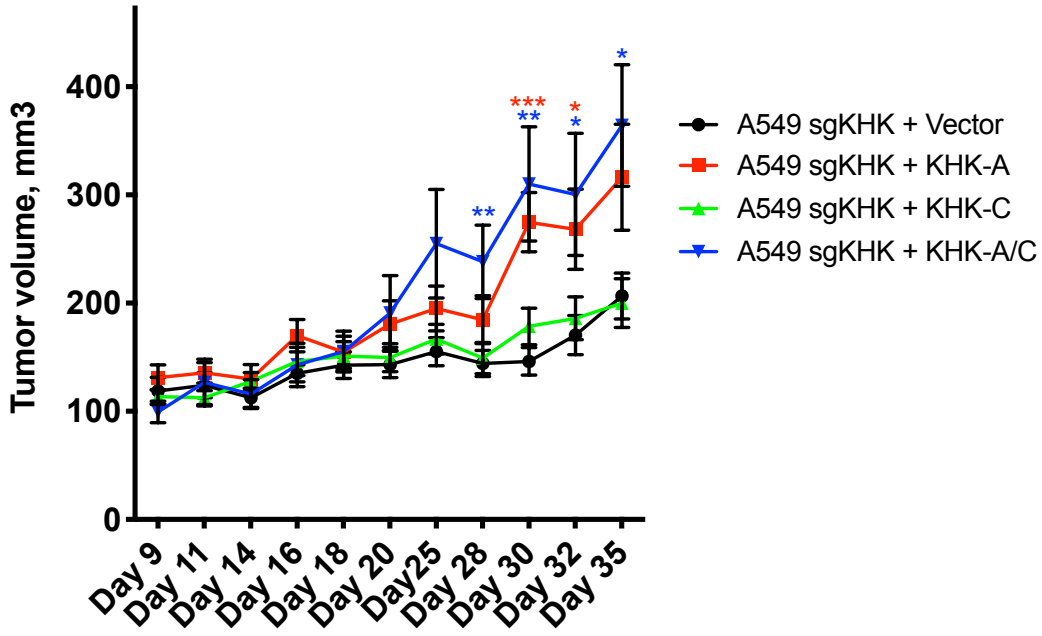

Figure 1. KHK-A, but not KHK-C restores growth of KHK KO tumors. A549 xenografts that were either KHK KO or KHK KO re-expressing either KHK-A, KHK-C, or both splice variants were generated and measured by calipers every 2-3 days. Tumor volume is plotted above.

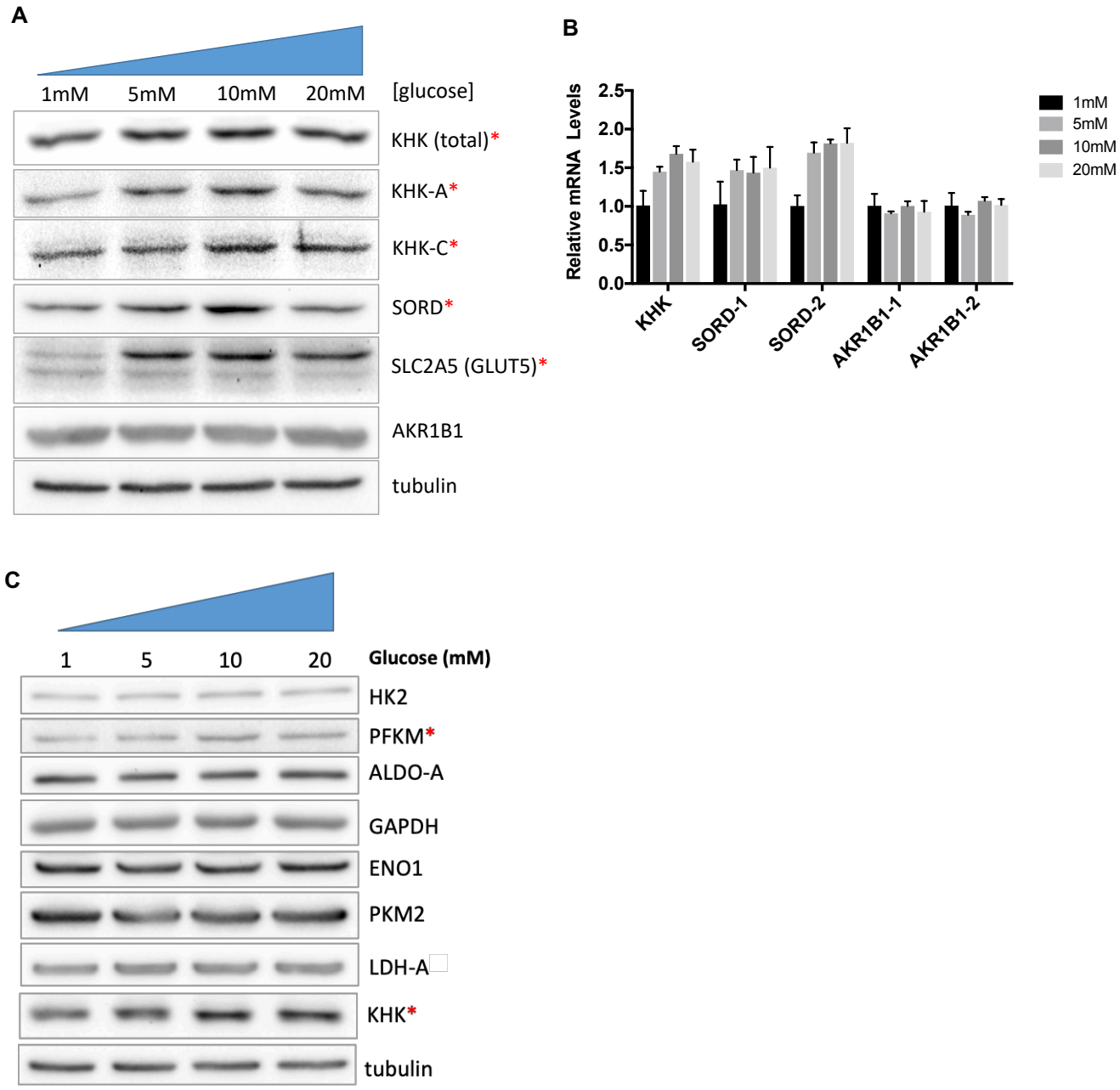

Figure 2. Effects of increasing glucose concentrations in media of A549 cells. A549 cells were serum starved and cultured in increasing concentration of glucose in the media. (A) Immunoblots of KHK and both splice variants, polyol pathway enzymes, and GLUT5. Protein levels of total KHK, KHK-A, KHK-C, SORD, and GLUT5 were elevated with increasing concentrations of glucose. (B) Relative mRNA levels of KHK, SORD, and AKR1B1 with increasing concentrations of glucose. (C) Immunoblots of glycolytic enzymes in the same

conditions are shown on the right. Only PFKM showed a glucose concentration-dependent increase in protein levels. Tubulin was used as a loading control in both sets of immunoblots in (A) and (C).

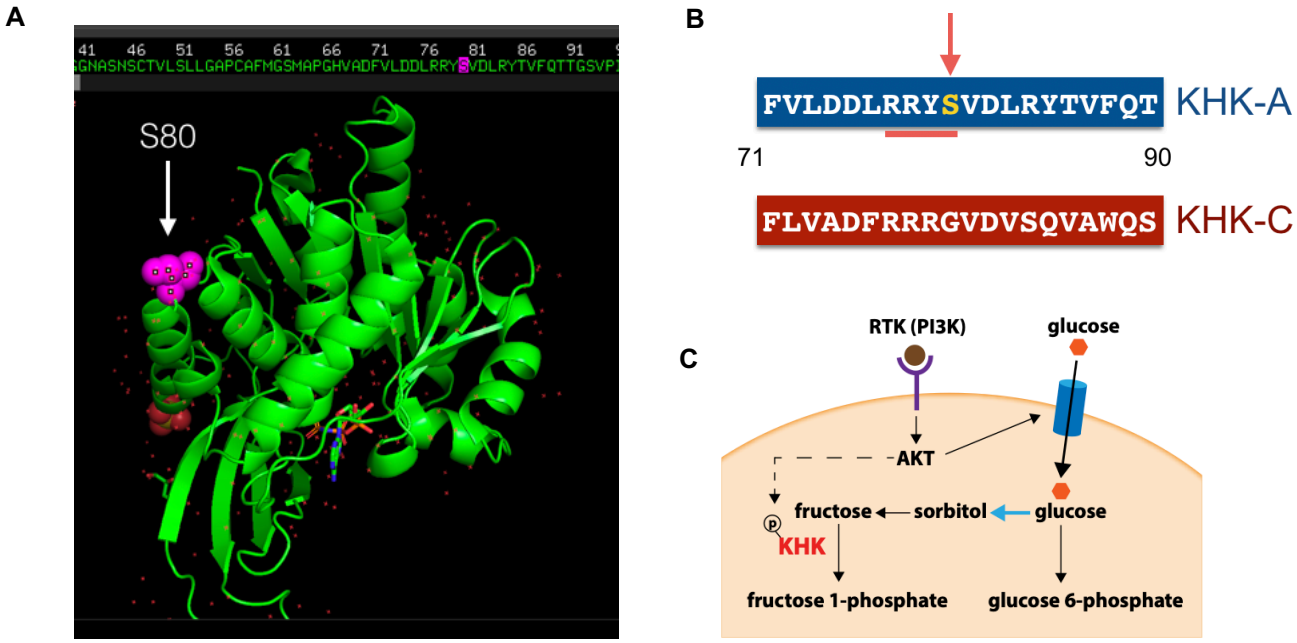

Figure 3. KHK-A contains the RXXS motif and may be phosphorylated at the Ser80 residue. (A) Crystal structure for KHK-A is shown on the left with the Ser80 residue indicated by the arrow. (B) KHK-A, but not KHK-C, has the RXXS motif and may therefore be a candidate substrate for phosphorylation by kinases like Akt. (C) Model of hypothesis for regulation of KHK and glycolysis by Akt.

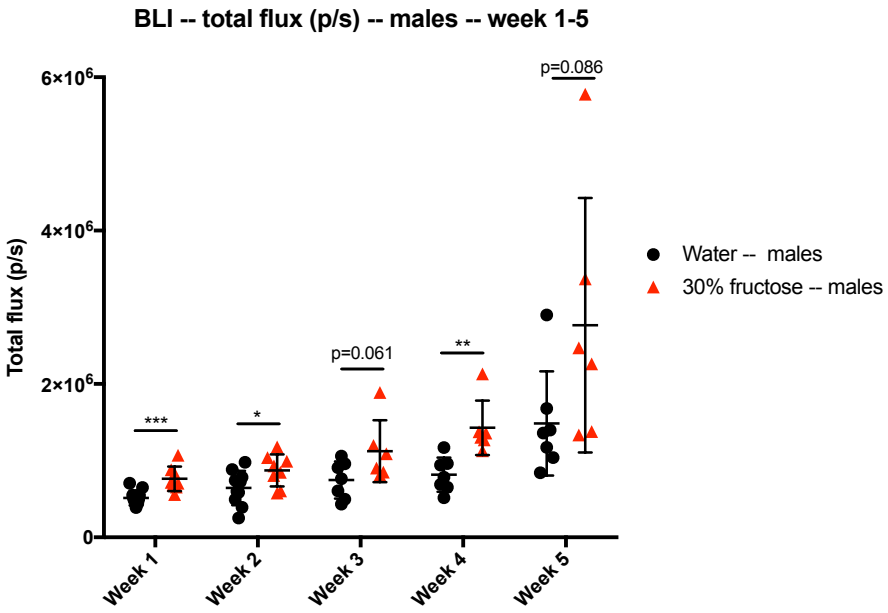

Figure 4. Bioluminescent Imaging of Kras^{G12D};p53$^{-/-}$ tumors. KP male mice placed in a group with control water or 30% fructose water and tumor growth was assessed by BLI over 5 weeks.

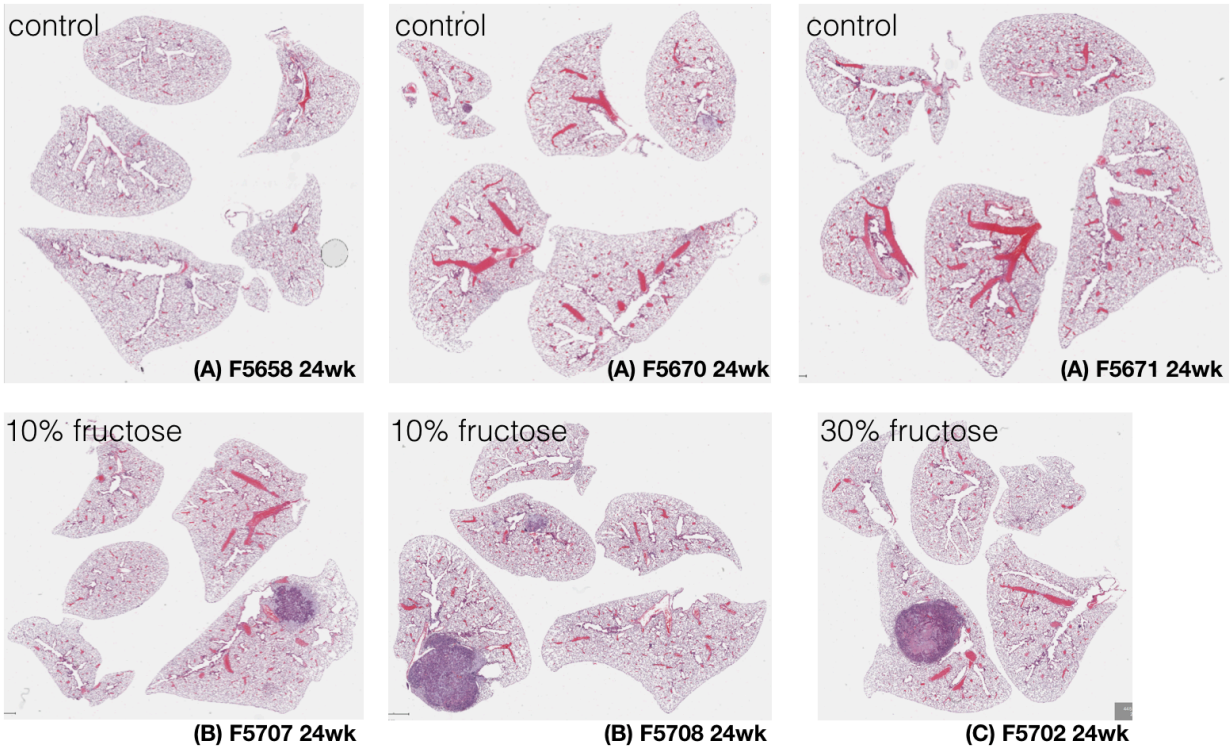

Figure 5. H&E (hematoxylin and eosin) staining of Lkb1$^{-/-}$;p53$^{-/-}$;PTEN$^{-/-}$ mice on control water or fructose water. LPP mice were placed in control a water group, 10% fructose water, or 30% fructose water. Sections of lung from female mice sacrificed at 24 weeks is shown in the figure.

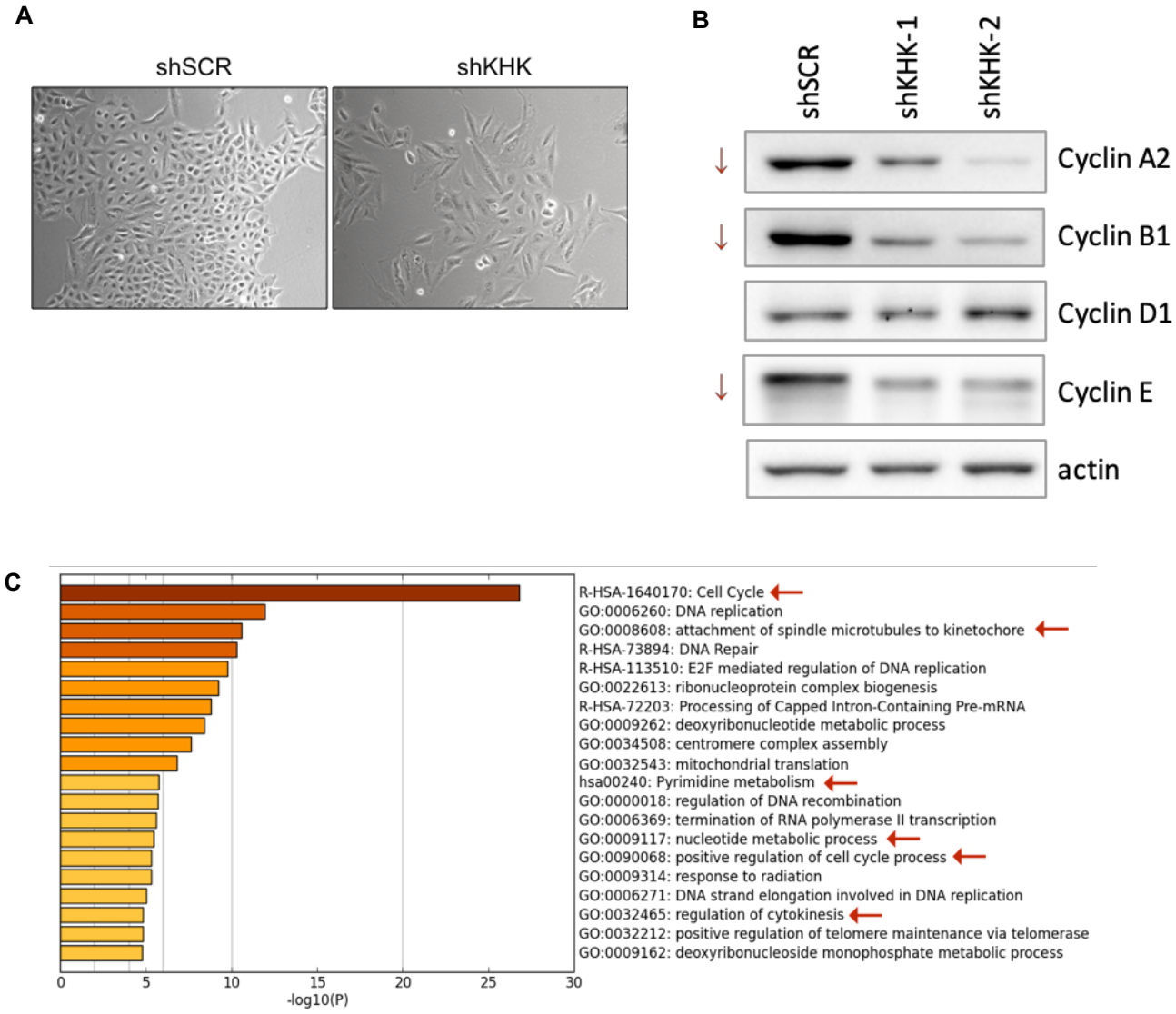

Figure 6. Potential connection of KHK with the cell cycle. (A) Light microscope images of A549 cells expressing a scrambled shRNA or shRNA against KHK. (B) Immunoblots of cyclin levels from lysate of A549 cells expressing a scrambed shRNA or 2 shRNAs against KHK. Actin was used as a loading control. (C) Analysis of gene sets whose expression correlate most highly with KHK expression in LUSC using Metascape software and data from cBioPortal.

Gene	Function	Relevance to Cancer	Log2 Fold Change	P-value	FDR
CHSY3 Chondroitin Sulfate Synthase 3	CHSY3 is a glycosyltransferase that has both glucuronyltransferase and N-acetylgalactosaminyltransferase activities.	Increased expression in colorectal cancer	2.73	< 0.005	< 0.005
ITPKA Inositol-Trisphosphate 3-Kinase A	Regulates inositol phosphate metabolism by phosphorylation of second messenger inositol 1,4,5-trisphosphate to Ins(1,3,4,5)P4.	Higher transcript levels found in primary lung cancers and metastases vs. normal tissues	2.44	< 0.005	0.01
XYLB Xylulose kinase	Phosphorylates D-xylulose to produce D-xylulose 5-phosphate, a molecule that may play an important role in the regulation of glucose metabolism and lipogenesis.	Higher transcript levels found in lung, breast, pancreas, and stomach cancers vs. normal tissues	2.34	< 0.005	0.001
KHK Ketohexokinase (fructokinase)	This gene encodes ketohexokinase that catalyzes conversion of fructose to fructose-1-phosphate.	Higher transcript levels found in lung and liver cancers vs. normal tissues	1.86	< 0.005	0.001
RDH10 Retinol Dehydrogenase 10	This gene encodes a retinol dehydrogenase, which converts all-trans-retinol to all-trans-retinal, with preference for NADP as a cofactor.	Higher transcript levels found in lung, liver, and pancrease cancers vs. normal tissues	1.58	< 0.005	0.001

Figure 7. Top five adenovirus-induced metabolic genes. RNA-sequencing was performed on RNA harvested from mock-infected versus wild-type adenovirus 5 (ADWT) infected normal human bronchial epithelial (NHBE) cells 8 hours post-infection. The top five upregulated genes are displayed here along with their potential association with cancer, the fold change in ADWT infected versus uninfected cells, p-value, and false discovery rate (FDR).

REFERENCES

Cha, Y. J. and H. S. Shim (2017). "Biology of invasive mucinous adenocarcinoma of the lung." Transl Lung Cancer Res **6**(5): 508-512.

Counihan, J. L., A. L. Wiggenhorn, K. E. Anderson and D. K. Nomura (2018). "Chemoproteomics-Enabled Covalent Ligand Screening Reveals ALDH3A1 as a Lung Cancer Therapy Target." ACS Chem Biol **13**(8): 1970-1977.

Hayward, B. E. and D. T. Bonthron (1998). "Structure and alternative splicing of the ketohexokinase gene." Eur J Biochem **257**(1): 85-91.

Huard, K., K. Ahn, P. Amor, D. A. Beebe, K. A. Borzilleri, B. A. Chrunyk, S. B. Coffey, Y. Cong, E. L. Conn, J. S. Culp, M. S. Dowling, M. F. Gorgoglione, J. A. Gutierrez, J. D. Knafels, E. A. Lachapelle, J. Pandit, K. D. Parris, S. Perez, J. A. Pfefferkorn, D. A. Price, B. Raymer, T. T. Ross, A. Shavnya, A. C. Smith, T. A. Subashi, G. J. Tesz, B. A. Thuma, M. Tu, J. D. Weaver, Y. Weng, J. M. Withka, G. Xing and T. V. Magee (2017). "Discovery of Fragment-Derived Small Molecules for in Vivo Inhibition of Ketohexokinase (KHK)." J Med Chem **60**(18): 7835-7849.

Kim, M. S., S. A. Krawczyk, L. Doridot, A. J. Fowler, J. X. Wang, S. A. Trauger, H. L. Noh, H. J. Kang, J. K. Meissen, M. Blatnik, J. K. Kim, M. Lai and M. A. Herman (2016). "ChREBP regulates fructose-induced glucose production independently of insulin signaling." J Clin Invest **126**(11): 4372-4386.

Kohn, A. D., S. A. Summers, M. J. Birnbaum and R. A. Roth (1996). "Expression of a constitutively active Akt Ser/Thr kinase in 3T3-L1 adipocytes stimulates glucose uptake and glucose transporter 4 translocation." J Biol Chem **271**(49): 31372-31378.

Koo, H. Y., M. Miyashita, B. H. Cho and M. T. Nakamura (2009). "Replacing dietary glucose with fructose increases ChREBP activity and SREBP-1 protein in rat liver nucleus." Biochem Biophys Res Commun **390**(2): 285-289.

Shackelford, D. B., E. Abt, L. Gerken, D. S. Vasquez, A. Seki, M. Leblanc, L. Wei, M. C. Fishbein, J. Czernin, P. S. Mischel and R. J. Shaw (2013). "LKB1 inactivation dictates therapeutic response of non-small cell lung cancer to the metabolism drug phenformin." Cancer Cell **23**(2): 143-158.

Thai, M., N. A. Graham, D. Braas, M. Nehil, E. Komisopoulou, S. K. Kurdistani, F. McCormick, T. G. Graeber and H. R. Christofk (2014). "Adenovirus E4ORF1-induced MYC activation promotes host cell anabolic glucose metabolism and virus replication." Cell Metab **19**(4): 694-701.

Thai, M., S. K. Thaker, J. Feng, Y. Du, H. Hu, T. Ting Wu, T. G. Graeber, D. Braas and H. R. Christofk (2015). "MYC-induced reprogramming of glutamine catabolism supports optimal virus replication." Nat Commun **6**: 8873.